Molecular recognition of organic and inorganic phosphates at the aqueous interface

Dissertation

Presented in Partial Fulfillment of the Requirements for the Degree Doctor of Philosophy

in the Graduate School of The Ohio State University

By

Jennifer Frances Neal

Graduate Program in Chemistry

The Ohio State University

2020

Dissertation Committee

Prof. Heather C. Allen, Advisor

Prof. Jovica D. Badjić

Prof. L. Robert Baker

Prof. Andrew A. May

Abstract

The air–water interface is a unique microenvironment to explore host–guest chemistry. In the following chapters, molecular recognition of a diverse set of organic and inorganic phosphates were explored at the aqueous interface. Chapter 1 provides a brief introduction to interfacial molecular recognition across synthetic, environmental, and biological systems. This literature review provides a background on supramolecular chemistry at the aqueous interface and the unique properties driving these interactions at the surface of water. Chapter 2 explores a biologically relevant phospholipid, 1,2-dipalmitoyl-sn-glycero-3-phosphatidic acid, binding to the amino acid arginine. Through a systematic evaluation of the binding sites by testing glycine and guanidinium chloride as control molecules, we determined that the guanidinium moiety was binding to the phosphate headgroup of the phospholipid. Interestingly, the interfacial binding affinity was 10,000-fold greater than the binding affinity determined through bulk solution measurements. The surface binding affinity was determined using infrared reflection absorption spectroscopy and the surface pressure-mean molecular area isotherms. Chapter 3 is a systematic evaluation of the driving forces of interfacial phosphate recognition using synthetic receptors. Four surface receptors were synthesized with long octadecyl chain(s) and different functional groups at the binding site in which guanidinium, thiouronium, and thiourea headgroups were tested. The number of alkyl chains was modulated (single chain versus double chain) to determine their effect on the supramolecular packing and binding affinity. Overall, we

ii

determined the driving forces influencing interfacial phosphate recognition as the chemical, physical, and supramolecular superstructural. The chemical nature of the headgroup influenced binding where the guanidinium > thiouronium > thiourea for phosphate affinity. The physical environment of the aqueous subphase influenced the binding selectivity over chloride in which high ionic strength with addition of sodium chloride hindered phosphate selectivity for the double chain guanidinium receptor. The supramolecular superstructural packing arrangement influenced phosphate binding because the single chain guanidinium did not bind to phosphate whereas the double chain guanidinium strongly bound to phosphate. These driving forces are crucial to developing the rational design principles of surface receptors that are selective towards aqueous phosphates. Chapter 4 explores the double chain guanidinium receptor's selectivity towards various anions. We found that the guanidinium receptor binds to sulfate> phosphate> iodide> nitrate >chloride~ bromide~ nitrite. Interestingly, the guanidinium receptor is selective for sulfate over phosphate even though the dehydration penalty for the sulfate anion is significant. Sulfate is a (-2) anion and the phosphate is a (-1) anion and charge differences could be influencing both the binding affinity and binding stoichiometry of the guanidinium interactions to either phosphate or sulfate. It was already previously shown in Chapter 3 that electrostatic interactions dominate over hydrogen bonding interactions alone because the charged guanidinium receptor had a stronger phosphate affinity than the neutral thiourea receptor. Therefore, it is not surprising that a (-2) anion would outcompete a (-1) anion at the surface of water. Infrared reflection absorption spectroscopy and vibrational sum frequency generation spectroscopy were both used to determine the guanidinium selectivity and essentially

provide an order of the relative anion affinities. Lastly, Chapter 5 explores a series of semi-soluble phosphoric and phosphonic acids at the aqueous interface. The relative protonation state and sodium binding properties were determined by systematically controlling the pH and sodium concentrations. Also, competitive binding interactions between protonation state and sodium complexation were explored by increasing amounts of sodium chloride at low pH. We have determined a critical sodium chloride concentration at pH 2 necessary to outcompete the acid-base equilibrium for the phosphonic acid semi-soluble species. The following chapters explore supramolecular chemistry at the air–water interface and provide new insights into studying these interactions. Each chapter is a diverse look into molecular recognition at the aqueous surface in which Chapter 2 is a biologically relevant system, Chapters 3 and 4 are synthetic receptors, and Chapter 5 is relevant for atmospheric and oceanic chemistries.

Dedication

This dissertation is dedicated to my husband Taylor Neal. You are a wonderful scientist and person and have constantly supported me throughout this process. Your chemical insights have helped me so much and your love for teaching and mentorship is contagious and motivational.

Acknowledgments

I would like to acknowledge my advisor Professor Heather Allen for supporting me through this process. I would also like to thank Professor Amar Flood (Indiana University) for all your help and research support. I would also like to thank my undergraduate research students who have dedicated so much of their time to research and understanding these interfacial systems. Alexander Grooms, Brittany Shook, Mia Zerkle, and Morgan Smeltzer have been instrumental in my research and contributed to both the experimental work and overall understanding of these complex supramolecular events. Also, the rest of the Allen group has been very supportive over the years. I would like to acknowledge Mickey Rogers for your help with research and allowing me to grow algae with you for your dissertation work. Also, to Ka Chon Ng and Kimberly Carter-Fenk for your help with various projects. The postdocs over the years including Wei Zhao (Indiana University), Ankur Saha, Lu Lin, Stephen Baumler, and Liwei Yan who have worked with me and helped me grow as a scientist. And lastly, I would like to thank my family and friends who have always been there for me. Thanks to my dad for supporting me during this process and flying out to see me present at an ACS meeting. You always believed in me and have made even the hardest times easier through your support.

Vita

Education

2012…………………….B.A., Chemistry & Environmental Studies, Lake Forest College

2015-2017, 2020……………………………………...Graduate Teaching Assistant,

Department of Chemistry and Biochemistry,

The Ohio State University

2017-2019…………………………………..…………….Graduate Research Assistant,

Department of Chemistry and Biochemistry,

The Ohio State University

Publications

Neal, J. F.; Zhao, W.; Grooms, A. J.; Smeltzer, M. A.; Shook, B. M.; Flood, A. H.; Allen, H. C. Interfacial Supramolecular Structures of Amphiphilic Receptors Drive Aqueous Phosphate Recognition. *J. Am. Chem. Soc.* **2019**, *141* (19), 7876–7886.

Neal, J. F.; Zhao, W.; Grooms, A. J.; Flood, A. H.; Allen, H. C. Arginine–Phosphate Recognition Enhanced in Phospholipid Monolayers at Aqueous Interfaces. *J. Phys. Chem. C* **2018**, *122* (46), 26362–26371.

Neal, T. A.; **Neal, J. F.**; Eippert, A. B.; Moore, C.; Allen, H. C.; Badjic, J. D. An easily accessible isospiropyran switch. *Org. Biomol. Chem*. **2019**, 17, 9124–9128.

Fields of Study

Major Field: Chemistry

Table of Contents

List of Tables

List of Figures

xiv

List of Abbreviations

ACS	American chemical society
ADP	Adenosine diphosphate
AMP	Adenosine monophosphate
ATP	Adenosine triphosphate
BAM	Brewster angle microscopy
CCD	Charge-coupled device
CW	Continuous wave
DPPA	1,2-dipalmitoyl-snglycero-3-phosphatidic acid
DPPC	Dipalmitoylphosphatidylcholine
EDTA	Ethylenediaminetetraacetic acid
EM	Electron-multiplying
FTIR	Fourier-transform infrared
HPLC	High performance liquid chromatography
IR	Infrared
IRRAS	Infrared reflection-absorption spectroscopy
LPA	Lysophosphatidic acid
MCT	Mercury cadmium telluride
MD	Molecular dynamics
MMA	Mean molecular area
MME	Mean molecular expansion
NDFG	Noncollinear difference-frequency generator
NMR	Nuclear magnetic resonance
PA	Phosphatidic acid
RA	Reflectance-absorbance
SF	Sum frequency
SFG	Sum frequency generation spectroscopy
SSA	Sea spray aerosols
TC	Tilted liquid condensed
UV	Ultraviolet
VSFG	Vibrational sum frequency generation spectroscopy

Chapter 1. Interfacial binding across synthetic, environmental, and biological monolayers

1.1 Introduction

The aim of this dissertation is to provide new insights into molecular recognition at the air–water interface. The development of receptor molecules (or hosts) capable of binding to ions (guests) in water is notoriously challenging.[1,2] The highly competitive nature of water as a solvent acts to hydrate both the host and guest molecules.[2,3] In addition to this, electrostatic interactions are effectively screened by the high dielectric environment of water.[4] The development of aqueous supramolecular systems will benefit from collaborative efforts between supramolecular and physical chemists.[5] In particular, the aqueous interface has some remarkable advantages over traditional bulk recognition but is nevertheless experimentally challenging and requires surface specific instrumentation to probe.

Interfaces are prevalent in binding across synthetic, environmental, and biological systems, and each system will be broken down into a separate chapter. This introductory chapter will focus on the unique properties of the air–water interface and the numerous literature examples employing Langmuir monolayers to study host–guest chemistry. We have chosen to focus on the air–water interface because of the unique properties at the surface of water. This interfacial regime provides advantages over traditional bulk

studies; however, a fundamental understanding of these events is still underdeveloped. There is a great opportunity to explore these simple binding interactions at the air–water interface to serve as a model for studying recognition events. As we have studied these interactions, we have begun to reveal the molecular driving forces. Ultimately, we seek to answer the question: what makes molecular recognition so special at the interface? This introduction provides an overview of binding at the aqueous interface and looks at these interactions across synthetic, environmental, and biological systems.

Before exploring recent examples in molecular interfacial recognition, it is important to understand the fundamental differences in host–guest chemistry at the air–water interface. In the case of binding at the air–water interface, the host is the molecular monolayer and the guest is a soluble aqueous species driven to the interface through binding interactions (Figure 1.1a). These noncovalent interactions stem from the balance in entropy and enthalpy at the interface for both host and guest and during the host–guest binding event. There is an intricate and delicate balance of thermodynamic gains and costs during binding. The enthalpy-entropy compensation is a well-known phenomenon in host-guest chemistry. Enthalpy-entropy compensation stems from the combined thermodynamic forces from the binding event which leads to more noncovalent interactions and thus a more negative enthalpy component, but also leads to a restriction in mobility because ultimately two separate entities are coming together, thereby decreasing entropy.[6] There are however some systems that are enthalpically disfavored and entropically driven.[7,8]

Monolayers have the advantage of preorganization[9,10] (i.e. all the headgroups are pointing into the water and the hydrophobic part is pointing up into the air) which is

thermodynamically paid for (entropically driven) by the hydrophobic effect. The hydrophobic part of the molecule (often greasy, long alkyl chains) are pointed up away from the water and into the air while the hydrophilic headgroup is well ordered and available for binding, essentially taking advantage of entropy at the interface. While use of preorganization is often employed as a tool to drive host–guest chemistry in bulk solution by means of rigid architectures,[11–13] the interface has the advantage that this entropic cost is paid for before the recognition event takes place. Preorganization undoubtably plays a vital role in host–guest chemistry which makes these interfaces a logical environment to explore.
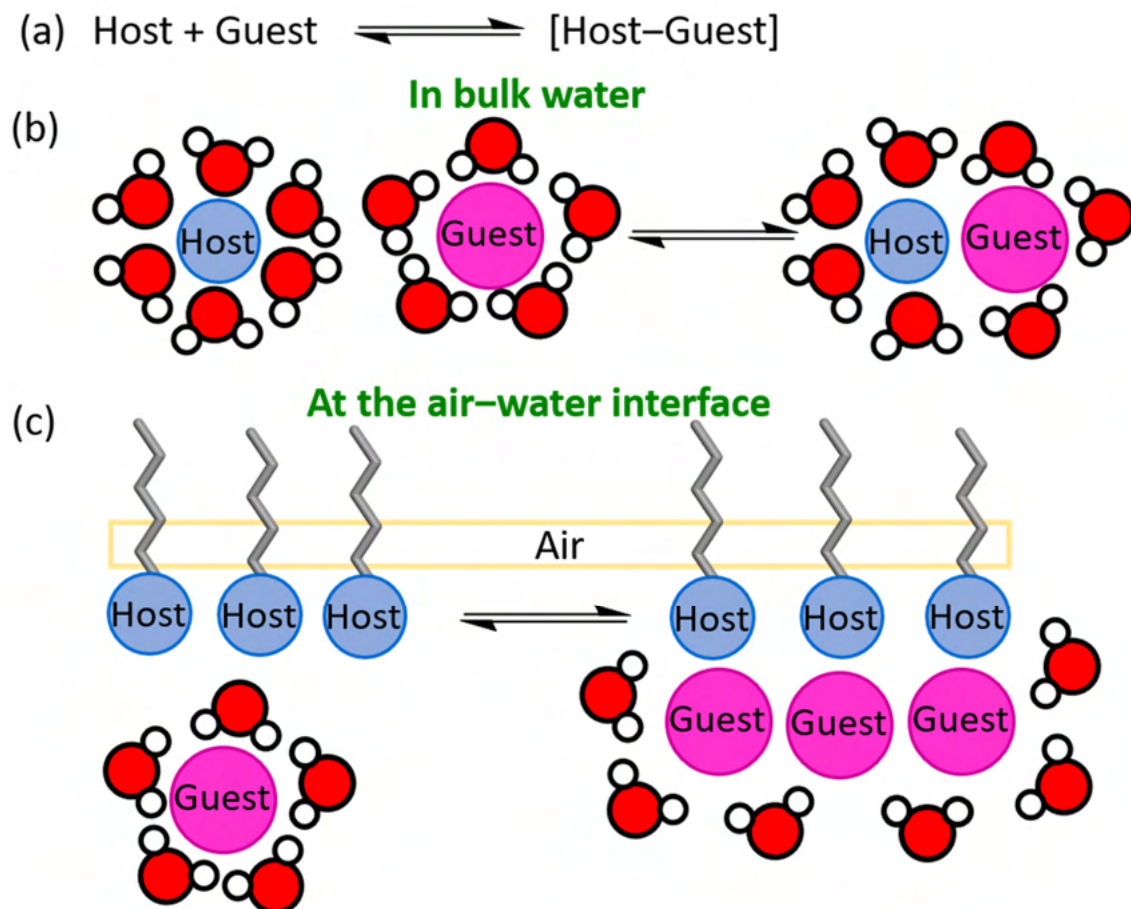
Figure 1.1 (a) Simple host-guest binding equilibrium, (b) solvent effects in host-guest binding in bulk solution, (c) interfacial advantage of preorganization at the air–water interface.

The nature of the noncovalent bond is also important in understanding these systems. The strength of the noncovalent interaction deeply depends on the type of noncovalent bond. These include electrostatic or ion–ion interactions which are generally the strongest (100-350 kJ/mol), ion-dipole interactions which are weaker (50-200 kJ/mol), ion-dipole (50- 200 kJ/mol), dipole-dipole (5-50 kJ/mol), hydrogen bonding (4-120 kJ/mol), cation-Π (5-80 kJ/mol), van der Waals (< 5 kJ/mol), others.[7,14] Hydrogen bonding interactions can have a range of binding energies depending on whether they are

weak or strong and are especially important in host guest chemistry because they provide directionality.[7] These noncovalent interactions provide the toolkit to building supramolecular architectures tuned to bind to a particular guest.

Solvent effects are also influential in host–guest complexation. The other aspect influencing this binding affinity enhancement at the air–water interface is the dielectric constant and the ever–changing hydration environment at the interface. The dielectric constant of bulk water is extremely high ($\varepsilon > 80$) which screens electrostatic interactions. For comparison, the dielectric constant of methanol is 33.3[15] and chloroform is $4.7.$[4] Binding in aqueous solutions has added challenges as there is a competition between hydrogen bonding between water solvating the guest molecules and the host binding to the guest molecules. Surface water molecules are in a much lower dielectric constant regime than in the bulk water. This dielectric value has been reported as $\varepsilon < 40$ by several groups through both theoretically and experimentally determined methods. Figure 1.2 schematically shows the changing dielectric at the interface of a monolayer surface or at a micelle or bilayer surface. The air–water surface evidently has a lower dielectric constant than a micelle or bilayer systems. In addition to the change in the dielectric constant of water, hydration at the air–water interface has been found to be different to that of bulk solution studies.[16–18]
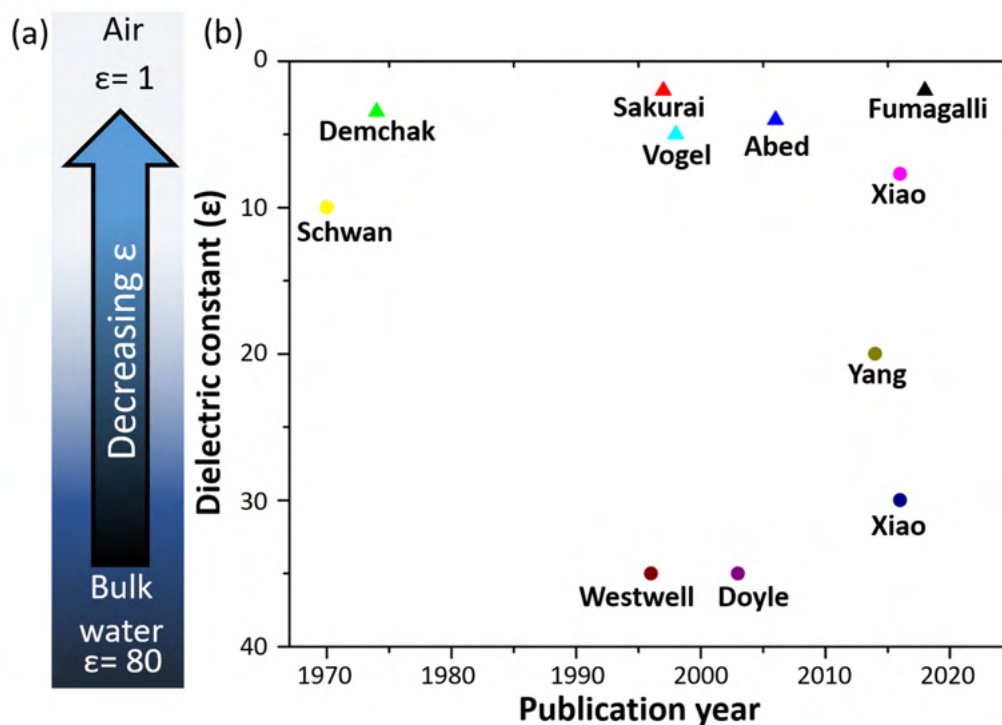
Figure 1.2 (a) Schematic of the change in dielectric constant transitioning from bulk solution to interface of water and (b) the reported dielectric constants at the surface of water (triangles) and at the surface of micelles or bilayers (circles) along with publication year taken from references.[19–28]

The complex nature of hydration and ion adsorption also plays a role in host-guest chemistry at the aqueous surface. Hofmeister's rules often seem to fail at the surface,[16,29–32] there has been a push towards explaining the unique phenomena of ion interactions as specific ion effects.[30,33,34] One interesting example of this found that the character of the anion (nitrate vs thiocyanate) showed different lanthanide extraction selectivity for a methylated ammonium monolayer.[34] The complex nature of hydration and ion interactions at the aqueous interface will continue to be an open source of investigation for interfacial molecular recognition. Binding affinity and selectivity are undoubtably influenced by the unique interfacial hydration effects.

1.2 Synthetic Receptors
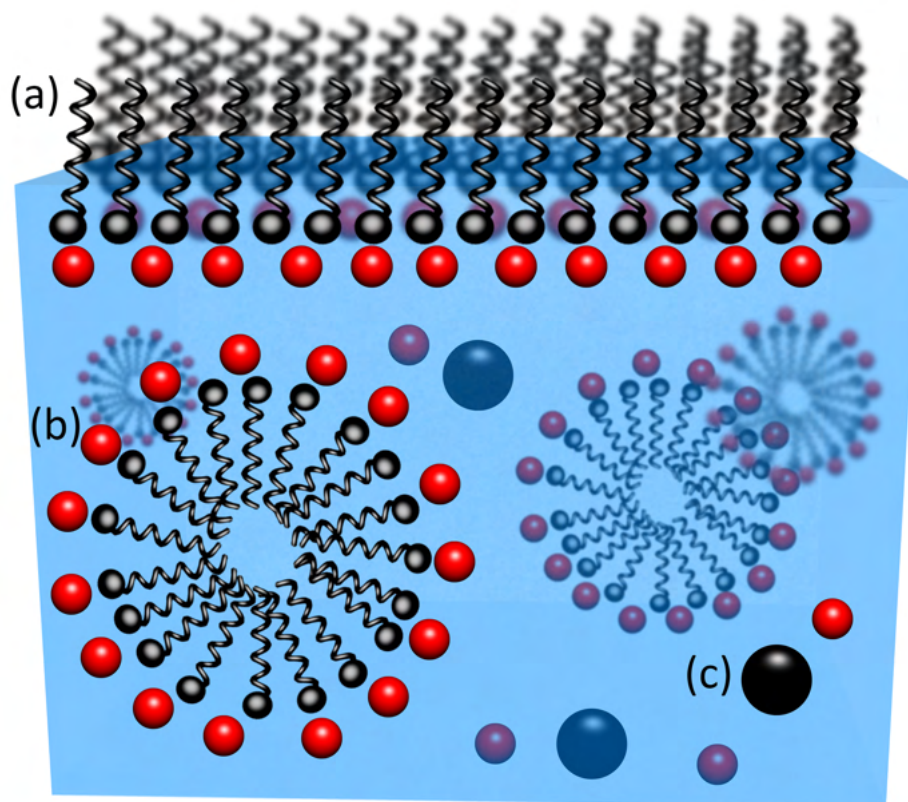
Figure 1.3 Apparent binding affinities between guanidinium and phosphate (a) at the surface of Langmuir monolayers $K = 10^6 - 10^7$ M^{-1}, (b) at the surface of micelles or bilayers $K = 10^2 - 10^4$ M^{-1}, (c) in bulk solution $K = 1.4$ M^{-1}. Modified from M. Onda *et al.*, J. Am. Chem. Soc., 1996, 118, 8524.

One of the exciting avenues for host–guest chemistry is the rational design of surface immobilized receptors. Chapters 3 and 4 explore a series of synthetic phosphate receptors and outlines the principle driving forces of these receptor–phosphate interactions at the air–water interface. Pioneering work by Kunitake on synthetic guanidinium amphiphiles demonstrated that the binding affinity is greatly enhanced at the surface of Langmuir monolayers. Figure 1.3 shows the binding affinities for a guanidinium–phosphate

interaction in which $K = 10^6 - 10^7$ M^{-1} at the air–water interface, $K = 10^2 - 10^4$ M^{-1} at the surface of micelles or bilayers, and $K = 1.4$ M^{-1} in bulk solution. There is a clear trend indicating that the binding affinity increases from the least organized in bulk solution to the most ordered at the air–water interface. This helps demonstrate that the preorganization of the system coupled with the decreasing dielectric constant must play a crucial role in driving the substantial differences in binding affinities. Theoretical work by the Kunitake group breaks down why the intermolecular interactions are strengthen at the aqueous surface relative to that of bulk water.[21,35,36] They attribute this as due to the dielectric change at the interface and the relative distance of the binding interaction to the interfacial regime which must span a short distance to be effective.

Figure 1.4 shows select examples of synthetic systems designed by the Kunitake group binding to various soluble molecules including an amphiphilic Kemp's acid[37], orotic and hydroorotic acid monolayers[38], among others.[39–42] The single chain guanidinium amphiphile shown in Figure 1.4a binds to phosphates in the form of adenosine triphosphate (ATP) and adenosine diphosphate (ADP) with extraordinary high binding affinities of 3.2×10^6 M^{-1} and 1.7×10^7 M^{-1}, respectively. X-ray photoelectron spectroscopy of multiple Langmuir-Blodgett transfers of the bound guanidinium amphiphile to the ATP or ADP substrate was used to determine these binding affinities.[43] Kunitake designed multiple receptors that were tailored to utilize hydrogen bonding and/or electrostatics as the principle driving forces for these interfacial binding interactions. An example of this is the neutral resorcinol-dodecanal cyclotetramer binding to soluble sugar ribose through hydrogen bonding interactions (Figure 1.4b).[44] Figure 1.4c also shows a mixed monolayer system of guanidinium and orotate

8

amphiphiles binding to flavin adenine dinucleotide driven by multiple hydrogen bonding sites and electrostatic interactions.[45] The use of mixed monolayers allows the binding site to be controlled to maximize interactions. The concept of a mixed monolayer receptor was also observed in a mixture of an oligopeptide amphiphile with a benzoic acid amphiphile.[46] In this system, the binding affinity was 10 times larger in the mixed monolayer than in the single component.[46]
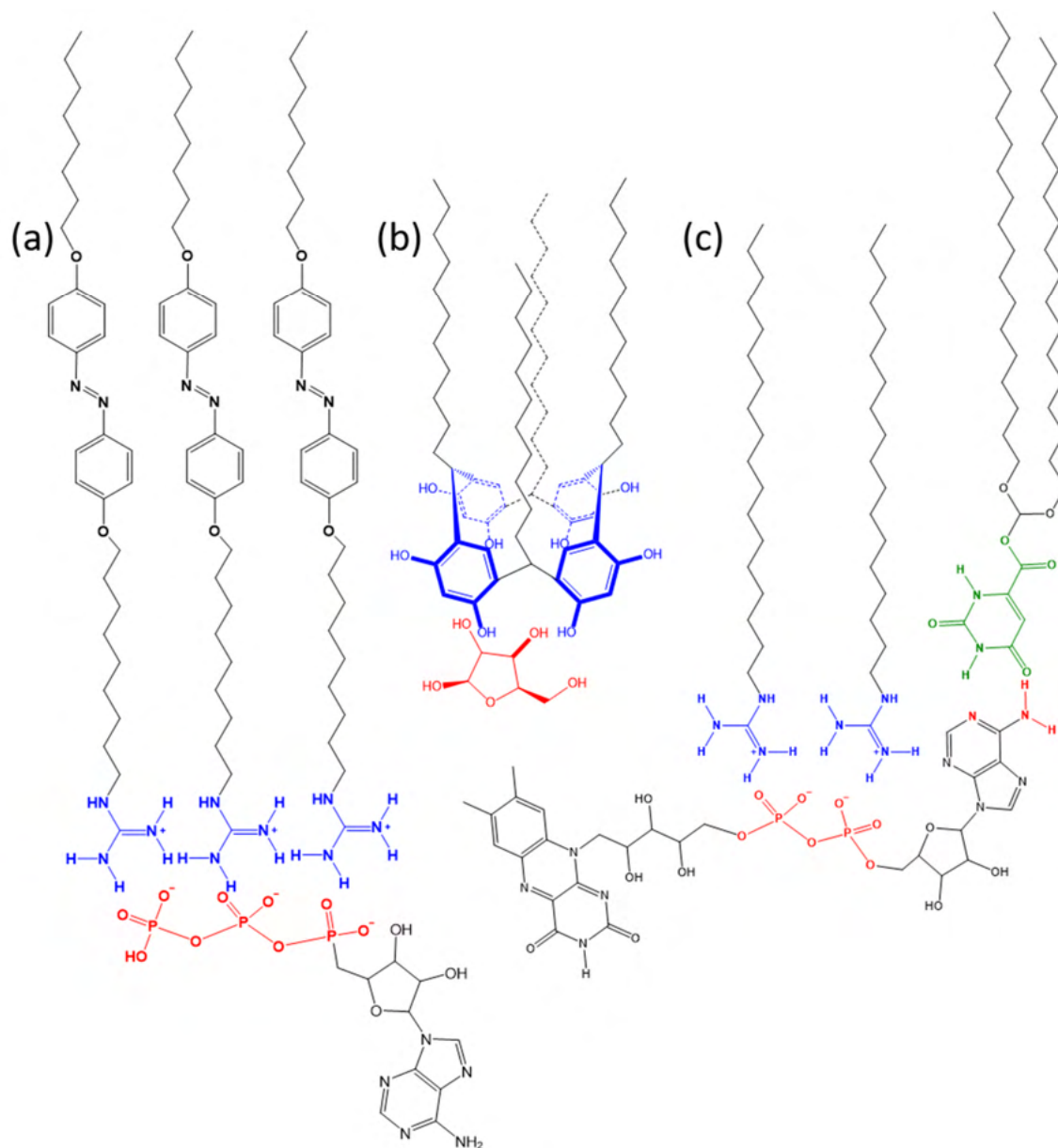
Figure 1.4 Selected examples of molecular recognition at the air water interface from the Kunitake group[43–45] (a) guanidinium amphiphiles binding to adenosine triphosphate, (b) resorcinol-dodecanal cyclotetramer binding to soluble sugar ribose, and (c) mixed monolayers of guanidinium and orotate amphiphiles binding to flavin adenine dinucleotide.

The Klärner group has brought the use of molecular clips and tweezers from the bulk solution to the air–water interface in several studies.[47–50] The electron rich molecular

tweezer is able to bind to the electron deficient guest molecule 1,2,4,5-tetracyanobenzene in the binding cavity as depicted in Figure 1.5a. This binding geometry agreed with their previous work[51] as well as a crystal structure of the complex.[50]   Furthermore, there are examples of cavitand hosts that have also been used as synthetic hosts at the aqueous interface.[52–56] Figure 1.5b shows an amphiphilic calixresorcinarene binding to phenylalanine.[57] The cavitand binding is assisted by a copper mediated binding and has enantioselective recognition for D-phenylaniline over the L enantiomer.
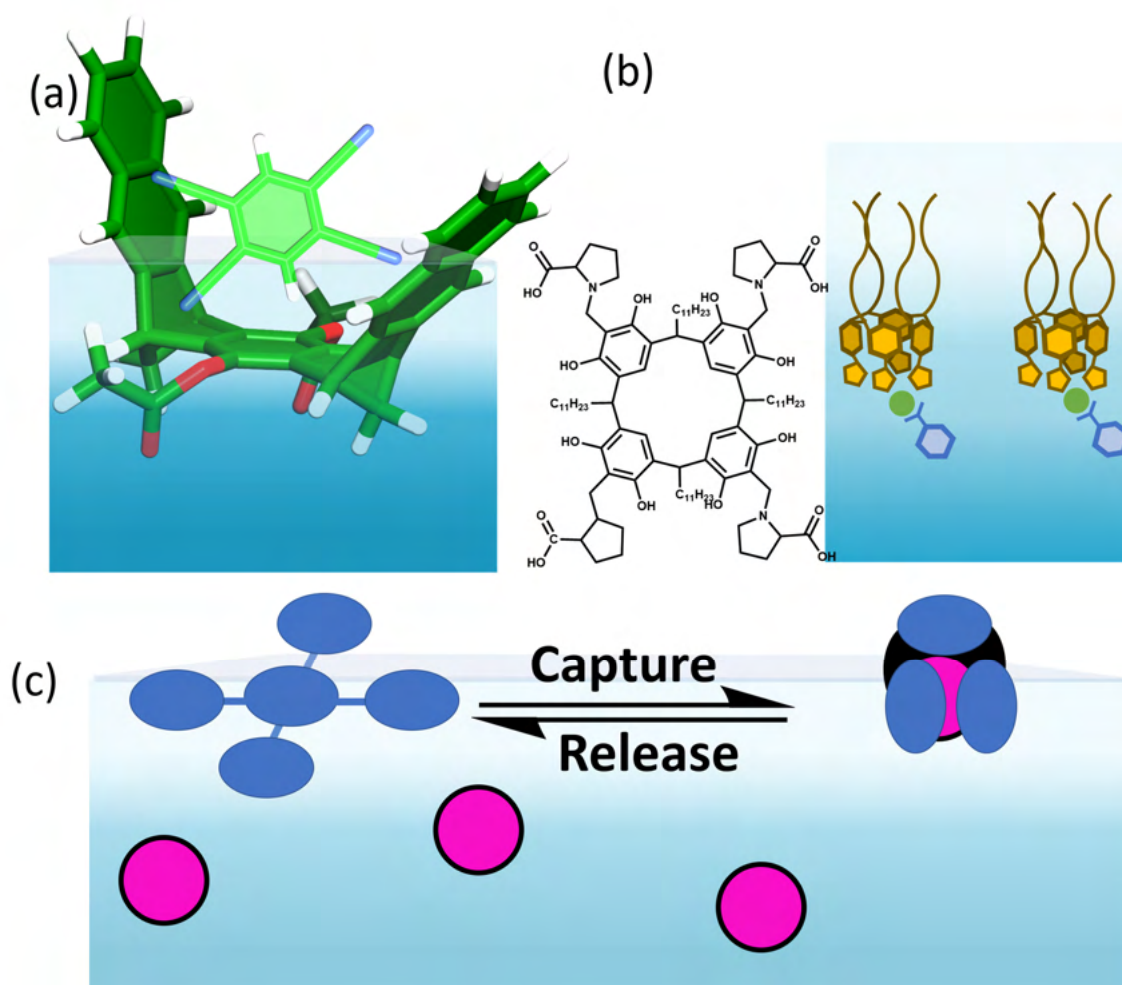
Figure 1.5 (a) Binding of tetracyanobenzene in the cavity of the molecular tweezer at the aqueous interface, (b) calixresorcinarene binding to phenylalanine, and (c) capture and release switchable steroid cyclophane to a naphthalene derivative.

11

The concept of switchable molecular recognition is appealing because it allows for the guest molecule to be captured and released and opens opportunities for recycling capabilities. Ariga *et al.* have developed a switchable steroid cyclophane at the aqueous interface that binds reversibly to a naphthalene derivative.[58–61] At large molecular areas the steroid cyclophane lays flat in a two dimension array while upon compressing the monolayer, it converts to a three dimension standing up conformation as depicted in Figure 1.5c.

Employing synthetic hosts at the aqueous interface has some additional benefits over bulk solution and remains an open area of investigation. The aqueous interface will continue to be a relevant area to explore for separations,[18,34,62] sensing,[63,64] environmental remediation.[5,65,66] Some studies have shown that the mechanical compression at the interface can be used as molecular trigger to conformational changes and these molecular machines could have use in interfacial molecular recognition.[67–70] It will be exciting to see what new synthetic hosts will be utilized at the air–water interface in the future.

1.3 Environmental
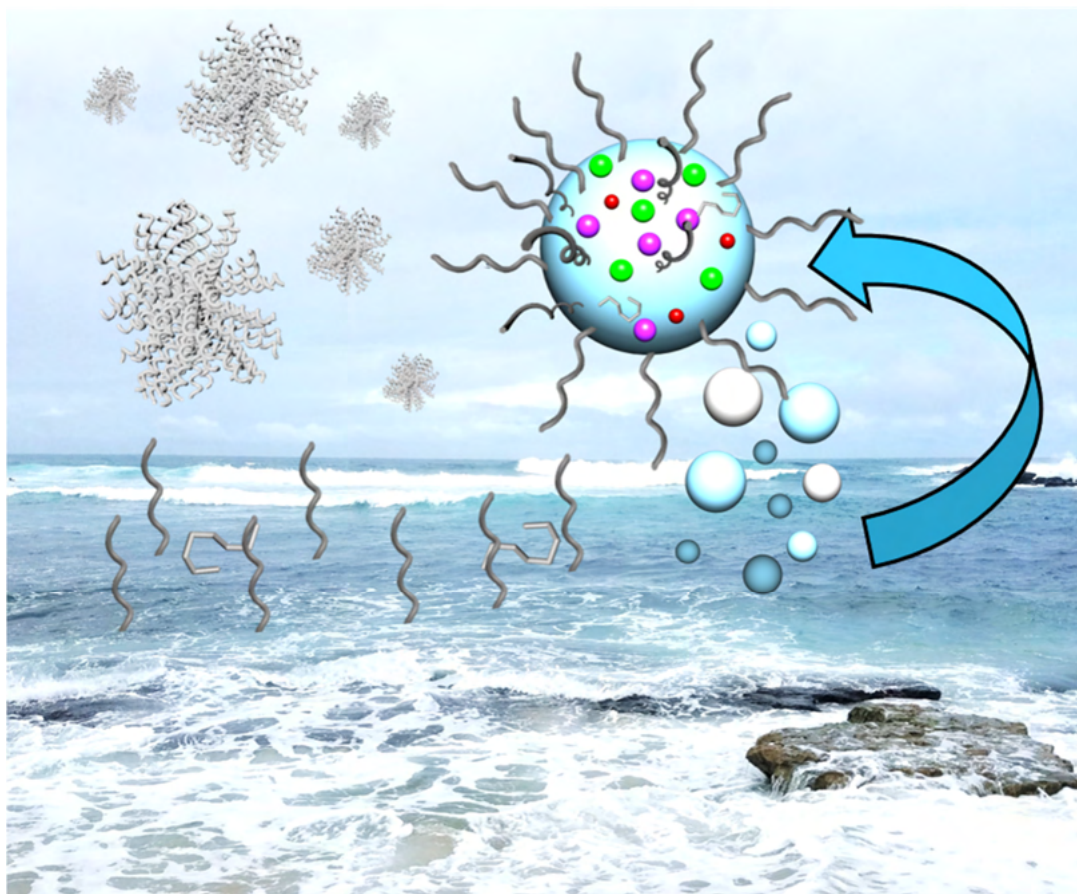
Figure 1.6 Schematic representation of the sea surface microlayer and sea spray aerosol which are both enriched with an organic coating.

In addition to the utility of host–guest chemistry in synthetic systems, non–covalent interactions also have an influential role in both freshwater and oceanic environmental systems. It is especially interesting to study monolayer films as a model system for the thin hydrophobic film coating of atmospheric sea spray aerosols and the ocean surface in

the sea surface microlayer. Chapter 4 features a set of semi-soluble organic phosphoric and phosphonic acid species and explores the concept of competitive binding interactions at high sodium chloride and low pH. Sea spray aerosols which are formed from bubble bursting or wave breaking at the ocean's surface are in part stabilized by the numerous interactions between the organic amphiphilic species present at the surface and the soluble ions (sodium, calcium, magnesium, trace metals, etc.), as well as both neutral and charged small organics, macromolecular proteins, and polymeric species (Figure 1.6). There are numerous articles that explain the composition of the sea surface microlayer, formation of these aerosols, and their relevance in climate science in more extensive detail.[71–75] We will focus on studying the binding event in the interfacial regime of these aqueous systems.

Recent work has shown that there is saccharide enrichment in the sea surface microlayer and sea spray aerosols[76–78] and this in part has been found to be driven by binding interactions of these saccharides at the surface of water.[79–84] Recent work linked electrostatic binding interaction between the negative sugar moieties on alginate and divalent cations to interfacial enrichment.[81] The neutral saccharide tested did not exhibit interfacial driving forces, demonstrating that binding helps facilitate interfacial transport.[81] The Allen group studied mixed monolayers of palmitic acid and galactocerebroside which contains a galactose sugar group anchored to the air–water interface by two alkyl chains.[85] Figure 1.7a shows a schematic representation of the hydrogen bonding interactions of the galactose with the carboxylic acid on the palmitic acid headgroup. Analysis of the surface pressure–mean molecular area isotherms of these mixed monolayers showed that there is attractive interactions and higher

14

thermodynamic stability at larger surface pressures (Figure 1.7b). This suggests that as

the molecular monolayer packs tighter, it becomes more stable as the hydrogen bonding

interactions begin to dominate the monolayer surface. This study demonstrated

intermolecular binding between two tethered sugar-surfactants, but the same event could

occur between a monolayer and a soluble saccharide.

The Walker group has shown that saccharides are driven to the surface of

phospholipid monolayers through noncovalent binding interactions using vibrational sum

frequency generation spectroscopy (VSFG).[80,82,83] The molecular reason behind this

enrichment was tracked by changes in the water region (specifically the 3250 cm^{-1} mode)

upon phospholipid-sugar binding.[82] The zwitterionic phospholipid dipalmitoyl

phosphatidtylchloline (DPPC) formed an insoluble monolayer surface and the positively

charged, glucosammonium saccharide bound to the negative phosphate at the surface of

the monolayer (Figure 1.7c,d). They determined that this DPPC–glucosammonium

binding affinity was 7.95×10^3 M^{-1} using a two–layer Langmuir model.[83] Another

example of phospholipids driving interfacial ion enrichment is through metal cation

interactions to a negatively charged surfactant headgroup at the air–water interface.
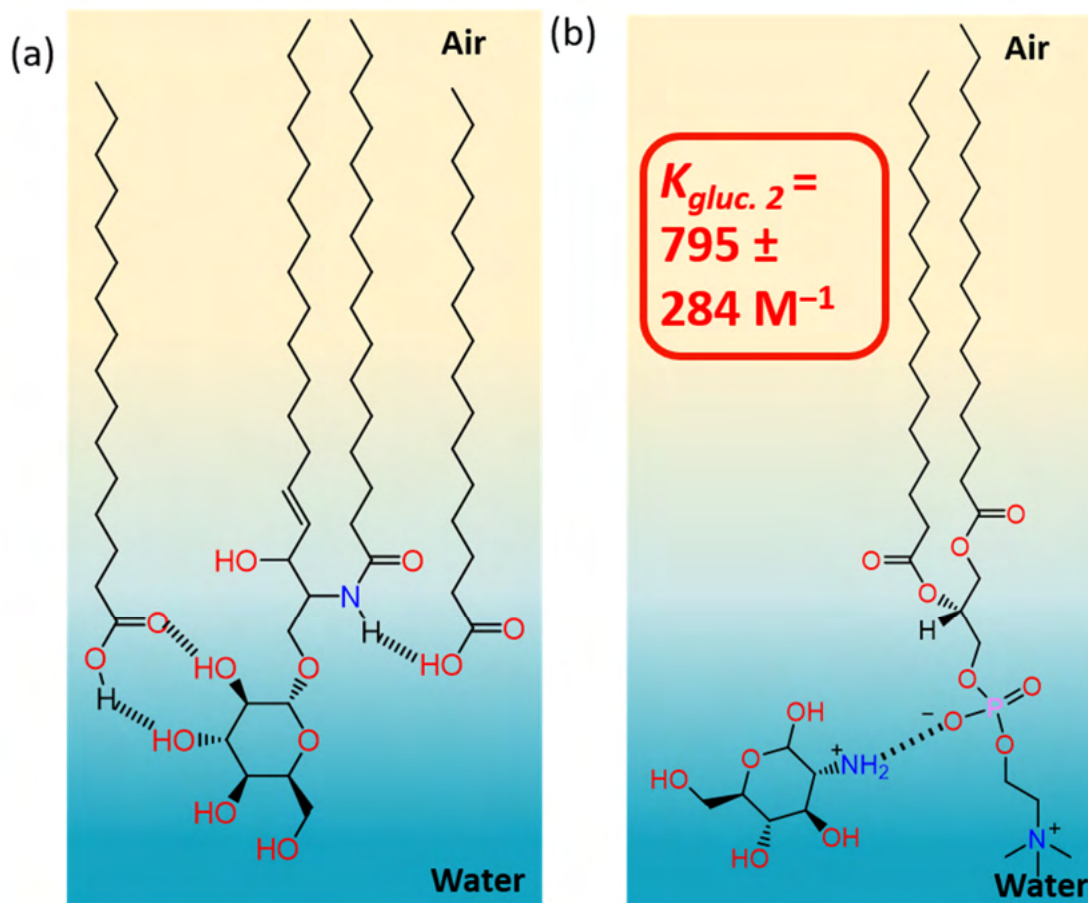
Figure 1.7 (a) Mixed monolayers of palmitic acid and galactocerebroside[85] and (b) electrostatic attraction from the negative phosphate on DPPC and the positive ammonium on the protonated glucoammonium drives this sugar molecule to the air–water interface as shown in Burrows *et al.*[83]

Previous work by the Allen group has shown that metal ions strongly interact with the negative phosphate moiety on a phospholipid headgroup.[86–91] Figure 1.8 shows an example of the phosphate systems with the phospholipid 1,2-dipalmitoyl-sn-glycero-3-phosphate. Zhang *et al.* found that the binding affinities of phosphate to a series of metal cations followed the order $Al^{3+} > Fe^{3+} > Zn^{2+} > Mg^{2+} > Ni^{2+} > Mn^{2+} \sim Ca^{2+}$.[91] They used a binding titration method as shown in Figure 1.8 where the metal of interest was titrated

beneath the monolayer and allowed to equilibrate to the surface and bind to the phosphate headgroup. By applying the Langmuir-Szyszkowski model, they quantified the surface adsorption constants as K= 700, 90, 48, 32, and 27 for Zn^{2+}, Mg^{2+}, Ni^{2+}, Mn^{2+}, and Ca^{2+} respectively.[91] Other work in the Allen group of the dipalmitoylphosphatidylcholine model system has shown that Sr^{2+} only weakly interacts but Zn^{2+} strongly interacts with the headgroup,[89] Mg^{2+} behaved similarly to monovalent cations in a 1:1 binding stoichiometry,[90] and divalent salts have a stronger binding affinity than monovalent salts to the headgroup through surface potential measurements.[88]

Figure 1.8 Modified schematic from Zhang *et al.*[91] showing the phosphate headgroup of a phospholipid monolayer interacting with metals titrated beneath the aqueous surface.

The long chain (fatty) carboxylic acids are one of the most ubiquitous Langmuir monolayer systems studied in the sea spray aerosol and oceanic communities. Fatty acids are important constituents of the organic film on sea spray aerosol surfaces and palmitic and stearic acids have been found to comprise two-thirds of the fatty acid

17

composition of sea spray aerosols.[92] The fatty carboxylate–sodium binding interaction is not only important in the atmospheric community but also has biochemical relevance as an important component of cell membranes.

Results from VSFG showed that K^+ had stronger ionic binding affinities than Na^+ to the carboxylate moiety on palmitate.[93]   A study that followed showed that Ca^{2+} have stronger binding affinities than Mg^{2+}[94] and the binding stoichiometry of this carboxylate–Ca^{2+} interaction went through a ionic bridging complex first (2 Ca^{2+} per COO^-) to a chelating bidentate complex (1 to 1) as the system reached equilibrium at low concentrations (<0.1 M). This binding stoichiometry changed to favor only a 2:1 configuration at high concentrations of calcium (>0.3 M).[95] IRRAS results of stearic acid demonstrated that Cd^{2+} and Pb^{2+} bound covalently to the carboxylate moiety whereas the Ca^{2+} interacts ionically.[96] Contact ion pairing between palmitic acid and sodium at high pH was found to stabilize the interaction and drive the carboxylate species to the interface.[97]

One interesting method to determine binding interactions between the molecular monolayer and soluble species is through equilibrium spreading pressure, also referred as equilibrium surface pressure. Equilibrium spreading pressure is a unique measurement of the true thermodynamic equilibrium between a monolayer (2D phase) and amorphous solid (3D phase) as depicted in Figure 1.9a.[98,99] This occurs when a solid surfactant is deposited onto the water surface and eventually there will be a constant surface pressure reached which is the surface pressure at equilibrium. There are also the equilibria between the monolayer and gas phase and the monolayer and liquid (bulk) phase but those are considered to be negligible for most equilibrium spreading pressure

experiments. Determining the equilibrium spreading pressure is a powerful piece of information that can give insights into binding and stability at the surface. As shown in Rudd *et al.* and Adams *et al.* equilibrium spreading pressure can be used to determine the binding interactions between a palmitate monolayer and sodium or calcium ions.[97,100] Furthermore, the palmitate calcium binding interactions were found to be more stable at low concentrations of calcium up to 1 mM concentrations. Upon exceeding 1 mM calcium, the palmitate monolayer was not thermodynamically stable and the equilibrium loss of the monolayer must also be considered at this point.[100] Current work is underway in the Allen group to utilize the thermodynamic parameters from an equilibrium spreading pressure temperature study to determine the enthalpy and entropy of binding between palmitate and sodium.
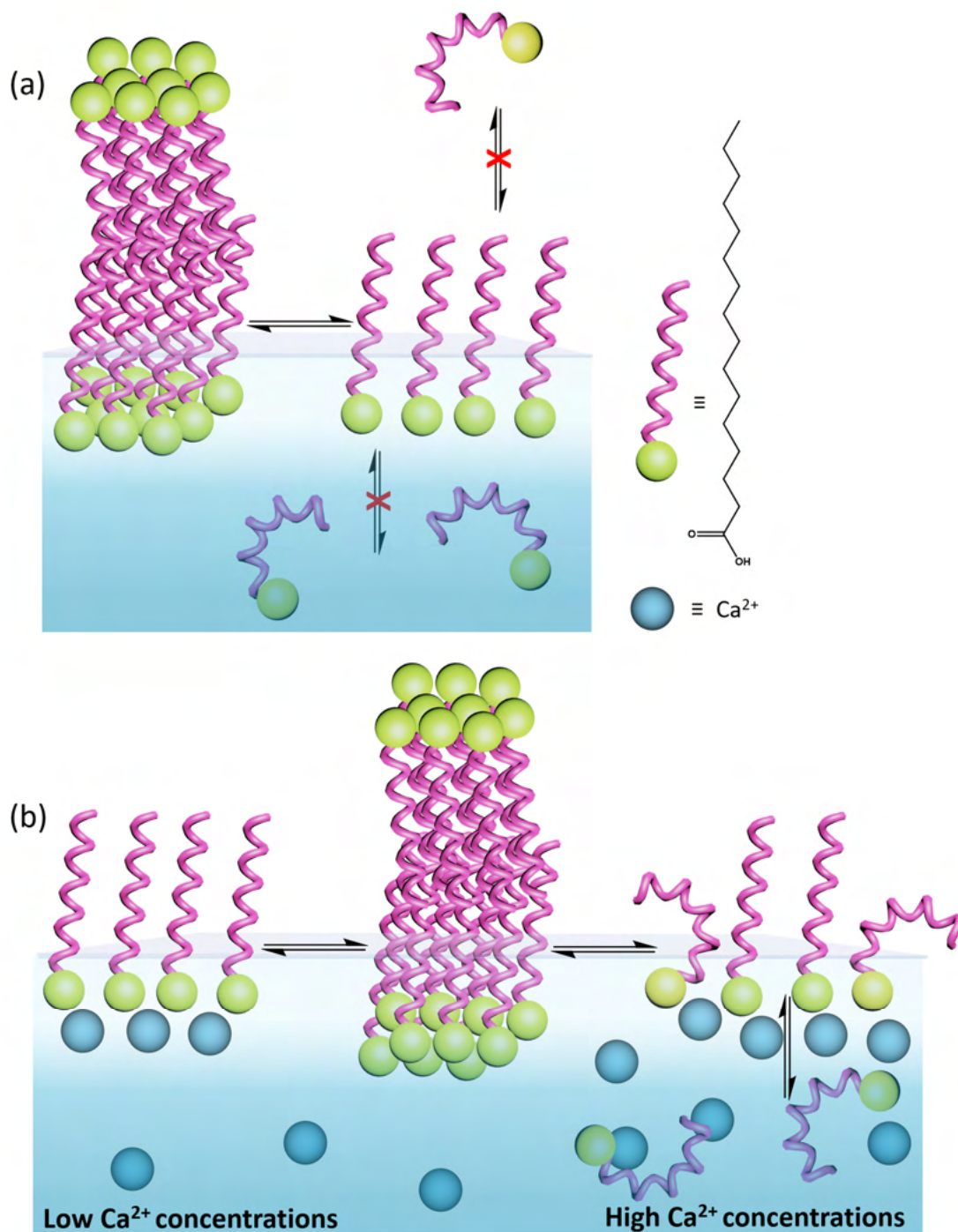
Figure 1.9 (a) Schematic representation of equilibrium spreading pressure and (b) equilibrium spreading pressure as a viable method to determine binding interactions between a monolayer of palmitic acid and calcium as shown in Rudd et al.[100]

20

Exploring the air–water interface in freshwater environmental systems is a growing field of interest. Particularly, lake spray aerosols which are aerosols produced from wave breaking processes in freshwater lake systems[101–104] will be a relevant model system to study at the aqueous interface in the future.

1.4 Biological
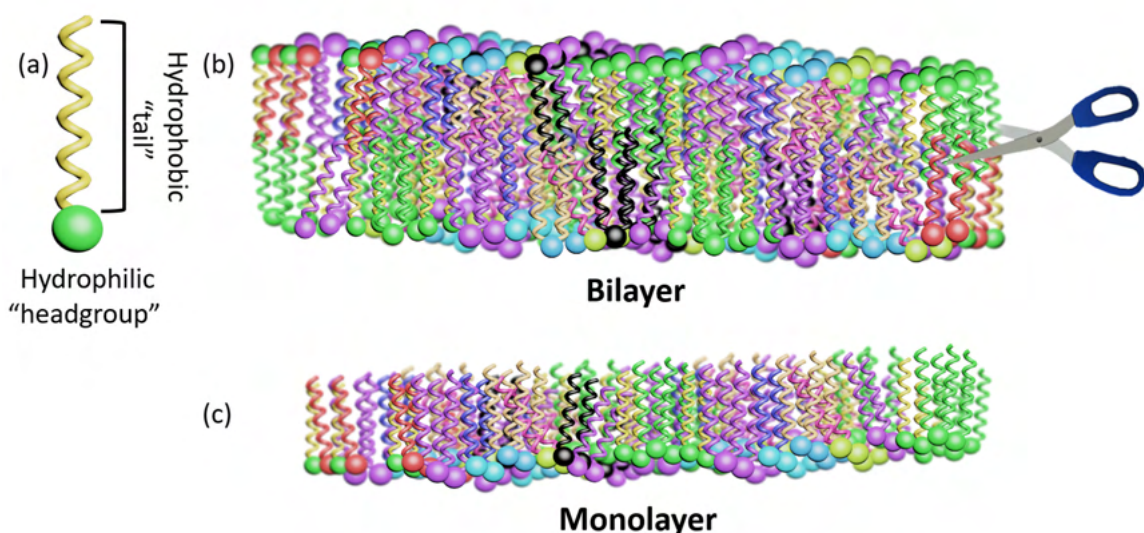
Figure 1.10 Schematic representation of the monolayer and bilayer systems.

There are numerous examples of biological systems utilizing Langmuir monolayer as a model to study binding interactions in membrane structures. The monolayer surface serves as half a bilayer structure and mimics the processes at the membrane surface thereby modeling the fundamental processes occurring in the interfacial region of a cell membrane.[105–108] Figure 1.10 shows the monolayer system where the lipids (comprised of a hydrophilic headgroup that is anchored into the water and a hydrophobic tail which is pointing away from water) can mimic the bilayer structure of a membrane. Chapter 2

explores a biologically relevant phospholipid monolayer binding to the soluble amino acid arginine. The phosphate to arginine binding affinity was quantified by surface pressure–mean molecular area and infrared reflection absorption spectroscopy and found to be enhanced at the surface of the phospholipid monolayer.[66] Various studies have explored phospholipid protein[105,109–115] and peptide[116–119] interactions as well as the constituent amino acids[66,120,121] to better understand these noncovalent interactions.

Additionally, one study explored a monolayer system of dioleylphosphatidylcholine and 1,1′,2,2′-tetraoleoylcardiolipin to study the binding interactions to methylene blue which is a cationic photosensitizer[122] (Figure 1.11). A better understanding of the binding mechanism between methylene blue and the lipids will help reveal the underlying response of methylene blue as it oxidizes cell membranes converting the reacting with the unsaturated lipids. The distance between the methylene blue and the membrane is very important as the lifetimes of the reactive oxygen species that the methylene blue produces under light radiation are short.[123,124] They found by surface pressure–mean molecular area isotherms and infrared reflection absorption spectroscopy that the methylene blue strongly interacted by electrostatic attraction to the model cell membrane. Interestingly the methylene blue affected the alkyl packing and carbonyl groups as well, which demonstrates that the methylene blue is close to the unsaturated chains in the binding arrangement. Several other studies have investigated the interactions between phospholipid monolayers and photosensitizers.[125–127]
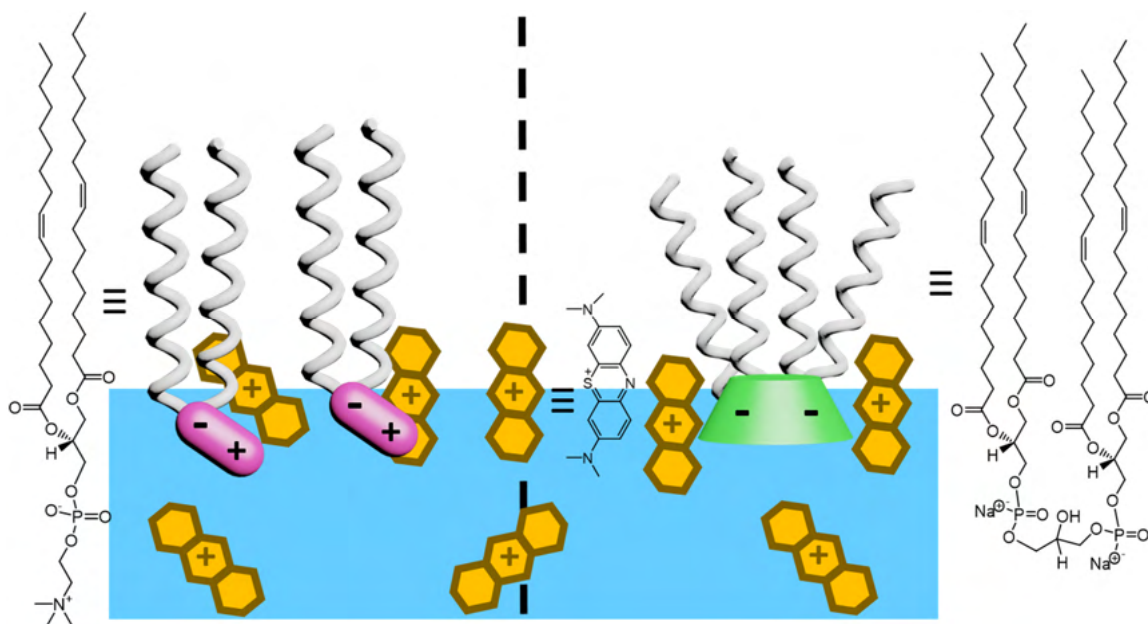
Figure 1.11 Monolayers of dioleylphosphatidylcholine and 1,1′,2,2′-tetraoleoylcardiolipin binding to cationic methylene blue at the air–water interface as shown in Schmidt *et al.*[122]

Langmuir monolayer model systems are also useful to study the interaction of drug molecules with simple phospholipid membrane systems. There are several studies modeling the interactions at the air–water interface with phospholipids and the antineoplastic drug paclitaxel also known as taxol[128–133] and the breast cancer therapy drug tamoxifen and derivatives,[134,135] and others.[136–139]The binding interactions of taxol with monolayers comprising of 1,2-dipalmitoyl-sn-glycerol-3-phosphocholine were found to be relatively weak and remained in the vicinity of the headgroup region.[131,133] A better understanding of the molecular interactions of these drugs molecules at the air–water interface will help further our biological understanding and possibly also allow for structural tuning of these molecules to better target molecular interactions.

The Cremer group has also done a lot of work studying Langmuir monolayers regarding their biological significance.[140–145] Figure 1.12a shows the interactions of

aqueous ibuprofen with the phosphatidylcholine headgroup of a 1,2-dilauroyl-sn-glycero-3-phosphocholine monolayer.[143] Interestingly, Sun *et al.* observed a multistep binding interaction where the first step is a entropically driven binding interaction and later step is an insertion into the lipophilic region. Other work by the Cremer group has looked at phospholipids binding to calcium.[140,144,145] Figure 1.12b shows the headgroup of the phosphatidylinositol which has three phosphates interacting with calcium ions. Bilkova *et al.* found that both the headgroup and carbonyl regions are binding with the calcium and this induces conformational rearrangements within the monolayer structure.[140] Work in the Allen group has also shown the importance of calcium interactions where the calcium-phosphate binding interaction results in significant dehydration of the phosphate headgroup of the phosphatidylcholine (Figure 1.12c).[86] These phospholipid model systems demonstrates that the monolayer can be a powerful tool to decipher the complex intermolecular interactions occurring in membrane bilayers.
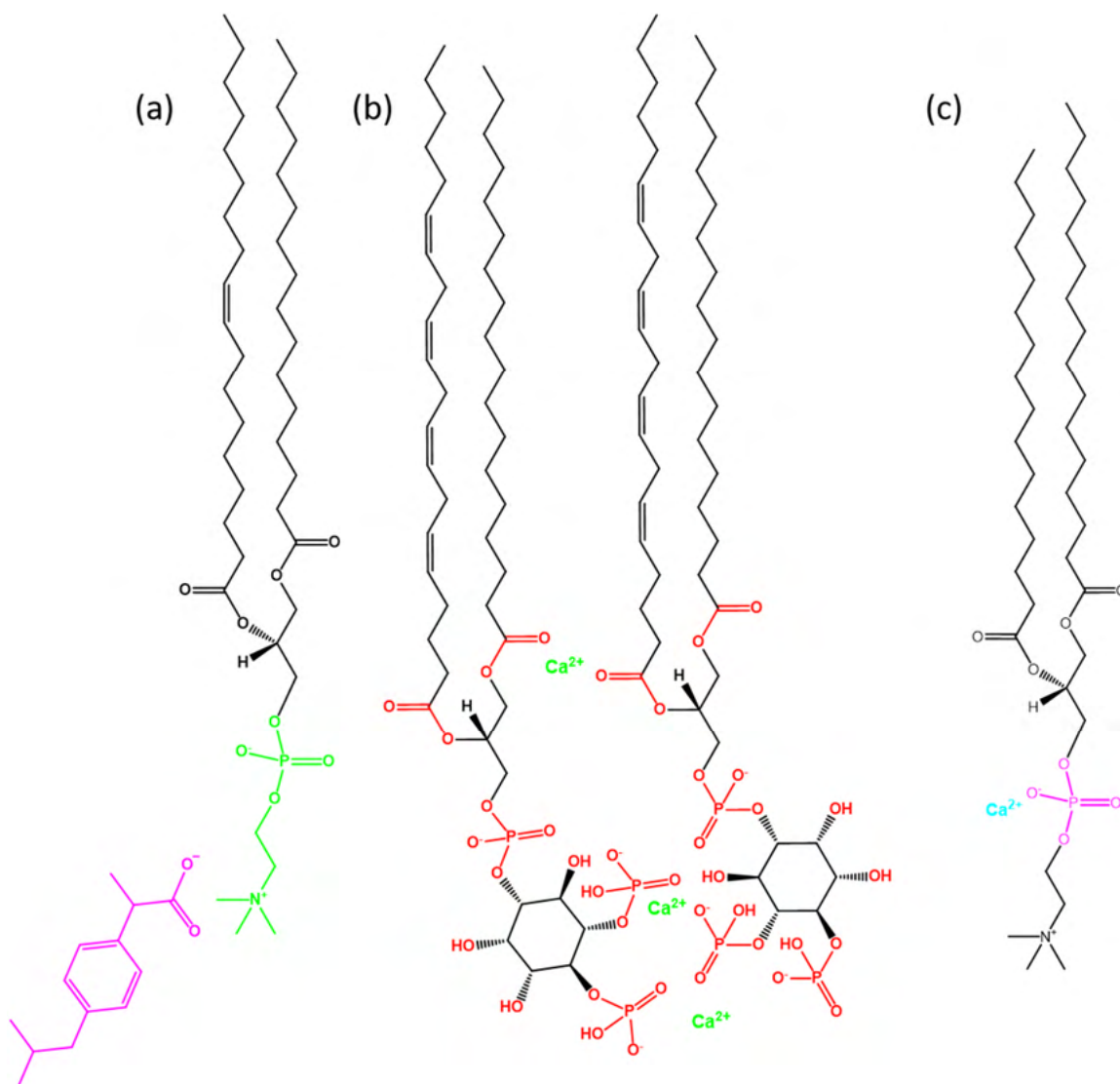
Figure 1.12 (a) Interactions of ibuprofen with the phosphatidylcholine headgroup of a 1,2-dilauroyl-sn-glycero-3-phosphocholine monolayer,[143] (b) phosphatidylinositol binding to calcium,[140] and (c) calcium binding and dehydrating the phosphatidylcholine headgroup.[86]

1.5 Conclusion and Outlook

Molecular recognition at the air–water interface is highly relevant across synthetic, environmental, and biological systems. The following chapters will explore these in more detail. The link between these distinct binding events is water and the unique

properties of this ubiquitous solvent. The field of host–guest chemistry at the aqueous

interface will continue to be an important avenue of exploration.
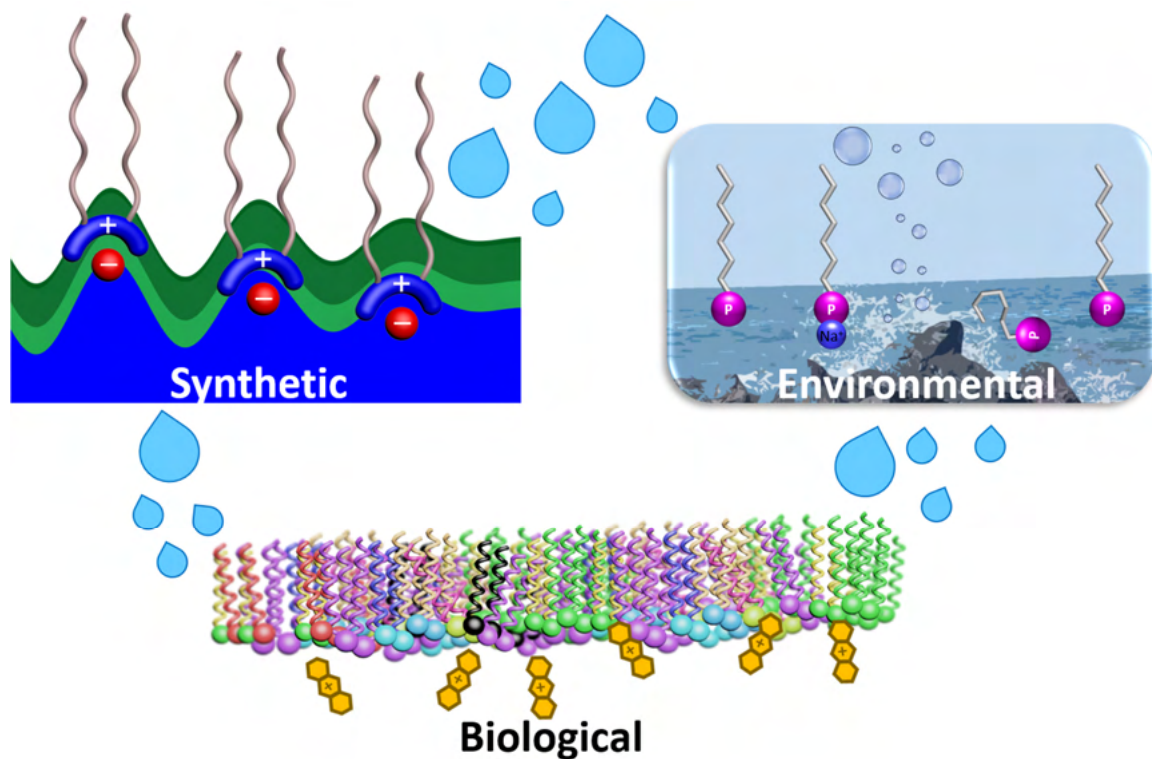
Figure 1.13 Binding at the air–water interface as explored through synthetic, environmental, and biological relevance.

Chapter 2. Guanidinium–phosphate binding enhanced at the surface of phospholipid monolayers

Abstract

There is a need to develop better receptors for use in the environmental remediation of anthropogenic aqueous phosphates. This need is in part driven by the growing world population which will require more phosphate fertilizers for use in agricultural purposes. Phosphate resources are limited and therefore we need better phosphate capture and recycling capabilities. Phosphate recognition has been mostly limited in the past to homogenous bulk studies whereas the air–water interface has been largely underexplored. The aqueous interface has some unique and beneficial properties over bulk solution such as a diminishing dielectric constant and the preorganization of Langmuir monolayers. We used a model system of phosphate binding to an amino acid, arginine using a Langmuir monolayer comprising of the phospholipid 1,2-dipalmitoyl-sn-glycero-3-phosphatidic acid as the phosphate source. The use of arginine allowed us to evaluate the guanidinium moiety binding to phosphate as a model system for the phosphate–guanidinium surface binding interactions. The binding affinity was quantified using

surface pressure isotherms and infrared reflection absorption spectroscopy by a Langmuir–type fitting. The molecular binding interactions were quantified in situ and the apparent surface binding affinity of the phospholipid–arginine complex was shown to be greater than 10^3 M^{-1}. The binding constant determined in bulk solution by NMR was on the order of 0.1 M^{-1}. Our study reveals that there is a greater than 10,000 fold increase in the binding affinity from bulk solution to the interface for the phosphate–guanidinium interaction. This remarkable increase in binding affinity demonstrates that the air–water interface provides a unique microenvironment that could be employed in phosphate remediation technologies to better remove phosphate from agricultural runoff.
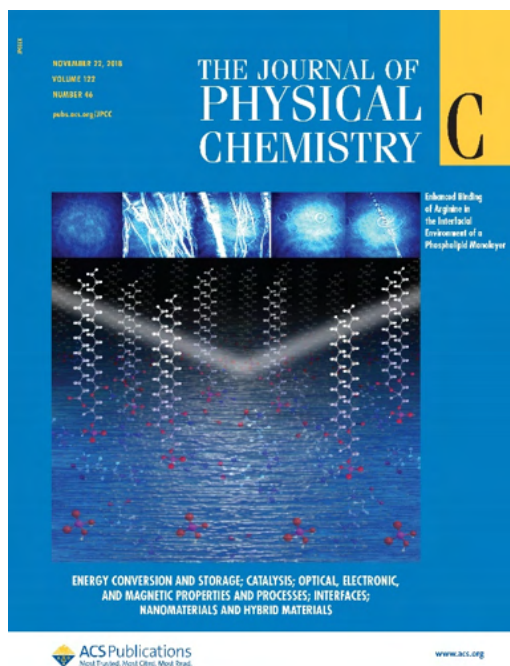
Figure 2.1 Cover image from the Journal of Physical Chemistry C with a representation of a phospholipid interacting with arginine at the air–water interface.

2.1 Introduction

Phosphorus is an integral component in the food-energy-water nexus.[146] Loss of phosphates in runoff to natural waters represents a net loss in the phosphate cycle and creates harmful environmental effects.[147–149] Algal blooms driven by the influx of phosphate impact aquatic life and fresh water supplies. The development of efficient sequestration materials for phosphate capture represents a possible solution to this problem. The rational design of phosphate receptors has been frequently studied in bulk solution.[11,150–153] The field of supramolecular host–guest chemistries at the air–water interface however is largely unexplored and presents some possible advantages over traditional host–guest chemistry in bulk solution. The air–water interface has a lower dielectric constant ($\varepsilon < 20$) than bulk water ($\varepsilon = 80$).[28,36] The lower dielectric constant at the surface of water helps to preserve strong electrostatic interactions. A study in bulk solution found that electrostatics only dominate binding stability in low dielectric solvents and in the gas phase.[4] Additionally, monolayers have the added advantage of preorganization.[9] The headgroups (i.e. binding sites) of the monolayer are compact and available for binding while the hydrophobic alkyl chains induce this organization by directing the headgroups into the aqueous phase. In order to understand phosphate recognition at the air–water interface, we chose the lipid 1,2-dipalmitoyl-snglycero-3-phosphatidic acid (DPPA, Figure 2.1a) and amino acid arginine (Figure 2.1b). The interaction between phosphate and amino acids (arginine) also has significance in biological[154–156] and atmospheric applications.[157,158]

DPPA molecules have a phosphate headgroup and two long C_{16} acyl chains that facilitate monolayer formation at the air–water interface. Arginine is a soluble amino acid with guanidinium, ammonium, and carboxylate moieties is an informative guest molecule to study the phosphate-guanidinium interaction. DPPA and arginine both possess vibrational modes that are easily accessible and informative for binding interactions. The pK_a of the guanidinium moiety is ~13.6[159] which means it will retain its positive charge, allowing for both electrostatic and hydrogen bonding non-covalent interactions.

Molecular recognition at the air–water interface is largely unexplored and remains an open area of investigation. At the aqueous interface, electrical double layers emerge, the structure of water is altered, and different driving forces enrich or deplete solutes to the interface relative to bulk.[160–164] Furthermore, the correlation between binding affinities in bulk solution to the nominally two dimensional (2D) affinities needs to be addressed in future work for a deeper understanding of recognition at the air–water interface.[5,165] Pioneering work by Kunitake and co-workers showed that binding at the air–water interface greatly enhanced affinities relative to bulk solution.[36,43,166–169] However, these binding affinities were determined using ex situ methods after transferring the Langmuir-Blodgett films of the monolayer bound to phosphate and taking X-ray photoelectron, UV vis spectroscopy, or other techniques.[43,167,168] It is possible that these ex situ analyses did not preserve the binding event, and therefore the results and methods presented here are all in situ. Herein, we test Kunitake's hypothesis of enhanced affinity at the interface with a system of inverted charge (i.e. negative phosphate monolayers with a positively charged soluble guanidinium species). We used surface pressure-area isotherms and infrared reflection absorption spectroscopy (IRRAS) to quantitatively determine binding

affinities. The phosphate-guanidinium complex at the air–water interface was 10,000 fold greater in binding affinity than compared to analogous bulk solution. This remarkable enhancement of the binding at the air–water interface supports our hypothesis that the interface has unique advantages over recognition in bulk solution and provides new avenues for exploration.
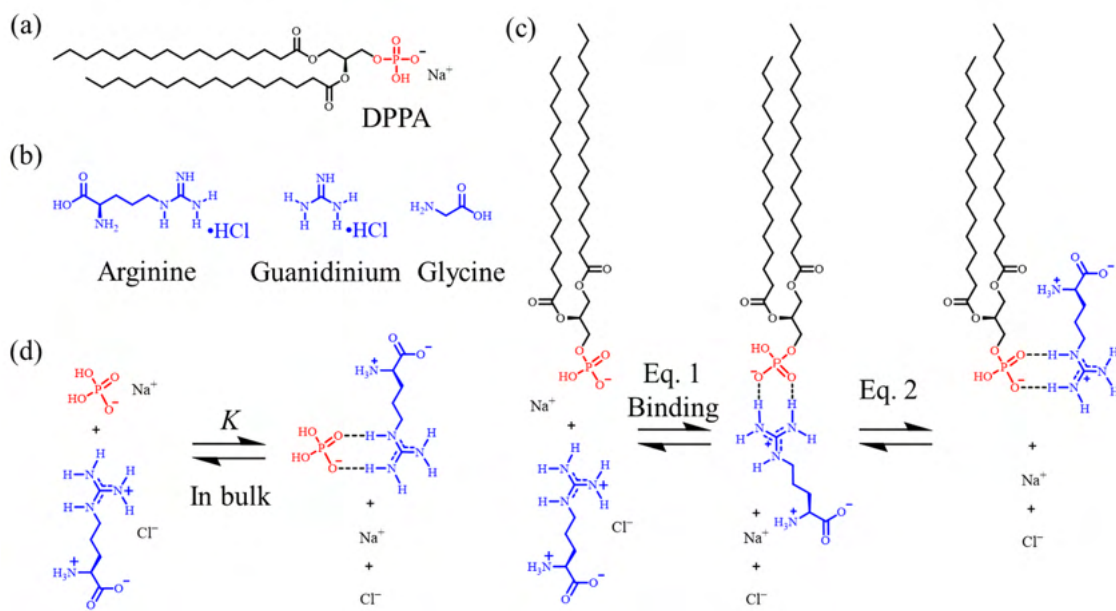
Figure 2.2 Structures of the materials: (a) 1,2-dipalmitoyl-sn-glycero-3-phosphatidic acid (DPPA), (b) L-arginine monohydrochloride, guanidine hydrochloride, and glycine. Proposed binding motif of the guanidinium-phosphate interaction with (c) DPPA at the air–water interface and (d) sodium phosphate in bulk water.

2.2 Materials and Methods

2.2.1   Materials

All materials were purchased in high purity and used without further purification. 1,2-dipalmitoyl-*sn*-glycero-3-phosphate sodium salt (DPPA) (≥99%, Sigma) was dissolved in a mixture of chloroform (HPLC grade, Fisher Scientific) to methanol (HPLC grade, Fisher Scientific) (4:1 v/v). The hydrochloric acid salt of arginine and guanidine were purchased to avoid pH adjustments since the guanidine moiety acts as a strong base. L-Arginine monohydrochloride (≥99.5%, Sigma), glycine (≥99.0%, Sigma), and guanidine hydrochloride (≥99%, Sigma) were dissolved in ultrapure water with a resistivity of 18.2 MΩ cm from a Barnstead Nanopure Filtration System (model D4741, Barnstead-Thermolyne Corporation, Dubuque, IA). The pH of the solutions was measured on an Accumet pH meter (Acuumet AB15, Fisher Scientific). The measured pH of the highest concentration tested represents the maximum deviation from the pH of pure water and is as follows: 6.4 for arginine, 6.4 for glycine, and 6.5 for guanidinium. At these pH values, the guanidinium moieties are positively charged and the amino group on the amino acids for glycine and arginine is protonation as an ammonium. For control experiments to test to see if trace metals affect the interpretation of the results, ethylenediaminetetraacetic acid (EDTA) (99.995%, Sigma) was used. Deuterium oxide (D_2O) (99%, Sigma) was purchased for select IRRAS experiments.

2.2.2 Instrumentation

2.2.2.1 Surface Pressure-Area Isotherms (Π-A)

Surface pressure (Π) – mean molecular area (A) isotherms were taken on a custom-built Teflon Langmuir trough (144.5 cm^2) with movable Delrin barriers control with KSV software (KSV NIMA, Finland). The Wilhelmy plate method was used by custom cut filter paper plates (Ashless grade filter paper, Whatman). The Hamilton syringe method using a microsyringe was used to deposit the Langmuir monolayer. After 10 minutes to allow for solvent evaporation, the Delrin barriers compressed at a constant rate of 5 mm/min per barrier and for constant Π experiments, once the desired Π was reached, the barriers maintained the Π by oscillation at 1 mm/min per barrier until the completion of the experiment. A schematic representation of the Π -A isotherm experiment is shown in Figure 2.3. The liftoff point of the DPPA isotherm was set to 47.5 Å^2/molecule. All experiments were run at 21.8 °C ± 0.7 °C and relative humidity 31% ±7%.
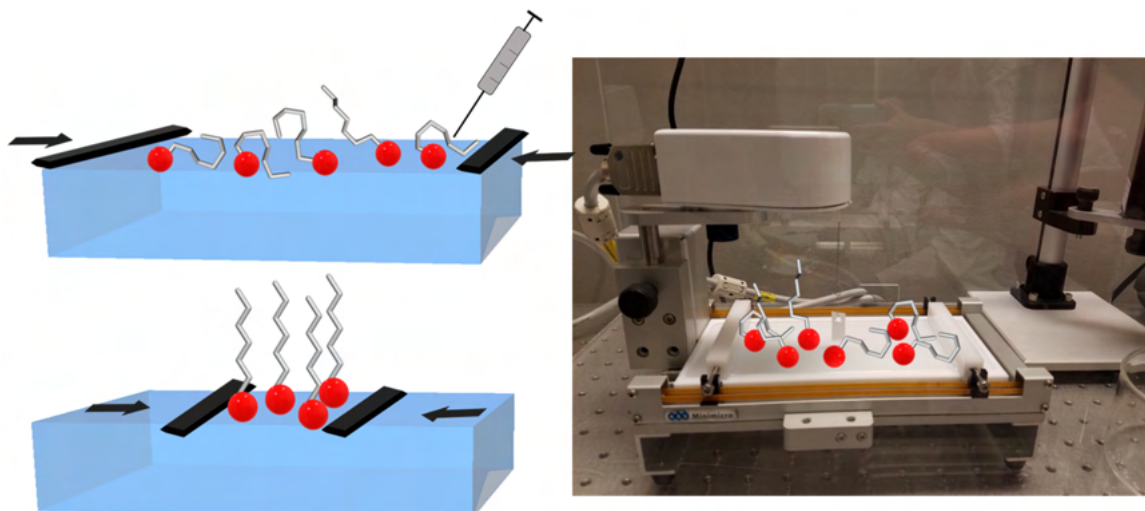
Figure 2.3 Schematic representation of spreading a monolayer and the compression of the monolayer during the Π-A isotherm.

2.2.2.2 Infrared Reflection-Absorption Spectroscopy (IRRAS)

A modified Pekin Elmer Fourier transform spectrometer (Spectrum 100, PerkinElmer) was used for infrared reflection-absorption spectroscopy (IRRAS) with a liquid nitrogen-cooled HgCdTe (MCT) detector. The Langmuir trough setup described above was placed inside the spectrometer with two gold plated mirrors that directed the infrared beam to collect the reflectivity off the monolayer surface at an incidence angle of 46 °. The spectra shown here are the reflectance-absorbance (RA) which is:

$$RA = -\log (R_m/R_0)$$

Each spectrum was recorded as a collection of 300 scans using unpolarized light in single beam mode. The data was processed with Origin (OriginLab 9). Because of the slanted baseline of the spectra, each spectrum was background subtracted by fitting a line across the region 1215-1134 cm^{-1}. Each spectrum shown here is also the result of averaging three independently collected spectra.

2.2.2.3 Brewster Angle Microscopy (BAM)

The theory of Brewster angle microscopy (BAM) is described in more detail in the literature.[170,171] A custom-built BAM was used for these imaging experiments (Figure 2.4). A 1.5 mW He-Ne laser source (Research Electro-Optics, Boulder, CO) emits linearly p-polarized light at 543 nm. This beam goes through a half-waveplate (Ekspla, Lithuania) and Glan polarizer to both attenuate and purify the p-polarized beam, respectively. The beam then reflects off the surface at the Brewster angle ($\sim 53°$) with a neutral density filter in the subphase to reduce the amount of scattering hitting going through the detection optics. The reflected beam goes through an objective lens (10X infinity corrected super long working distance) (CF160 TU Plan EPU, Nikon Instruments, Melville, NY) and a tube lens (MXA22018, Nikon Instruments, focal length 200 mm) to magnify and focus the beam into the detector. The camera is a back illuminated EM-CCD camera (iXon, DV887-BV, Andor Technology, Concord, MA) with 512 X 512 active pixels and each pixel is 16 µm X 16 µm. Each image was cropped in ImageJ to show the most focused region of the image.
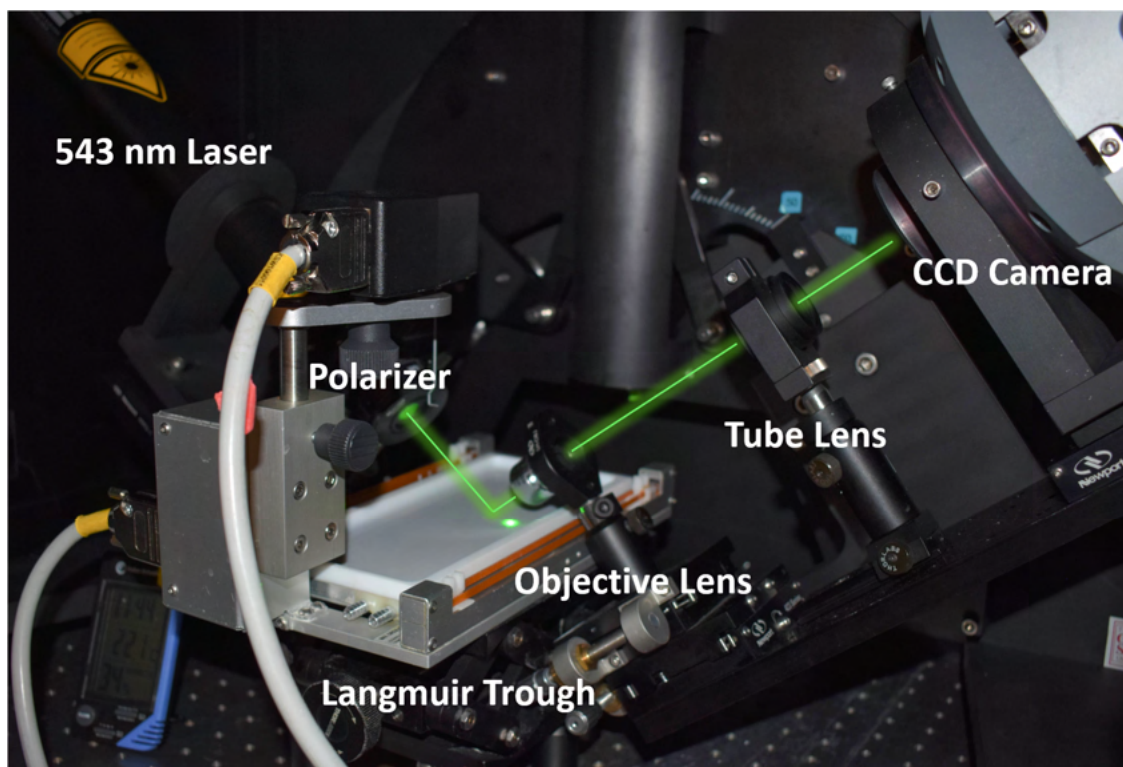
Figure 2.4 Brewster angle microscopy microscope setup.

2.3 Results and Discussion

2.3.1 Binding interactions of DPPA with arginine and guanidinium confirmed by Π-A isotherms and IRRAS

We sought to quantitatively interpret the binding of molecular monolayers composed of DPPA to arginine, glycine, and guanidinium in the aqueous subphase. Π-A isotherms and IRRAS were found to be effective means to determine this binding interaction in situ and gave a positive binding response for the arginine and guanidinium subphases. Figure 2.5a shows the phases of the Π-A isotherms of DPPA which are shown on the plot and read from left to right. These are the gaseous-liquid expanded region where the molecules are the most spread apart from one another, the tilted liquid

condensed, the untilted liquid condensed, and finally the collapse where the molecules are forming 3D structures and aggregates. Figure 2.5b shows a mean molecular expansion (MME) with increasing amounts of arginine (0.001 – 20 mM) in the subphase. This expansion is attributed to arginine molecules from the bulk subphase interacting with the molecular monolayer composed of DPPA molecules. Furthermore, the phase transitions of the DPPA isotherm change with arginine in the subphase. The untilied liquid condensed phase that is present in the water trial and lower arginine concentrations trials is absent from the trails at high concentrations of arginine. This means that the DPPA molecules are unable to form as close interactions with each other in the monolayer in this highly condensed region of the isotherm. Both the MME and change in phase transition strongly suggest that the DPPA is binding to arginine molecules.

Figure 2.5c shows the Π-A isotherms of DPPA with increasing glycine in the subphase. Glycine was chosen as a simple amino acid to differentiate between the ammonium moiety of the amino acid backbone and the guanidinium moiety on the side chain of arginine. Since glycine is one of the simplest amino acids with just a hydrogen as the side chain moiety, it serves to deconvolute the ammonium and guanidinium interactions since they both could possibly be interacting with the negative phosphate headgroup of DPPA. As seen in these control experiments, the DPPA Π-A isotherms do not show a significant change upon glycine addition. There is however a very small expansion of 0.43 Å^2 (taken at 10 mN/m) at 100 mM glycine. At this high concentration of glycine, we attribute this expansion to the ammonium binding to the phosphate headgroup since the ammonium also serves as a possibility hydrogen bonding donor. The results from these control experiments suggest that the guanidinium functional group

is mainly responsible for the binding interaction between DPPA and arginine. The MME is also observed with 5 mM guanidinium in the subphase in Figure 2.5d which further supports our hypothesis. Another reason why the glycine might not be interacting with the DPPA molecules is because of the negative charge on the carboxylate moiety which is adjacent to the ammonium. The proximity of the carboxylate to the ammonium on the free amino acid provides the ability for the ammonium to form stabilizing hydrogen bonding to the carboxylate. Since this intramolecular interaction likely outweighs any intermolecular interactions, it follows that the glycine is not intermolecularly interacting with DPPA.
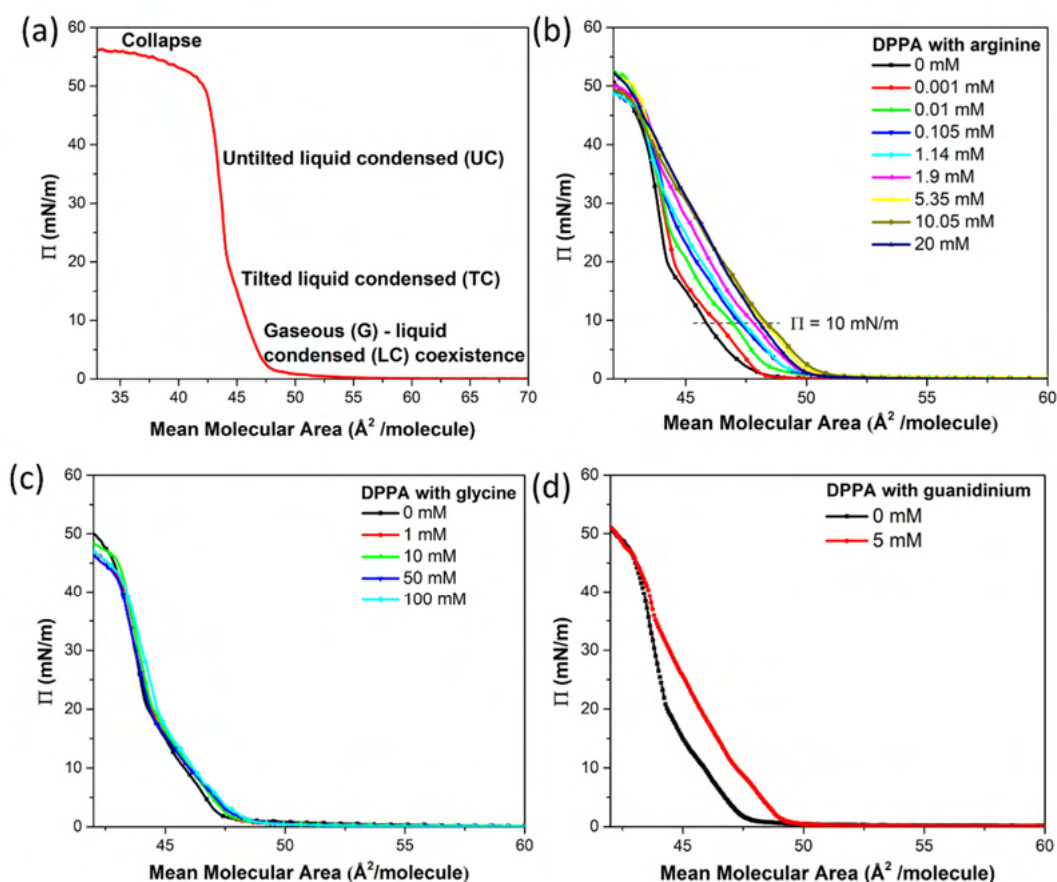
Figure 2.5 Π-A isotherms of DPPA on: (a) water showing the phases of the monolayer, (b) arginine showing a large monolayer expansion, (c) glycine showing a minimal change, and (d) guanidinium showing a monolayer expansion.

The Π-A isotherms provided strong evidence that DPPA is interacting with arginine. The expansion in the monolayer and changes in the phase behavior as indicated above are useful measurements to elucidate interactions. Another way to analyze this information is to plot the compressibility modulus which is a measure of the monolayer fluidity. The compressibility modulus is given as $C_s^{-1} = -A_\Pi(\partial\Pi/\partial A_\Pi)_T$ where the A_Π is the mean molecular area at each corresponding Π. The values from the compressibility modulus give a sense of the rigidity of the monolayer, where higher values correspond to

a more rigid monolayer. In Figure 2.6, the compressibility modulus was plotted for

DPPA on water, a low concentration of arginine, and a high concentration of arginine to

compare the extremes of the isotherms. Data shown here is the result of averaging at

least three spectra, and the shaded region of the plot is one standard deviation. As can be

seen by the change in the compressibility around 43.5 Å^2, the DPPA monolayer becomes

less rigid with the addition of arginine in the subphase. This agrees well with the

interpretation of the isotherms for which the untitled condensed phase was absent at high

arginine concentrations. These results suggest that the binding interactions between

arginine and DPPA hinders the available space to form the highly-compacted, untilted

condensed phase. Therefore, the results from the compressibility modulus indicate the

monolayer becomes more fluid with arginine than in the absence of arginine.
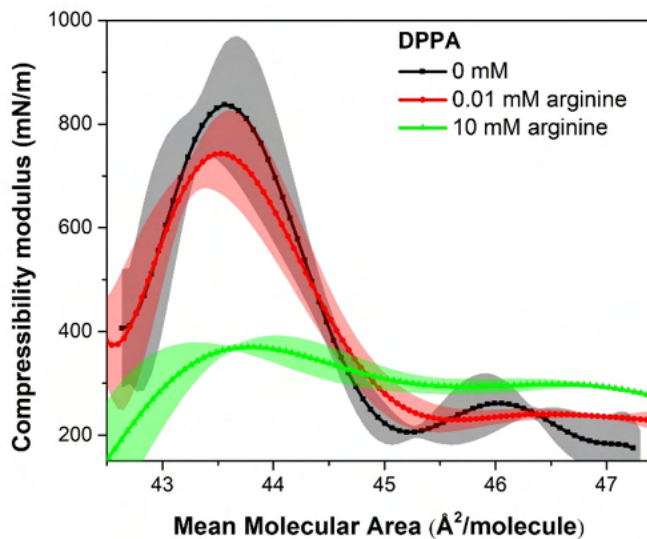
Figure 2.6 Compressibility modulus of the DPPA monolayer at a high and low extremes
of arginine concentrations. The shade region represents one standard deviation above and
below the mean.

To explore the DPPA-arginine interaction further, we used interface sensitive IRRAS measurements. The IRRAS spectra of DPPA in Figure 2.7 shows the asymmetric PO_2^- stretch at 1167 cm^{-1} which has shown to be sensitive to hydration and binding. [86,172–174] We exploit this phosphate stretch of DPPA to determine whether the phosphate headgroup is interacting with arginine, glycine, or guanidinium. Figure 2.7a shows the phosphate peak of DPPA with increasing concentrations of arginine. This mode changes in both intensity and broadness, which supports an DPPA-arginine binding interaction. Figure 2.7c shows a similar result with DPPA and guanidinium which suggests that the guanidinium moiety of arginine is contributing to this binding interaction. The spectra of DPPA with glycine do not change which demonstrates that the ammonium functional group is not acting as the binding unit for this interaction. There is a minimal change in the phosphate peak at 100 mM for glycine (as also shown in the Π-A isotherms) which suggests at this concentration, glycine is interacting with the phosphate headgroup. However, this is a concentration 10,000 times less than the comparable spectral change with the DPPA-arginine interactions.
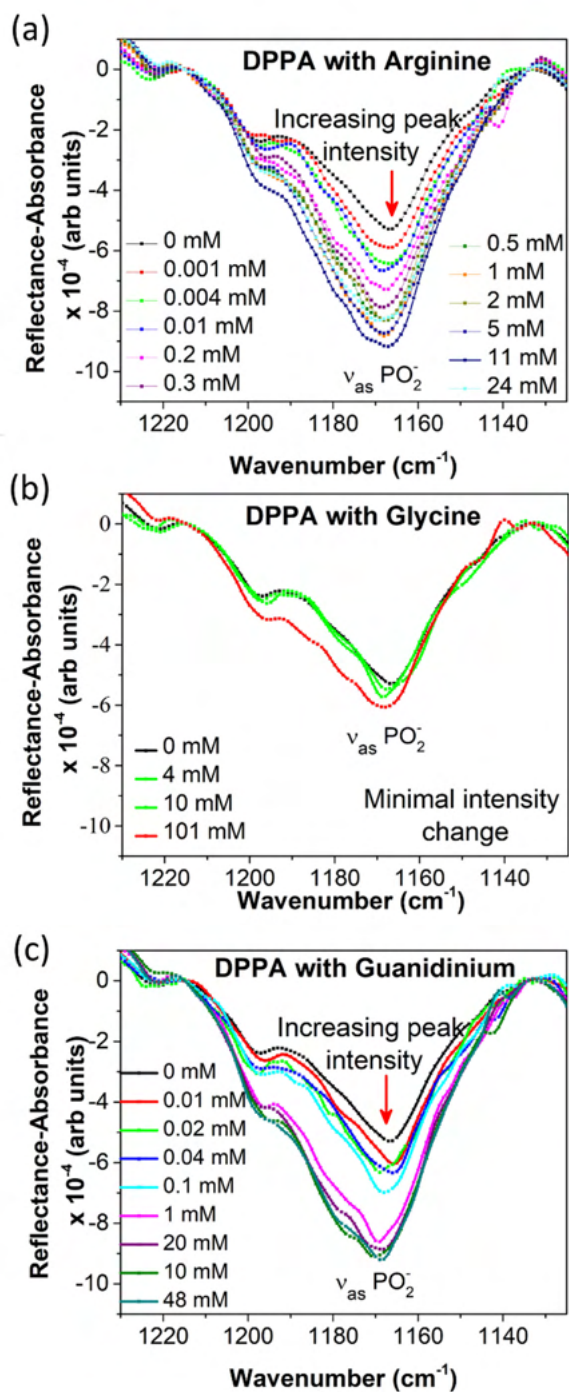
Figure 2.7 IRRAS spectra of DPPA on: (a) arginine, (b) glycine, and (c) guanidinium with increasing concentrations. The v_{as} PO2$^-$ of DPPA showed a very similar increase in intensity with both arginine and guanidinium chloride in the subphase.

2.3.2   Quantifying surface binding affinity of the DPPA-arginine interaction

With the knowledge that DPPA is interaction with the guanidinium moiety of arginine, we wanted to quantify this binding affinity. The MME from the Π-A isotherms (taken at a Π of 10 mN/m) and the peak intensity from the asymmetric phosphate mode of the IRRAS spectra were taken and plotted as a function of arginine concentration. These results were fit to a generalized Langmuir model with the assumption that the binding is a 1:1 equivalence of DPPA to arginine.

$$I = I_{max} \frac{[Arginine]}{K + [Arginine]}$$

In this equation, I is the intensity of the ν_{as} PO_2^- mode of DPPA or the MME of DPPA at 10 mN/m, I_{max} is the maximum intensity recorded for these methods, *[Arginine]* is the bulk concentration of arginine, and K is the apparent equilibrium dissociation constant.
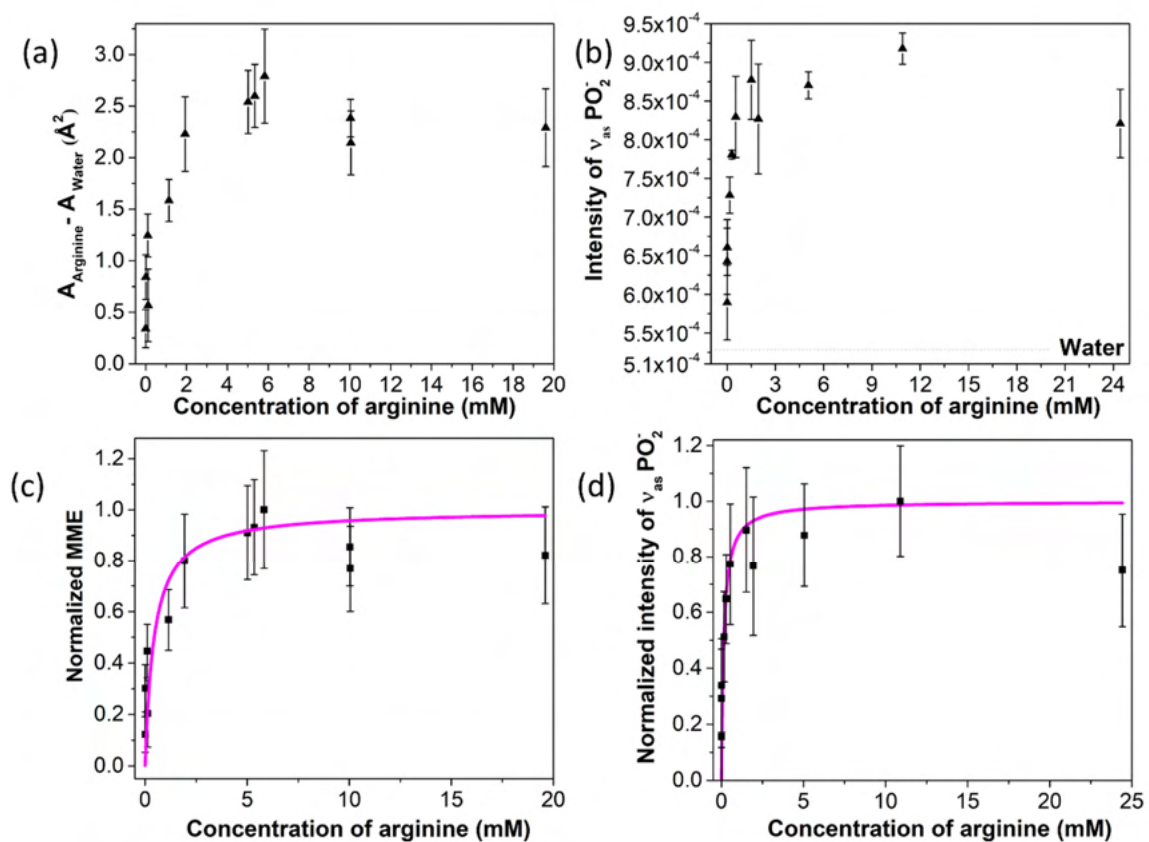
Figure 2.8 Plots showing the (a) mean molecular expansion (MME) and (b) ν_{as} PO$_2^-$ intensity as a function of arginine concentration. The normalized versions of these plots are shown in (c) and (d), respectively.

Figure 2.8a,b shows the plots of MME and ν_{as} PO$_2^-$ intensity as a function of arginine concentration, respectively. Figure 2.8c,d shows the normalized plots with the highest intensity of the plot corresponding to "1" and "0" is the intensity of DPPA on water. Based on these fitting results, the binding affinity of DPPA to arginine is 2.3 (0.9) x 10^3 M^{-1} for the Π-A isotherms and 6.8 (2.8) x 10^3 M^{-1} for IRRAS. This binding affinity is very large as compared to the analogous bulk binding affinity with sodium phosphate monobasic and arginine by ^{1}H NMR titrations. Neal *et.al* has more experimental details

44

of this NMR study but the main result is that the binding affinity is on the order of 0.1 M^{-1} in bulk solution.[66] The interface provides a remarkable advantage over aqueous bulk binding. Comparing the affinities from bulk to the air–water interface, there is a 10,000 times enhancement in the binding affinity at the interface. Table 2.1 summarize the binding affinities using the three different methods. This nicely demonstrates that the interface can provide a unique microenvironment to enhance affinities.

Method	Binding affinity (M^{-1})
Π-A isotherms (surface)	2.3 (0.9) × 10^3
IRRAS (surface)	6.8 (2.8) × 10^3
^{1}H NMR (bulk)	0.1

Table 2.1 Binding affinities of the phosphate-arginine interaction determined using Π-A isotherms and IRRAS as *in-situ* interfacial techniques and NMR for bulk solution.

2.3.3   Monolayer Morphology by BAM

DPPA-arginine binding properties were further studied by use of BAM in the collapse phase of the monolayers. The collapse mechanisms are characterized by monolayer loss mechanism (i.e. the monolayer forms aggregate structures or there is loss into the bulk solution). Figure 2.9 shows BAM images of the collapse phase of DPPA with concentrations of arginine (0 mM, 0.01 mM, 0.1 mM) in the top row which represents the low concentrations tested and (1 mM, 5 mM, 10 mM) in the bottom row which is the upper range of concentrations tested. The scale bar in these images is 100 μm. The morphology of the DPPA monolayers in the collapse phase is especially

interesting because it is different at low and high concentrations of arginine. The top images which show the DPPA on low concentrations of arginine reveals a striated crystalline morphology while the lower images at high arginine concentrations show the appearance of a homogeneous sheet. The difference in the images of the collapse phase indicates that there is change in the binding motif depending on the concentration of arginine. As already shown in the binding curves for DPPA-arginine with Π-A isotherms and IRRAS, there is a noticeable saturation point which also corresponds well to this change in morphology observed in the BAM images.

It is important to note that the morphology does not change leading up to the collapse phase. Figure 2.10 shows the morphology of the monolayer in the condensed region leading up to collapse on water, 0.1 mM arginine, and 10 mM arginine, respectively (a,b,c).
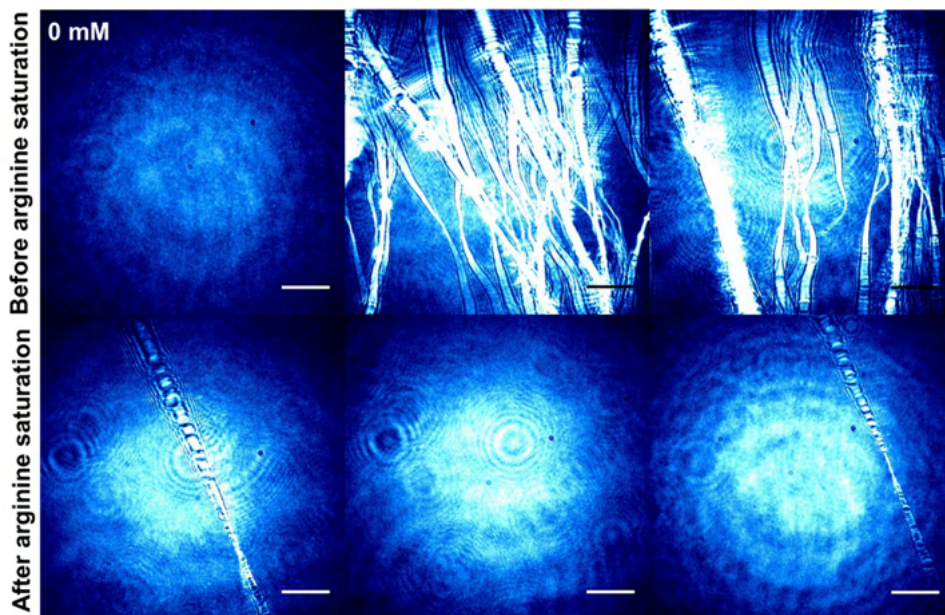
Figure 2.9 BAM images of DPPA in the collapse phase. The top row shows DPPA at the collapse on water, 0.01 mM, and 0.1 mM arginine and the bottom row shows DPPA on higher concentrations of arginine 1 mM, 5 mM, and 10 mM. The scale bar is 100 μm.
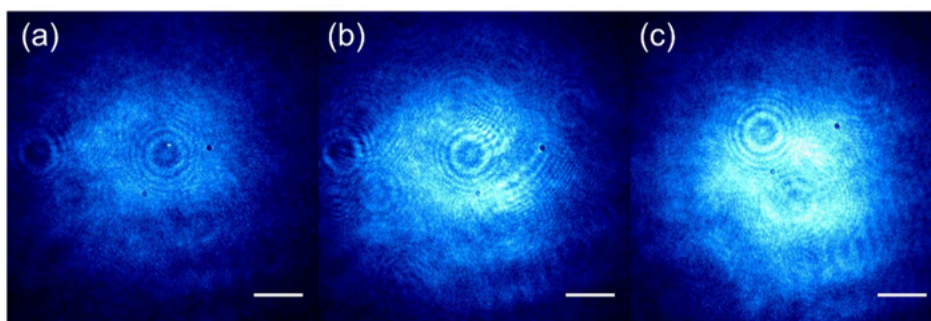
Figure 2.10 BAM images in the tilted condensed phase on (a) water, (b) 0.1 mM arginine, and (c) 10 mM arginine. Scale bar is 100 μm.

2.3.4   Possibility of the carbonyl of DPPA binding to the ammonium on arginine

It is clear from the work shown about that the guanidinium moiety of arginine is responsible for the binding to the phosphate headgroup of DPPA. It is also worth noting that the DPPA molecules have two ester backbones which are electron rich. To elucidate the binding of the carbonyl of DPPA to arginine, IRRAS spectra was taking using D_2O to avoid the large bending mode from H_2O from obscuring the spectra. The spectra shown in Figure 2.11 are of the carbonyl band of DPPA at approximately 46 $Å^2$ per molecule in the TC region of DPPA (spectra were taken in petri dishes instead of the Langmuir trough). The carbonyl band at 1738 cm^{-1} and 1720 cm^{-1} has been shown in the literature to correspond to the hydrated and more dehydrated carbonyl stretch.[175,176] Upon arginine addition there is a change in the carbonyl environment with a decrease in the 1720 cm^{-1} stretch (Figure 2.11). We attribute that the arginine molecules are interacting with the DPPA carbonyl group possibility through hydrogen bonding with the ammonium headgroup. Furthermore, there are additional peaks in the IRRAS spectra at 1605 cm^{-1} and 1585 cm^{-1} which we assign to the v (C-N) modes of arginine with possible

contribution from the v (COO⁻). [177–179] The presence of these peaks strongly suggests that

the arginine molecules are approaching the surface and binding to the DPPA molecules.

The nature of the IRRAS equation is that the reflectance-absorbance includes the arginine

subphase in both the numerator and denominator of the equation, especially removing the

vibrational components. These additional IRRAS experiments support our conclusions

that arginine is binding to DPPA at the interface and also provide support that the binding

motif might be a chelation instead of monodentate.
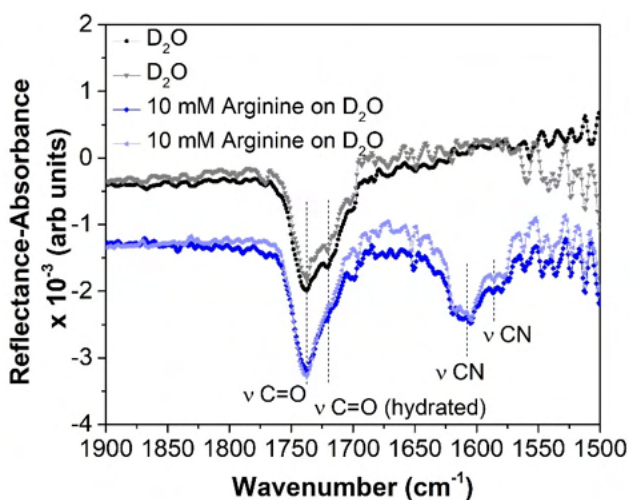
Figure 2.11 BAM images in the tilted condensed phase on (a) water, (b) 0.1 mM arginine, and (c) 10 mM arginine. Scale bar is 100 μm.

2.3.5 Control experiments with the metal chelating agent ethylenediamine tetraacetic acid (EDTA)

The air–water interface is a very sensitive microenvironment. To validate the

integrity of our experiments and to rule out any possibility of trace contaminants

affecting our results, we conducted a series of control experiments with ethylenediamine

tetraacetic acid (EDTA). EDTA is a chelating agent with four possibility binding sites

with carboxylic acids moieties. These carboxylic acid moieties also make this molecule a

strong acid and only small amounts can be used without acidifying the solution and

possibly changing the binding affinity by changing the speciation of arginine. We

therefore opted to use μM concentrations and considering the trace contaminates are

likely in the nM range, this seemed like an acceptable concentration to try. Shown in

Figures 2.12 and 2.13, the interpretation of the results from these experiments is not

affected with or without EDTA. This helps validate our data and supports the claim that

trace level contaminates are not affecting our results.
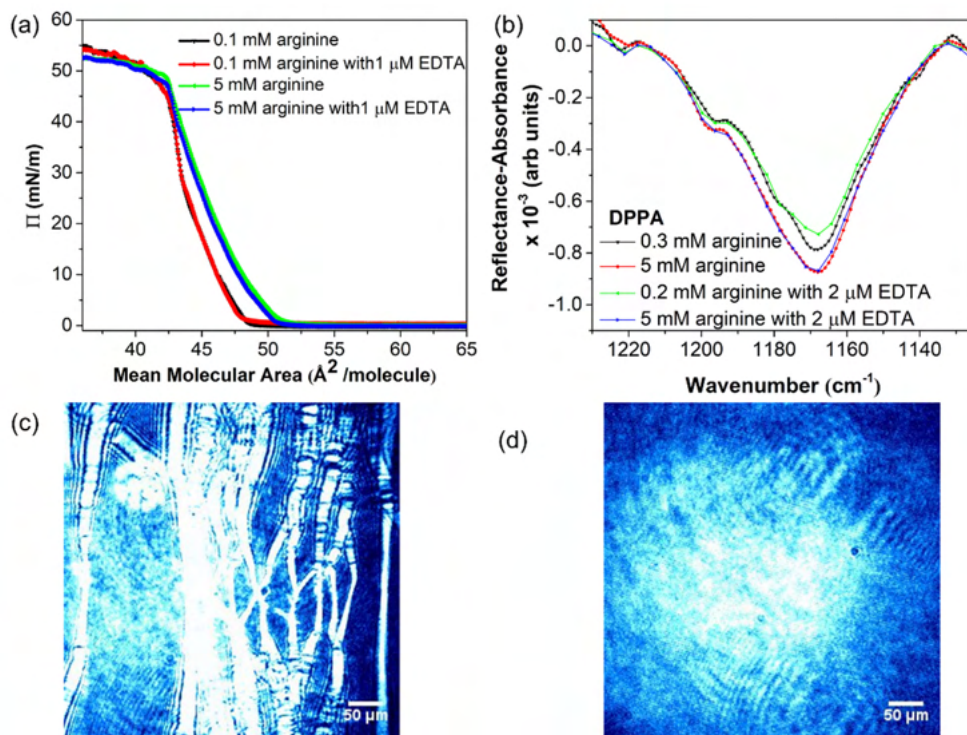
Figure 2.12 Experiments with EDTA do not affect our results. Shown here are DPPA experiments: (a) Π-A isotherms with 0.1 mM and 5 mM arginine with 1 μM EDTA, (b) IRRAS at 0.3 mM and 5 mM arginine with 2 μM EDTA, and (c) BAM image in the

collapse phase with 0.1 mM arginine with 2 µM EDTA, and (d) BAM image in the collapse phase with 5 mM arginine with 2 µM EDTA.
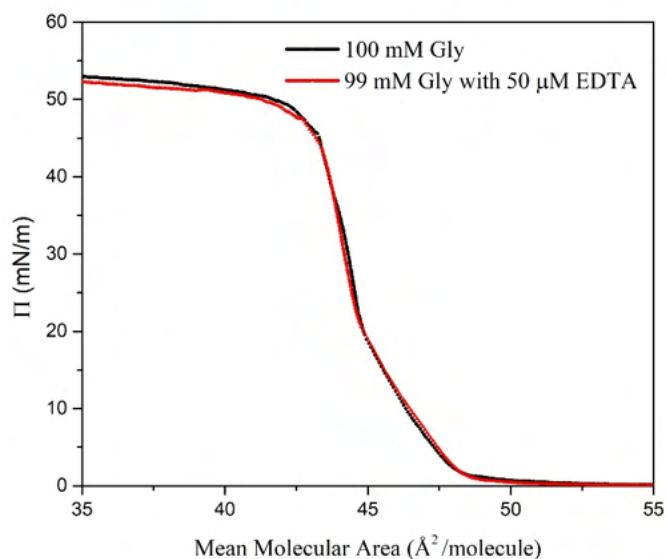
Figure 2.13 Π-A isotherm of DPPA on 100 mM glycine (black) and 100 mM glycine with 50 µM EDTA (red).

2.4 Conclusion

We explored the interfacial binding properties of the phospholipid DPPA to aqueous solutions of arginine, glycine, and guanidinium. The DPPA showed enhanced binding to the guanidinium moiety on arginine and also guanidinium in solution through electrostatic assisted hydrogen bonding on the negatively charged phosphate headgroup of DPPA. Π-A isotherms and IRRAS were used to quantitatively determine the apparent binding affinity using a Langmuir type fitting. The DPPA-arginine binding interaction was found to be on the order of 10^3 M^{-1} which is significantly higher than that determined for the bulk solution equivalent of 0.1 M^{-1}. The large difference between the apparent

binding affinity at the surface and in bulk solution suggests that the interfacial

microenvironment is different than that of bulk solution. At the aqueous interface, the

change in dielectric constant, hydration properties, and the preorganization of Langmuir

monolayers are all properties that help enhance binding affinities. Results from IRRAS

show that the guanidinium moiety of arginine is responsible for the binding mechanism

to phosphate. We utilized control experiments with glycine and guanidinium chloride to

confirm this. Lastly, BAM imaging of the molecular monolayer helped confirm that there

is a morphological change in the collapse structure before arginine saturation and after

arginine saturation consistent with our Π-A isotherm and IRRAS results. To the author's

knowledge, this was the first time IRRAS was used to quantify binding affinity and could

open new avenues for research in molecular recognition at the aqueous interface.

Chapter 3. Chemical, physical, and supramolecular superstructural driving forces of aqueous interfacial phosphate recognition
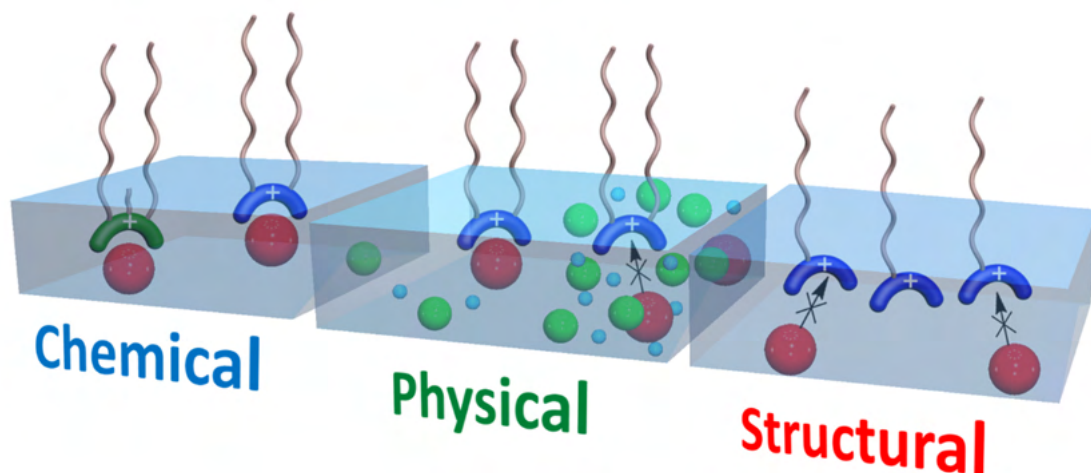
Figure 3.1 The driving forces for phosphate recognition at the aqueous interface were determined to be the chemical, physical, and supramolecular superstructural.

Abstract

The air–water interface is a largely underexplored area for phosphate recognition. We have chosen a set of four homologous molecules in which we have tuned their chemical and structural packing by modulating headgroup (guanidinium, thiouronium, and thiourea) and molecular packing (one alkyl chain versus two alkyl chains). In doing so, we have identified the principle driving forces for phosphate recognition at the air–

water interface. These are the chemical, physical, and supramolecular superstructural features. We found that phosphate affinity was greatly influenced by the chemical moiety of the headgroup where guanidinium > thiouronium > thiourea. Furthermore, the guanidinium receptor displayed higher phosphate selectivity over chloride than the thiouronium receptor. At high ionic strengths with sodium chloride >10 mM, the guanidinium receptor was not selective for phosphate over chloride due to significant charge screening. At lower concentrations, < 10 mM NaCl, the guanidinium receptor retained selectivity for phosphate demonstrating that the physical nature of the aqueous solution is integral in maintaining phosphate selectivity. Lastly, the supramolecular superstructural features showed that the single alkyl chain guanidinium did not bind to phosphate at all while the double alkyl chain guanidinium formed strong interactions with phosphate. This shows that the packing structure within the molecular monolayer is an important design principle for phosphate recognition.

3.1 Introduction

There is a need to continuously improve the design principles of aqueous phosphate recognition to aid in phosphate environmental remediation. The development of phosphate receptors is necessary for a modern sustainable society where phosphate usage is growing.[2,150,180,181] Phosphate is a non–renewable resource with reserves limited to 50–100 years worldwide[147,182] and the demand for phosphate fertilizers grows with the increasing global population.[182,183] Phosphate fertilizer eventually gets transported via runoff into water supplies and causes phosphate–driven harmful algal blooms.[147,184,185] These algal blooms negatively impact aquatic life and threaten freshwater supplies.[186] In

addition to the environmental issues of phosphate eutrophication, phosphate is also a non–renewable resource and loss of phosphorus impacts future food security. Thus, there is a vital need to develop ways to capture phosphate and remove it from water to potentially be recycled in this modern anthropogenic phosphate cycle.

There are however several challenges to phosphate capture. Phosphate has a high dehydration energy ($\Delta G_{hyd} = -465$ kJ/mol) and the receptor will need to overcome this energetic cost to capture phosphate.[187] Furthermore, the large dielectric constant of bulk water ($\varepsilon=80$)[4] acts to screen electrostatic interactions. In order to overcome some of the inherent disadvantages of phosphate binding in bulk water, we have exploited the unique properties at the interface of water.

The dielectric constant at the air–water interface is much lower than bulk water and decreases to as low as ($\varepsilon=2$) in the topmost layers.[28] Hydration environments of ions at the air–water interface have also been found to be altered relative to the bulk counterpart. [16,17] Furthermore, Langmuir monolayer have the advantage of preorganization which is expected to enhance binding affinity.[9] The long hydrophobic tails are pointing away from the water which leaves the hydrophilic part, or binding site anchored in the water and available for phosphate anions. We expect that these unique properties at the aqueous interface will be beneficial to drive phosphate capture.

Prior work by the Kunitake group has shown that binding affinity is enhanced at the monolayer interface.[36,43,168] They used guanidinium amphiphiles binding to adenosine triphosphate which had binding affinities of $10^7 \, M^{-1}$. They ascribed that was due to the unique properties at the air–water interface and also multivalency.[43] In this study, we

have explored a series of simple amphiphilic receptors to determine the fundamental principles of interfacial phosphate recognition.

The receptors studied here are in part inspired by biology bearing guanidinium, thiourea, and thiouronium functional groups. The guanidinium and thiourea moieties have been known to bind to phosphate selectively.[188–191] Long octadecyl chains anchored the receptors to the air–water interface and the number of chains was varied from one to two to determine how organization and packing affects the binding affinity. We tuned both the headgroup functional groups and alkyl chains to determine and distinguish their phosphate binding abilities. The charged guanidinium and thiouronium moieties are almost isosteric while the thiourea was the only charge neutral receptor tested. Four receptors were synthesized (Figure 3.2) The double alkyl chains drive the receptors into a U-shaped packing arrangement. The U-shaped guanidinium (**U-guan$^+$**), thiouronium (**U-thiouro$^+$**), and thiourea (**U-thiourea**). A single chain guanidinium was also tested (**S-guan$^+$**).

The guanidinium moiety of **U-guan$^+$** and **S-guan$^+$** is in a trigonal planar geometry with the positive charge distributed across the three nitrogen atoms by resonance and multiple possible hydrogen–bonding donor sites available to interact with phosphate anions.[192–194] The thiouronium functional group is still largely unexplored in the supramolecular chemistry community but there are a few examples that demonstrate its strong affinity for oxyanions.[195–199] The large polarizable sulfur atom on the thiouronium headgroups can prove charge–assisted hydrogen bonding to phosphate anions. Lastly, the thiourea group is the only neutral receptor tested. It has the advantage of hydrogen bonding but does not bear a positive charge whereas the other receptors have the

55

synergistic effects of electrostatic assisted hydrogen bond donation. The headgroup interactions will be tested as well as the physical packing arrangement of the molecules by modulating the number of alkyl chains.

The binding properties of these receptors were studied at the air–water interface in preorganized Langmuir monolayers. Surface sensitive techniques of surface pressure area isotherms (Π-A) and infrared reflection absorption spectroscopy (IRRAS) were used. We preferred to use in situ methods over ex situ method which require Langmuir–Blodget transfer of the monolayer (sometimes several transfers are necessary) to a solid support before analysis can be done using X-ray photoelectron spectroscopy, UV-vis spectroscopy, and others.[167,200]

IRRAS proved to be a valuable technique as it showed a phosphate binding response for the charged **U-guan⁺** and **U-thiouro⁺** receptors. The Π–A isotherms were not informative to binding and showed a null response for the **U-guan⁺** receptor even though it was interacting with phosphate. We attribute this outcome as due to the large size of the two octadecyl alkyl chains and the macroscopic changes in molecular area of the headgroup was not affected. Furthermore, a competition study between phosphate and chloride revealed that the charged **U-guan⁺** and **U-thiouro⁺** were selective for phosphate over chloride anions. This is not expected based on the Hofmeister series. The hydration energy of the phosphate anion is greater than that of the chloride anion. The selectivity of the **U-guan⁺** receptor amongst many competing anions is the topic of Chapter 4 in this dissertation. Furthermore, high ionic strength of sodium chloride revealed that charge screening effects weaken the electrostatic interactions and phosphate selectivity was not observed at concentrations >10mM sodium chloride. We have determined that the

principles of phosphate recognition depend on the nature of the binding site (chemical), the electrostatics and charge-screening effects (physical), and the molecular organization of the receptors in the monolayer (supramolecular superstructural). The results from our study will help advantage the rational supramolecular design of synthetic phosphate receptors where the molecular details of the interfacial interactions are still largely underexplored.
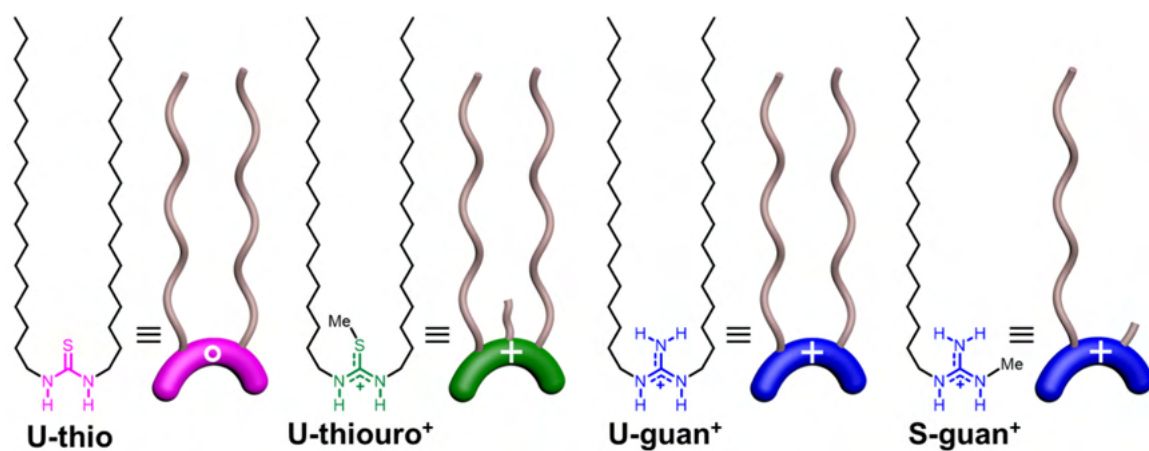
Figure 3.2 The structures of the octadecyl-based phosphate receptors studied here. The U-shaped neutral receptor **U-thio**, the U-shaped and charged receptors **U-thiouro⁺** and **U-guan⁺**, and the single chain and charged **S-guan⁺** receptor.

3.2 Methods and Materials

3.2.1 Materials

Receptors were synthesized by Dr Wei Zhao in collaboration with Professor Amar Flood's lab at Indiana University. Details of the synthetic procedure and characterization are included in the Supporting Information for the corresponding publication.[65] The **U-thio**, **S-guan⁺**, and **U-thiouoro⁺** receptors were dissolved in chloroform (HPLC grade, Fisher Scientific) and the **U-guan⁺** receptor was dissolved in a mixture of chloroform and

methanol (HPLC grade, Fisher Scientific) (4:1 and 10:1 v/v chloroform to methanol were both tested).

The **U-thiouro⁺** receptor was tested as both a chloride and iodide salt, and counterion did not affect the results (Figure 3.3).
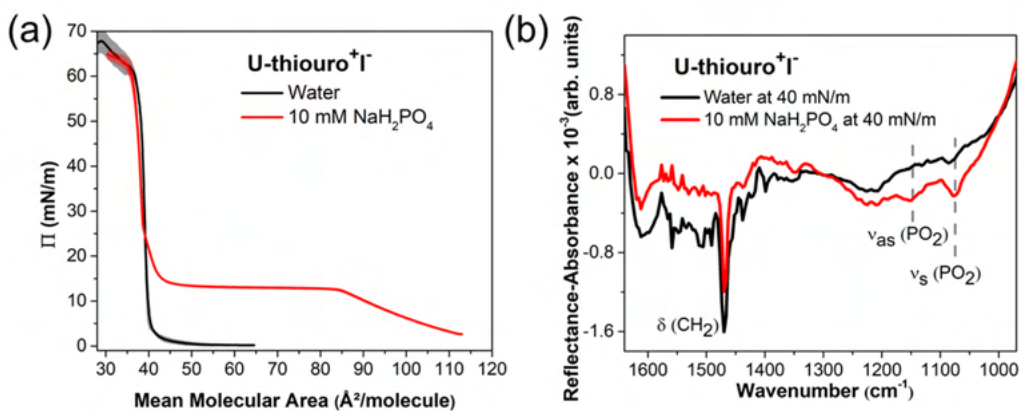
Figure 3.3 The iodide counterion for the **U-thiouro⁺** receptor was tested as a comparison to the chloride counterion which is shown in the remainder of this text.

A series of important control experiments are included with the following commercially available products: eicosane (Aldrich, 99%), perfluorotetradecanoic acid (Alfa Aesar, 96%), and tripalmitin (Sigma, ≥99%). These compounds were chosen because they should not possess any affinity for phosphate. The perfluorinated fatty acid should render the carboxylate deprotonated at the near neutral conditions of the phosphate solutions. Although the sodium counterion will interact with the carboxylate, we should not observe interactions between the phosphate and carboxylate. Eicosane is a long chain alkane with no hydrophilic headgroup. Although it does not organize into a monolayer, it does form an oil like surface on water and phosphate. Finally, tripalmitin is a triglyceride with an ester backbone. This molecular should also not possess affinity

towards phosphate. These control experiments are extremely important to access the validity of our results of the receptors interacting with phosphate.

All aqueous solutions in this study were made using ultrapure water with a resistivity of 18.2 MΩ·cm (Milli-Q Advantage A10). Phosphate solutions as received and filtered were both tested. Sodium phosphate monobasic monohydrate (Sigma, ≥99.5%) and sodium phosphate monobasic monohydrate (Fisher, ACS grade) was filtered three times using an activated carbon filter (Whatman Carbon Cap 75, Sigma) to ensure purity and determine whether there was a difference in solutions of commercially available phosphate. The concentration of the filtered Fisher brand phosphate was calibrated by Raman spectroscopy (Figure 3.4) and Figures 3.5-3.6 show the same conclusions as the unfiltered Sigma solutions.
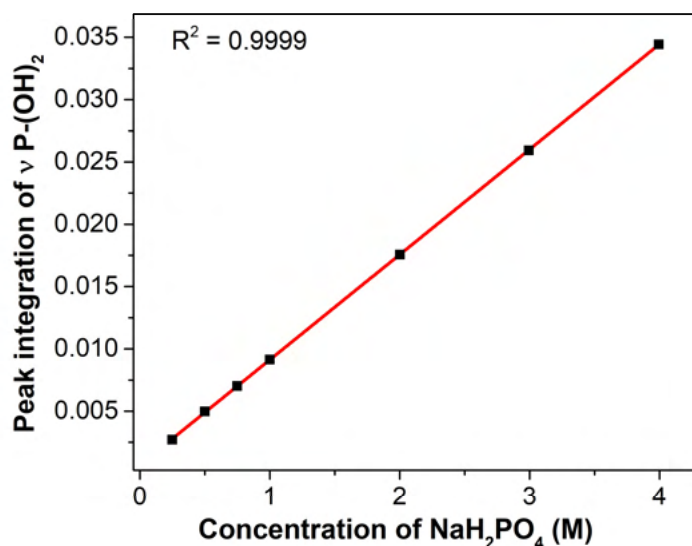
Figure 3.4 Raman calibration curve for the filtered phosphate solutions.
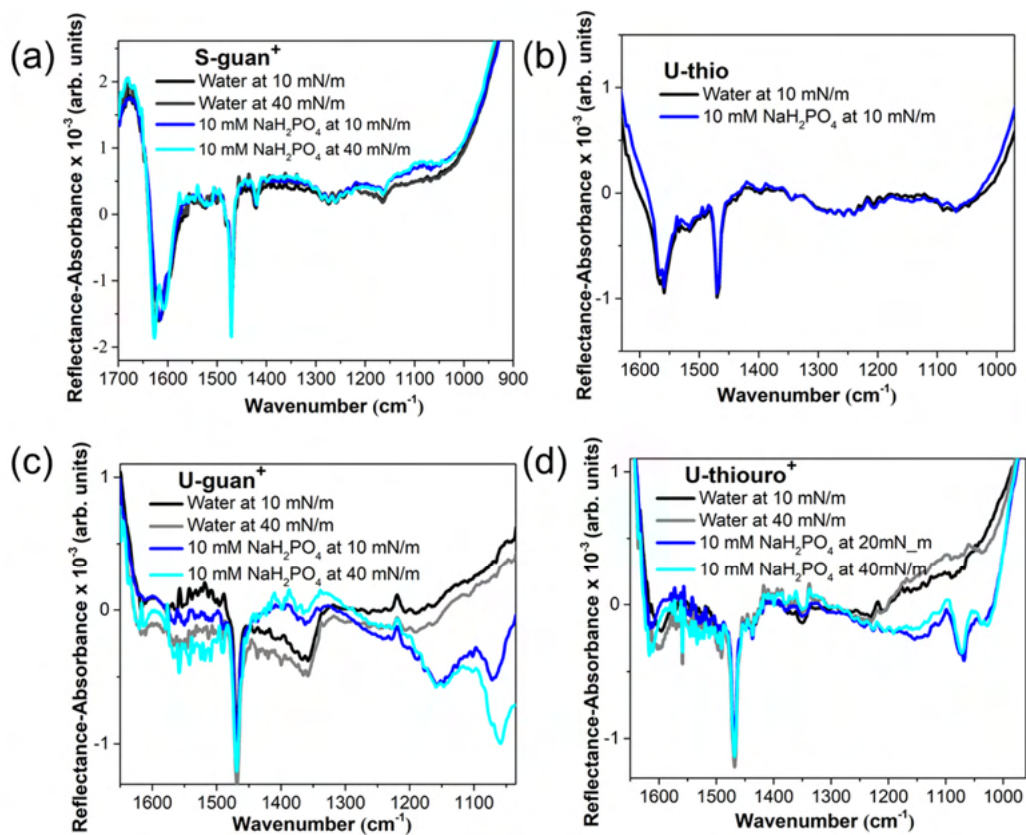
Figure 3.5 IRRAS spectra of (a) **S-guan⁺**, (b) **U-thio**, (c) **U-guan⁺**, and (d) **U-thiouro⁺** on water and 10 mM filtered phosphate. The results from the filtered phosphate solutions agree with the results from the unfiltered phosphate solutions shown later.
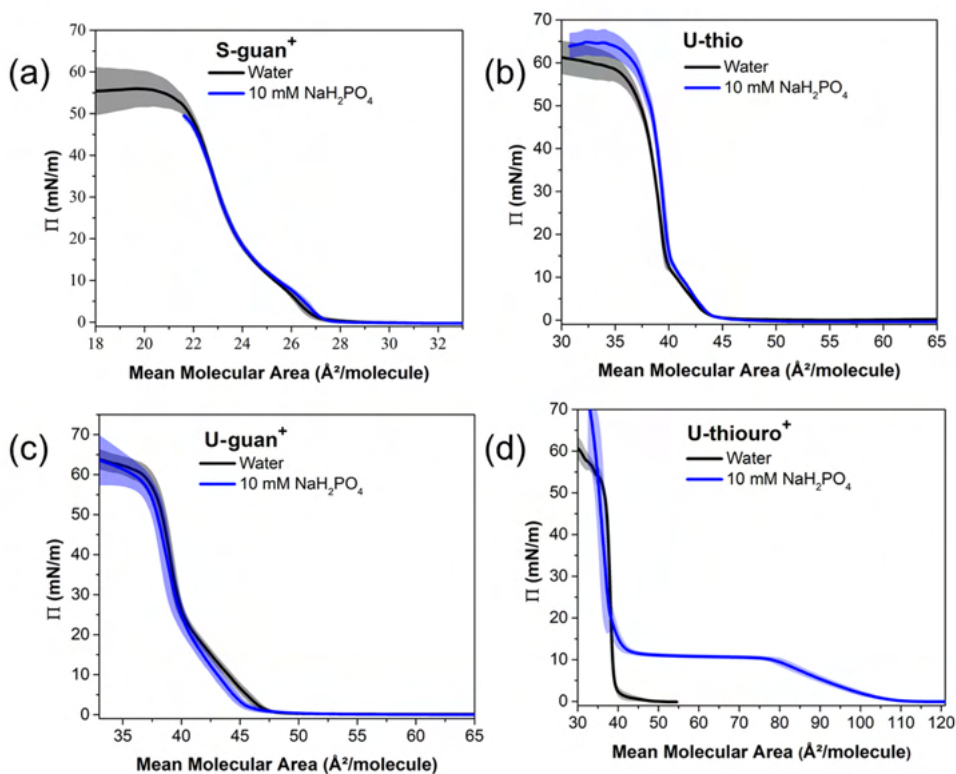
Figure 3.6 Π-A isotherms of (a) **S-guan⁺**, (b) **U-thio**, (c) **U-guan⁺**, and (d) **U-thiouro⁺** on water and 10 mM filtered phosphate. The results from the filtered phosphate solutions agree with the results from the unfiltered phosphate solutions shown later.

Therefore, unfiltered phosphate solutions were used for the other studies in this chapter because filtration was unnecessary for this project. To ensure purity of the phosphate even more, ~70 mg of phosphate was mixed with 600 μL of CDCl₃ (Cambridge Isotope Laboratories, Inc.) to extract out possible organic impurities into the organic layer and the CDCl₃ was added to an NMR tube to ensure purity of the salts. The NMR sample was then tested by ^{1}H NMR (250 MHz). Magnesium chloride hexahydrate (Fisher, ACS grade) prepared the same way was also tested. Please note that the peak at 7.24 ppm is CHCl₃ (symmetric peaks surrounding it are ^{13}C satellites, due to small

abundance of $^{13}CDCl_3$) and the peak at 1.56 ppm is water. As seen in Figure 3.7, there are no organic peaks seen in the spectra from phosphate spectra but there is a broad feature in the magnesium chloride spectra possible due to organics extracted into the chloroform NMR tube.
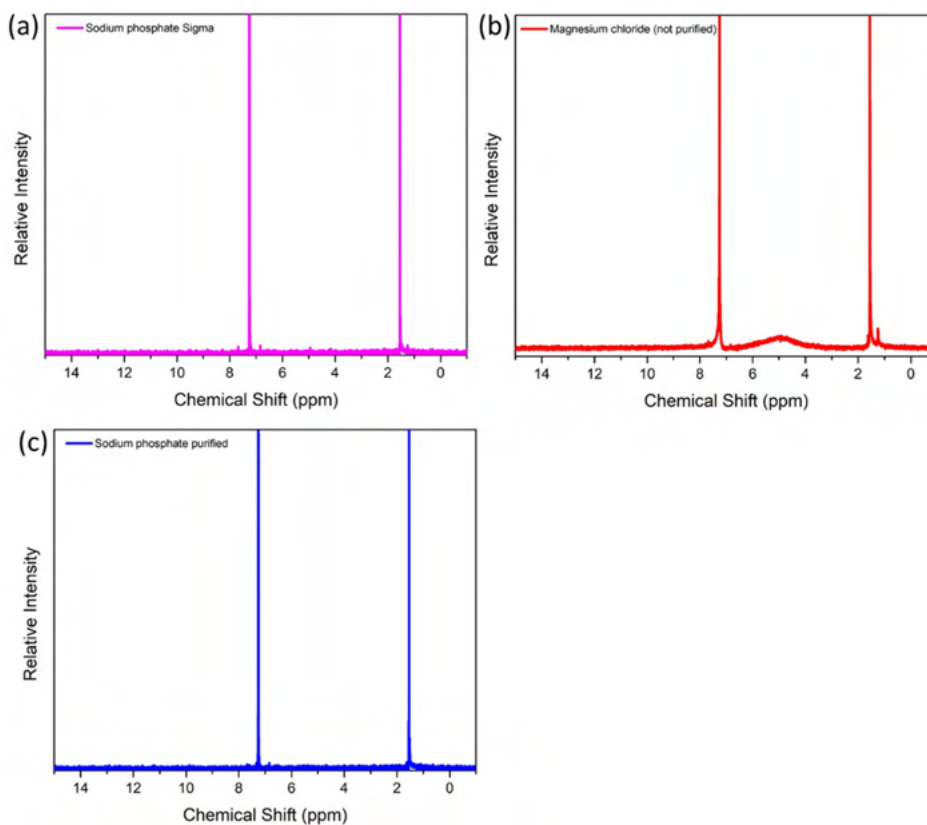
Figure 3.7 ^1H NMR in CDCl$_3$ of the organic extraction from (a) unfiltered sodium phosphate, (b) unfiltered magnesium chloride, and (c) filtered sodium phosphate.

The pH of the aqueous solutions was recorded using a Thermo Scientific Orion Versa Star Pro (± 0.002 pH units). The pH of water from the Milli-Q system is approximately 5.7 (+/- 0.2) and this lower pH than what might be expected is due to atmospheric carbon dioxide acidifying the solution. The 10 mM phosphate solution had a pH of 4.7 and the

filtered solution was ~5.3 which could be attributed to changes in speciation during the filtration process.

3.3 Results and Discussion
3.3.1   Determination of phosphate binding by IRRAS

IRRAS spectroscopy was found to be an effective means to determine the binding interactions between the receptors and aqueous phosphate. The low frequency region (1600—950 cm^{-1}) has valuable vibrational modes including the C-N stretches of the receptors as well as the phosphate modes. All IRRAS spectra were taken at $\Pi=40mN/m$ although lower Π were also taken (Appendix). Figure 3.8 shows the IRRAS spectra of the **S-guan⁺**, **U-guan⁺**, **U-thio**, and **U-thiouro⁺** receptors. It is clear from these spectra that the spectra of the **U-guan⁺** and **U-thiouro⁺** receptors on 10 mM phosphate are different than their corresponding spectra on water. It is also apparent the **S-guan⁺** and **U-thio** do not show any spectral changes from water to the 10 mM phosphate solution. This gives an initial indication that the **U-guan⁺** and **U-thiouro⁺** receptors are interacting and binding to phosphate while the **S-guan⁺** and **U-thio** receptors are not binding to phosphate.
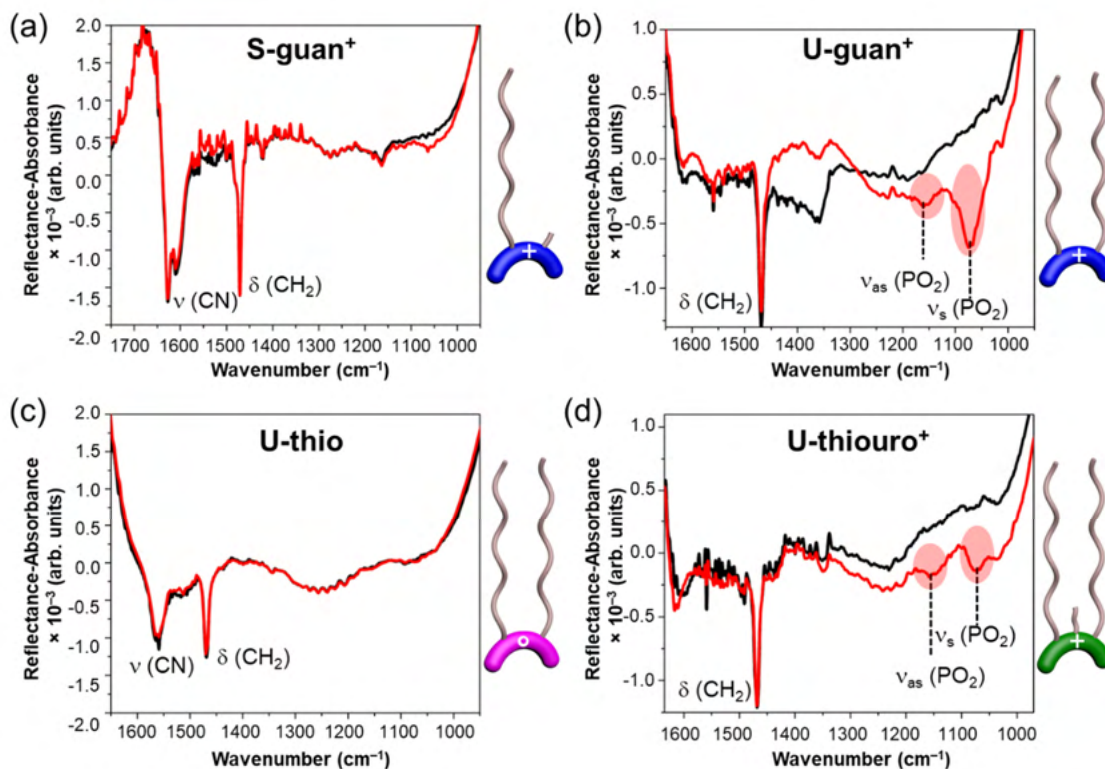
Figure 3.8 The IRRAS spectra of the receptors in the condensed phase at Π =40mN/m. (a) **S-guan$^+$**, (b) **U-guan$^+$**, (c) **U-thio**, and (d) **U-thiouro$^+$**. The phosphate stretching modes, which are attributed to receptor–phosphate binding, are marked in red on the spectra.

The **U-guan$^+$** and **U-thiouro$^+$** show clear binding signatures from phosphate at approximately 1158 cm^{-1} and 1074 cm^{-1}. These correspond to phosphate's asymmetric (ν_{as} PO$_2$) and symmetric (ν_s PO$_2$) modes.[201,202] It is important to remember that these modes would not appear in the absence of phosphate binding. Due to the nature of the IRRAS equation, -log (R/R$_0$) where the phosphate is included in both R and R$_0$ of this equation. It was still important to verify the effectiveness of this technique and conduct a series of control experiments to verify that the phosphate is binding to the receptors.
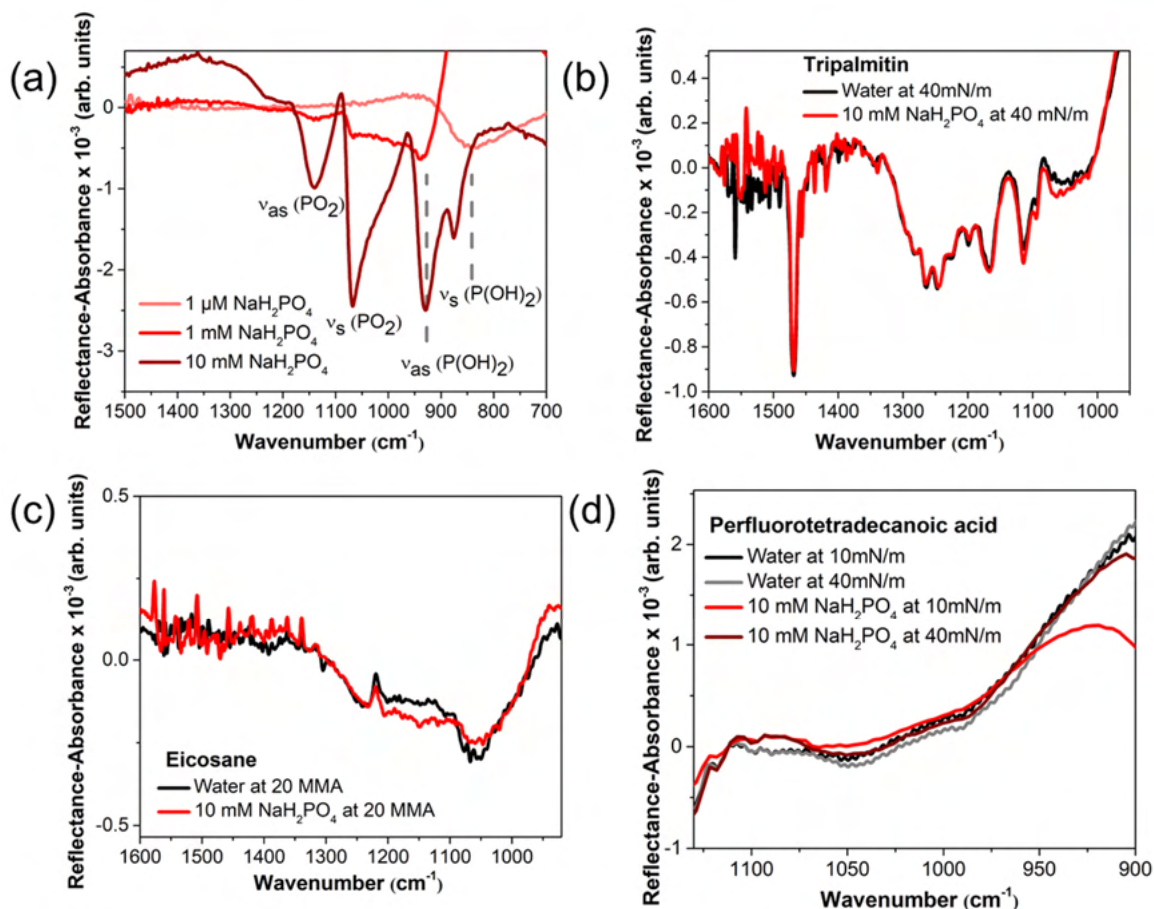
Figure 3.9 IRRAS spectra of (a) sodium phosphate where in this case the R_0 is a water without phosphate. Control experiments with (b) tripalmitin at 40 mN/m with and without phosphate, (c) eicosane at 20 MMA with and without phosphate, and (d) perfluorotetradecanoic acid with and without phosphate at 10 mN/m and 40 mN/m verify the effectiveness of this technique.

The control experiments are shown in Figure 3.9. First the spectral position of phosphate dissolved in water were determined by taking IRRAS spectra of water and then the phosphate solutions where in this case, R_0 is water and R is the phosphate solution. Figure 3.9a shows phosphate IRRAS spectra where the peaks are at 1137, 1067, 929, and 875 cm^{-1} correspond to the PO$_2$ asymmetric (ν_{as} PO$_2$), PO$_2$ symmetric (ν_s PO$_2$), P(OH)$_2$ asymmetric (ν_{as} P(OH)$_2$), and P(OH)$_2$ symmetric (ν_s P(OH)$_2$) stretching

modes,[201–203] respectively. These peaks were only observed at high concentrations > 1 mM phosphate. The control experiments were done with carefully selected molecules in order to avoid ambiguity with molecules that could bind with phosphate. Eicosane is a C_{20} hydrocarbon with no binding sites, tripalmitin is a triglyceride with three ester linkages, and perfluorotetradecanoic acid has a carboxylate headgroup. The fluorinated version of this molecule was chosen to avoid ambiguity with pKa at the interface and will undoubtably be negatively charged at neutral pH.

The phosphate modes are not present in the IRRAS spectra of these control molecules. This suggests there is no interaction between the molecules and phosphate. This makes sense since these molecules should not possess affinity towards phosphate and verifies the IRRAS technique to distinguish binding interactions. We have used this technique to track the receptor-phosphate binding interactions. The phosphate modes observed in IRRAS for the rest of this discussion are a response of the phosphate binding to the receptor molecules.

3.3.2 U-guan$^+$ and U-thiouro$^+$ phosphate binding interactions

There was further spectroscopic evidence that the **U-guan$^+$** and **U-thiouro$^+$** were interacting with phosphate. These phosphate modes underwent a blue shift of approximately 20 cm^{-1} and 5 cm^{-1} for the ν_{as} PO$_2$ and ν_s PO$_2$ modes respectively. This blue shift is due to the hydration environment around phosphate being altered from strongly hydrated with waters solvating the phosphates to less hydrated as the receptor phosphate bound state. This type of interfacial blue shift has been observed before and there is literature precedence to describe this change in hydration.[86,204,205] Therefore, the net hydrogen bonding of the phosphate is weaker with the receptor than in the displaced

portion of the total hydration sphere. This weaker hydrogen bonding is compensating by the strong electrostatic ion–ion interactions for the phosphate bound to the receptor in the low dielectric medium.

In addition to the phosphate modes, there is also evidence from the receptor vibrational modes that indicate a binding interaction is taking place. The mode at 1362 cm^{-1} in the U-guan+ spectra is tentatively assigned to the N–C–N stretch based on a similar structure tetramethyl guanidine.[206] This mode diminishes upon phosphate addition providing support that there is an interaction. Furthermore, **U-thiouro$^+$** with p and s–polarization shows a narrowing of the C–N stretch (with additional contribution from the N–H bend)[207,208] at approximately 1600 cm^{-1} and a blue shift of ~ 12 cm^{-1} of this mode in a way that correlates with phosphate interaction (Figure 3.10).
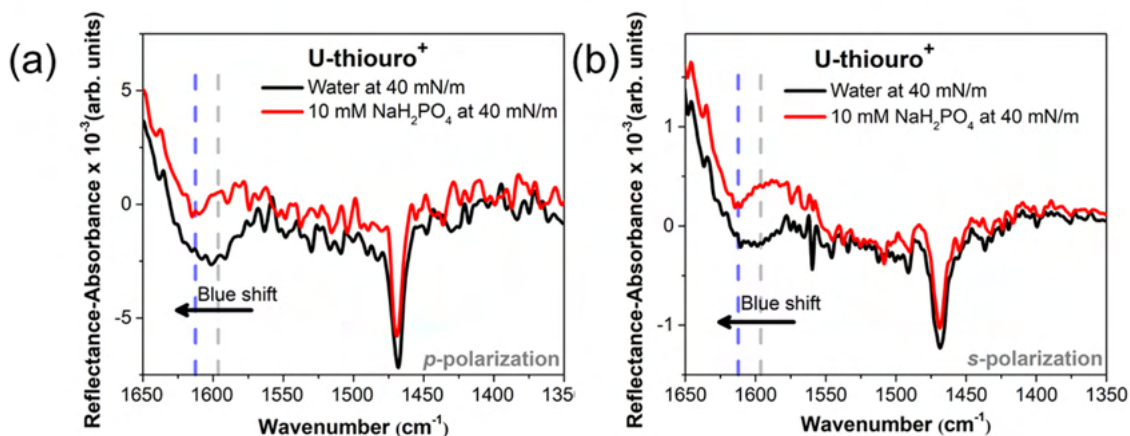
Figure 3.10 Polarization IRRAS spectra with (a) p-polarization and (b) s-polarization for the **U-thiouro$^+$** receptor on water and 10 mM phosphate.

3.3.3 Receptor size and the ambiguity of Π-A isotherms

Surface pressure-mean molecular area (Π-A) compressional isotherms have literature precedence to determine molecular interactions between a molecular monolayer and species dissolved in the subphase.[66,209–211] As shown in Figure 3.11a-c, **S-guan$^+$**, **U-guan$^+$**, and **U-thio** show almost no change between the isotherms on water and the 10 mM phosphate solution. This suggests that there is no interaction between these receptors and phosphate; however, it was just shown above that the **U-guan$^+$** is binding to phosphate. It is now important to recognize that the Π–A isotherms might not be sensitive to binding as this technique is showing a physical change in the monolayer area and the large alkyl chains have a larger effect on the area than the headgroup (binding region). Figure 3.11d of **U-thiouro$^+$** shows a large expansion in mean molecular area and the origin of this will be discussed later.

The Π–A isotherms of the single alkyl chain **S-guan$^+$** should be more sensitive to binding because of the higher packing density. If **S-guan$^+$** were binding to phosphate, the phosphate anions would be driven in-between the receptor headgroups and changes in the molecular area (by Π–A isotherms) would confirm a binding interaction. The lack of a

change in the isotherm for the **S-guan$^+$** further supports the lack of interaction.
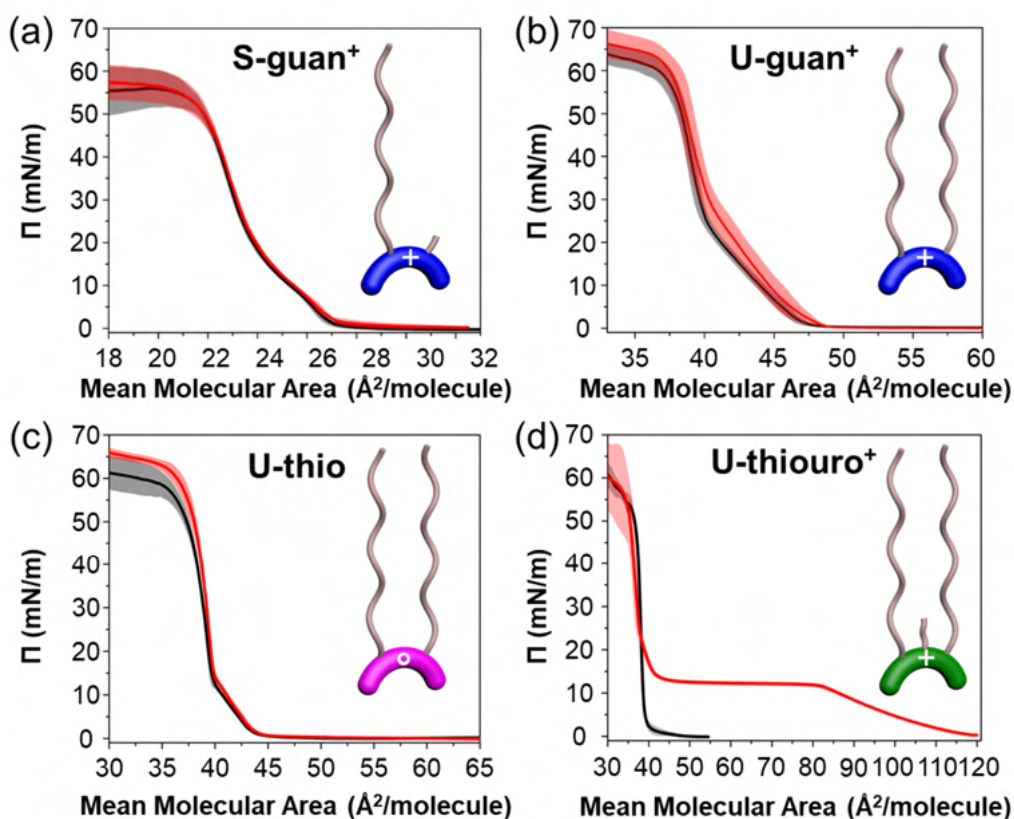
Figure 3.11 Surface pressure (Π)–mean molecular area (A) isotherms of (a) **S-guan$^+$**, (b) **U-guan$^+$**, (c) **U-thio**, and (d) **U-thiouro$^+$** on 10 mM phosphate (red) and water (black). The shaded region corresponds to one standard deviation above and below the mean. The **U-thiouro$^+$** shows a significant monolayer expansion upon phosphate addition.

The **U-guan$^+$** however is binding to phosphate and does not show a response via Π–A isotherms. Figure 3.12 shows the hypothesized binding mechanism for the **U-guan$^+$** and phosphate interaction. This cartoon representation shows the phosphate driven beneath the monolayer and not in–between the **U-guan$^+$** receptors molecules. A binding motif such as this explains why there was no change in the Π–A isotherm observed for this binding interaction.
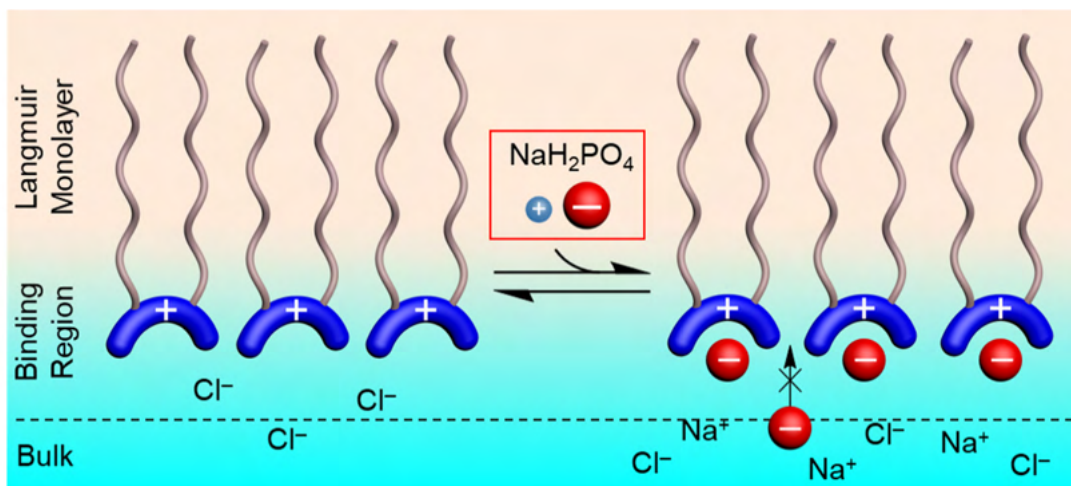
Figure 3.12 A schematic representation of **U-guan$^+$** interacting with phosphate beneath the guanidinium headgroup. In this binding configuration, there is no expansion or compression of the monolayer as the large alkyl chains impedes this macroscopic change.

3.3.4   Supramolecular superstructural impacts on phosphate recognition

It is important to appreciate the unique microenvironment present at the air–water interface. Receptors at the air–water interface are anchored into the subphase and tethered to the interface by means of the hydrophobic effect. In this confined space, the molecules are extremely close together (i.e. compacted) and it is not unreasonable to assume that receptor–receptor interactions can occur via the alkyl chains and headgroups through noncovalent interactions. We suggest that guanidinium–guanidinium interactions are occurring via the close neighboring headgroups. There has been recent literature to suggest that guanidiniums can form like charged ion-pairs.[212–217] We find that the **S-guan$^+$** receptor does not interact with phosphate while the **U-guan$^+$** receptor does interact which supports our hypothesis about the importance of supramolecular superstructures within the molecular interface.

Although the IRRAS results proved to be more valuable than the Π–A isotherms, the

Π–A isotherms were still informative for the **U-thiouro**[+] receptor. The Π–A isotherms

showed a mean molecular expansion of 59.6 Å^2 from water to the phosphate solution,

where the mean molecular area was 39.4 (±0.6) Å^2 on water and 99.0 (±0.7) Å^2 on 10

mM phosphate, taken at a surface pressure of 5 mN/m. The 59.6 Å^2 expansion is too

large to rationalize as contributing solely due to phosphate anions because the radius of a

phosphate anion is 0.2 nm (~12.6 Å^2).[187] We attributed this expansion as the result of

supramolecular superstructural changes within the monolayer. The alkyl chains and

methyl group on the thiouronium headgroup undergo reorganization upon phosphate

binding. This was the only receptor where we observed this reorganization. In order to

further understand this, IRRAS spectra of the **U-thiouro**[+] receptor were taken at 5, 10,

and 40 mN/m on both water and 10 mM phosphate (Figure 3.13a, b). The peak at 1468

cm^{-1} is assigned to the CH$_2$ scissoring (δ CH$_2$) and peaks at 2963, 2924, 2883, and 2850

cm−1 are the CH$_3$ asymmetric (ν_{as} CH$_3$), CH$_2$ asymmetric (ν_{as} CH$_2$), CH$_3$ symmetric (ν_s

CH$_3$), and CH$_2$ symmetric (ν_s CH$_2$) stretching modes, respectively. In Figure 3.13a, the

scissoring mode at 1468 cm^{-1} is in the same relative position on water and on the 10 mM

phosphate solution at various Π's. The lower intensity of this mode is due to larger

molecular area (i.e. less molecules being surveyed). We can infer that the packing lattice

of the monolayer is consistent through the addition of phosphate. We observe the

hexagonal packing throughout this. [218] Therefore, the change in the isotherm is not due to

changing in packing structure of the monolayer.

Figure 3.13b shows the **U-thiouro**[+] receptor at 5 and 10 mN/m which corresponds to

low surface coverage and at 40 mN/m which corresponds to the high surface coverage in

the condensed phase. We observe a red shift in the ν_{as} CH_2 and ν_s CH_2 stretching modes going from low to high surface coverage (i.e. more expanded to condensed). Please note in that the spectra are plotted on different intensity scales on the y–axis to magnify this red shift.
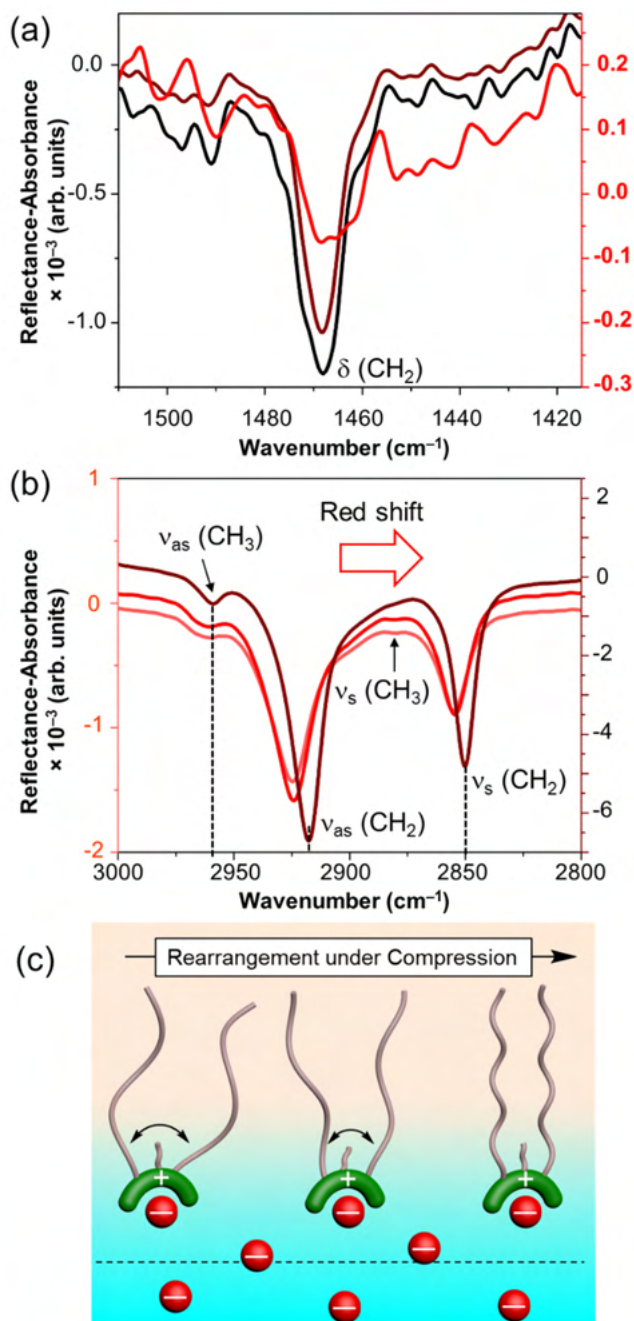
Figure 3.13 IRRAS spectra of the **U-thiouro⁺** receptor reorganizing upon phosphate addition. (a) CH_2 scissoring mode (1468 cm⁻¹) of the **U-thiouro⁺** receptor at 10 mN/m (red) and 40 mN/m (dark red) on 10 mM phosphate and on water (black). (b) The alkyl stretching modes with 10 mM phosphate at 5 mN/m (light red), 10 mN/m (red), and 40 mN/m (dark red). The alkyl modes for the **U-thiouro⁺** receptor on water is shown as a black dotted line for reference. (c) Schematic depiction of the reorganization of the **U-thiouro⁺** receptor headgroup as the headgroup interactions with phosphate and the alkyl chains change conformations.

Reorganization and phase changes upon intermolecular interactions have been observed before in some biological systems with phospholipids binding to calcium ions,[160,219,220] proteins,[221,222] and cholesterol.[223–225] The **U-thiouro⁺** receptor was the only receptor that we observed transition from a more disordered monolayer to a more ordered one. One possible explanation for this finding is that the bulky methyl group on the positively charged sulfur atom of the thiouronium undergoes a reorganization as it accommodates the large phosphate guest anions. As the phosphate anions donate electron density to the positive receptor headgroup, the thiouronium may begin to transition from more sp^2 to sp^3 character and gain rotational freedom in the process.

3.3.5 Charge screening and lack of phosphate selectivity at high ionic strength NaCl solutions

It was also important to begin to unravel the complexity of anion selectivity at the air–water interface. If these receptors were utilized in freshwater systems, there would be a plethora of competing anions. We decided to first determine the receptor's selectivity towards phosphate over chloride. Chloride is prevalent in natural waters (0–100 mg L⁻¹).[226] Figure 3.14a shows the IRRAS spectra of the **U-guan⁺** receptor with phosphate to chloride at a 1:1 molar ratio at 10 mM and 1 mM conditions. At a 1:1 equivalence, the phosphate modes remain present which suggests the **U-guan⁺** receptor is selective for phosphate over chloride at equal equivalence. We increased the relative amount of chloride to evaluate the 1:10 molar equivalence as shown in Figure 3.14b. Interestingly, by increasing the concentration to 10 mM NaH_2PO_4 : 100 mM NaCl, the phosphate modes diminish. At this high ionic strength solution, the receptor has lost selectivity for

the phosphate anions. We believe that at high ionic strength, charge screening can diminish the electrostatic interactions[227–229] between the **U-guan$^+$** and phosphate anions.
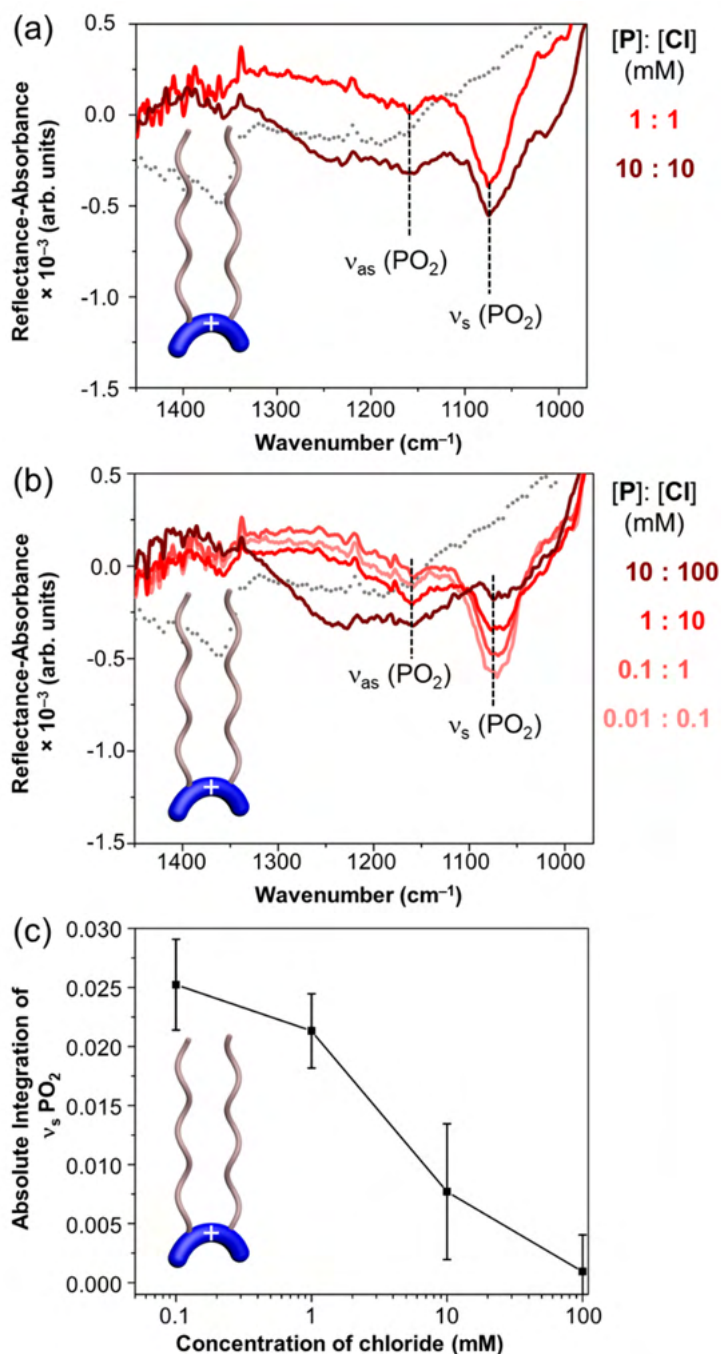
Figure 3.14 Competition between phosphate and chloride for the **U-guan$^+$** receptor at
Π=40 mN/m. (a) **U-guan$^+$** receptor shows selectivity for phosphate over chloride at a 1:1
molar concentration (at 1 mM and 10 mM). (b) The **U-guan$^+$** receptor at a phosphate to
chloride equivalence of 1:10 shows an inconsistent phosphate selectivity. At high
concentrations NaCl, significant charge screening limits phosphate interactions. (c)
Integration of the phosphate mode from (1120 – 1020 cm^{-1}) shows that chloride
concentrations must be less than 10 mM to limit the negative effects of charge screening.

To evaluate this result further, we tested the 1:10 equivalence at a variety of ionic strengths from 0.1 to 10 mM NaCl (Figure 3.14b). The phosphate modes are present at low chloride concentrations between 0.1 to 10 mM which implies that the **U-guan$^+$** receptor is selective for phosphate over chloride in this concentration range. It is important to note that as we go across this concentration range, the Debye length shrinks from ~30 to 1 nm.   Figure 3.14c shows the integration of the phosphate mode ν_s (PO)$_2$ (1120 – 1020 cm^{-1}) as a function of concentration of NaCl. There is a trend when the concentration of NaCl is at or below 1 mM the phosphate integration reaches a plateau. In order to effectively mimic the chloride concentration in natural waters, we retested the 1:10 equivalence at a chloride concentration of 1 mM NaCl (Figure 3.15). This was done also to limit the effects of charge screening at high ionic strengths. Figure 3.15 shows that the **U-guan$^+$** receptor has selectivity for phosphate over chloride up to a factor of 1000. The integration of the phosphate mode as a function of phosphate concentration with a constant 1 mM chloride background concentration shows this high selectivity for phosphate over chloride (Figure 3.15b). This selectivity is characterized as *anti*–Hofmeister behavior ($H_2PO_4^- >> Cl^-$).[29,188,230–232] The chloride anion would typically have a higher selectivity than phosphate because it has a smaller hydration energy (-381 kJ/mol). Furthermore, this goes against the expectations from Collins' rule which is when anions and cation have matching hydration enthalpies, they will form ion pairs.[233,234]
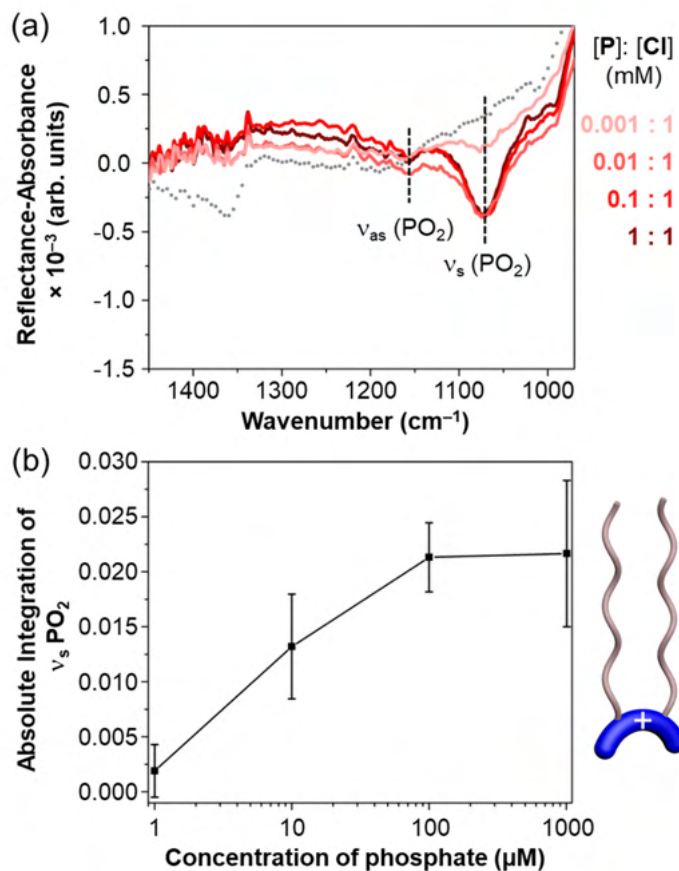
Figure 3.15 (a) A constant chloride concentration of 1 mM shows that the **U-guan⁺** receptor is selective for phosphate over chloride at up to 1:1000 ratios of chloride to phosphate. (b) The integration of the phosphate mode at constant chloride further supports the high selectivity of the **U-guan⁺** receptor towards phosphate.

We also tested the **U-thiouro⁺** receptor's phosphate selectivity over chloride (Figure 3.16). At a 1:1 molar equivalence of phosphate to chloride, the **U-thiouro⁺** receptor showed the presence of the phosphate modes which suggests it is selective for phosphate at this ratio. At an equivalence of 1:10 however, the **U-thiouro⁺** receptor shows a decrease in phosphate intensity. We can infer that the **U-thiouro⁺** receptor shows selectivity for phosphate over chloride at concentrations up to 1:10 phosphate to chloride ratio. Interestingly, the **U-guan⁺** receptor is more selective than the **U-thiouro⁺**

receptor for phosphate (Figures 3.15 and 3.16). There are several reasons to explain this finding, but the exact origin is the topic of future research. The calculated electrostatic potential of the truncated dimethyl guanidinium and dimethyl thiouronium can be found in the Supporting Information of Neal *et al.*[65] This electrostatic potential map shows that the hydrogen atoms on the (N–H) binding motifs are similar for both the **U-guan⁺** and **U-thiouro⁺** receptors. Although the electrostatic potentials are similar, the guanidinium moiety has two more potential hydrogen bonding donors than the thiouronium headgroup. Additionally, the **U-thiouro⁺** receptor undergoes a reorganization upon phosphate addition which induces a free energy penalty. This energetic cost is paid upon phosphate binding and is the most probable cause for the disparity in selectivity for the two receptors.
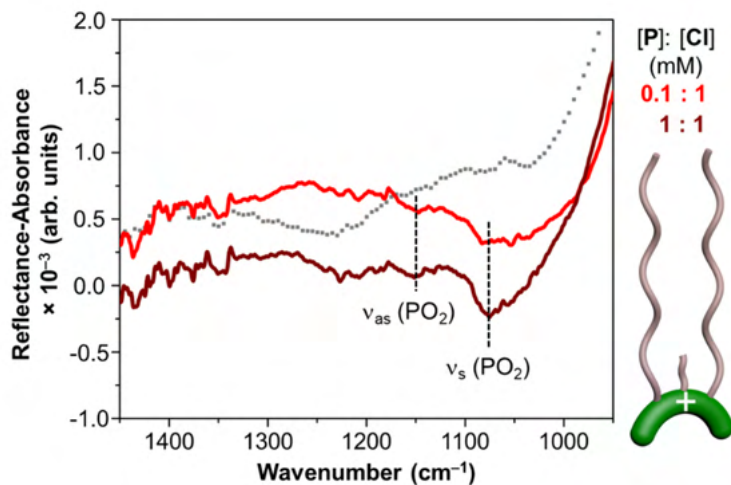
Figure 3.16 The **U-thiouro⁺** receptor shows phosphate selectivity over chloride at 1:1 molar equivalence. At 1:10 equivalence there is a sharp drop in phosphate selectivity which is seen as a diminishing of the phosphate intensity.
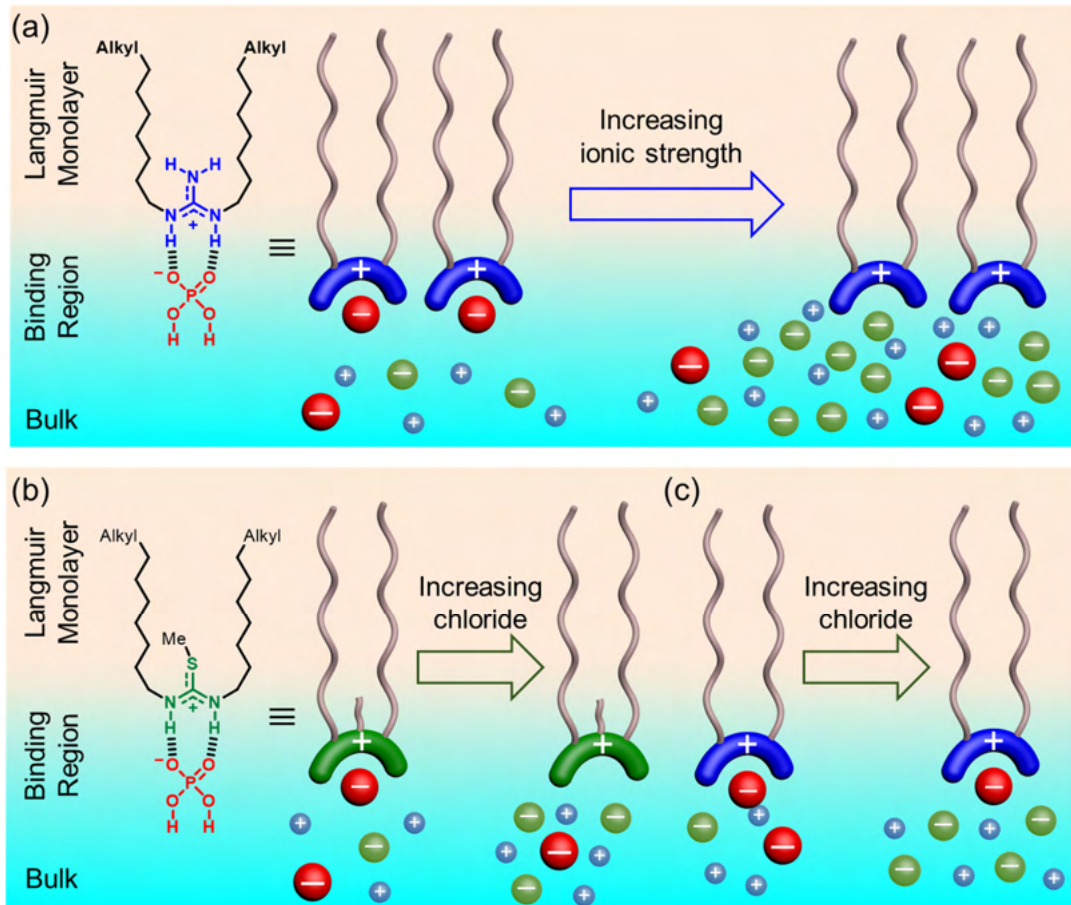
Figure 3.17 A schematic representation of the (a) charge screening at high ionic strength for the **U-guan$^+$** receptor and (b) the **U-thiouro$^+$** receptor outcompeting chloride for phosphate with 10–fold selectivity and (c) the **U-guan$^+$** receptor outcompeting chloride for phosphate at 10^3–fold selectivity.

These selectivity experiments help reiterate the importance of electrostatics in driving interfacial phosphate recognition. The **U-guan$^+$** and **U-thiouro$^+$** receptors showed stronger binding affinities to phosphate while the neutral receptor **U-thio** did not interact with phosphate. Furthermore, when electrostatic interactions are screened by high chloride concentrations, the hydrogen bonding of the **U-guan$^+$** receptor is not enough to bind to phosphate (Figure 3.17a). We saw this also with the **U-thio** receptor which did

not interact with phosphate and is consistent with the effects of charge screening. Furthermore, the **U-guan⁺** and **U-thiouro⁺** show selectivity for phosphate over chloride which is shows that the guanidinium and thiouronium functional groups promote phosphate binding through charge-assisted hydrogen bonding to the phosphate anions Figure 3.17b,c).

3.3.6 Additional phosphate receptors studied

In addition to the **U-guan⁺**, **U-thiouro⁺**, **U-thio**, and **S-guan⁺** receptors, we also tested a few additional receptors that were not pursed further for reasons outlined below. Initially, we sought to tune the supramolecular superstructural packing by also testing a series of glycol anchored receptors. The glycol anchor was supposed to be embed the receptor into the water subphase and act to pull the receptor headgroup further down into the water layers. By acting to anchor the receptors deeper into the interfacial waters, we could test how the distance to the surface impacts phosphate binding affinity. Although these molecules were synthesized, there were some preliminary issues in our attempts to deposit these molecules as organized monolayers.

Figure 3.18a shows the glycol anchored **S-guan⁺ (glycol)** monolayer on water. The condensed region of the monolayer has a mean molecular area of less than 10 $Å^2$/molecule. The small area occupied by the **S-guan⁺ (glycol)** is not due to the size of the alkyl chain but instead due to desorption of the partially soluble molecular monolayer into bulk solution. Because the **S-guan⁺ (glycol)** monolayer was not stable on the surface of water, we did not pursue further studies with phosphate. For reference, the cross-sectional area of a fatty acid is approximately 20.5 $Å^2$/molecule[235,236] which is greater than double the condensed region of the **S-guan⁺ (glycol)** receptor.

Figure 3.18b shows the other glycol anchored receptor that we tested, the **S-thio (glycol)** monolayer on water. As seen in the isotherm for the **S-thio (glycol)** receptor, there is a rise in surface pressure at a mean molecular area of ~90 $Å^2$/molecule. This suggests that there is some long-range ordering of the molecules at this large mean molecular area. We believe that the glycol anchoring group is not orientated down into the subphase but instead forming a network of glycol groups hydrogen bonding with each other. This hydrogen bonding network prevents the monolayer from forming a condensed region indicative of a single chain. We did not pursue further phosphate studies with this molecule for these reasons.
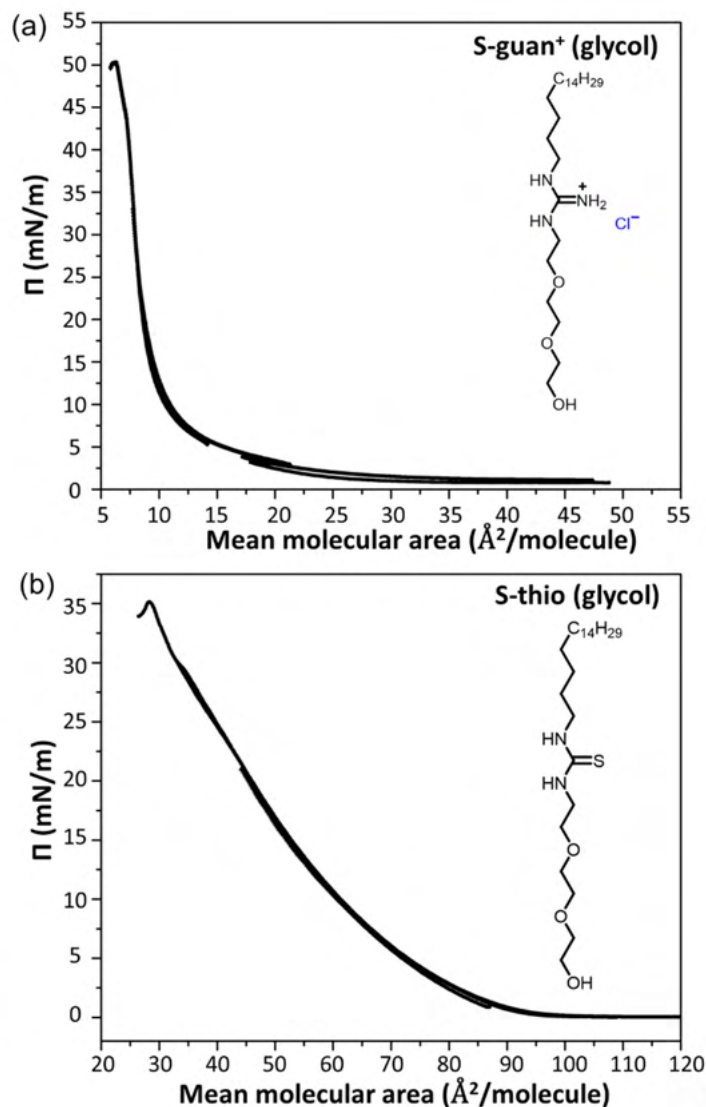
Figure 3.18 Π-A isotherms of the (a) **S-guan+ (glycol)** receptor and (b) **S-thio (glycol)** receptor on water.

Lastly, we tested the **S-thio** receptor which is a single alkyl chain thiourea. Results from these studies of this receptor proved to be inconclusive. The Π-A isotherm of the receptor on water is shown in Figure 3.19a. The Π-A isotherm has a condensed region defined by a single phase and a liftoff point and collapse region that is consistent with

approximately a single alkyl chain species. The IRRAS spectra of the **S-thio** receptor on

water and 10 mM phosphate are shown in Figure 3.19b. The signature phosphate modes

that were present for the **U-guan⁺** and **U-thiouro⁺** receptors binding to phosphate are not

present for the **S-thio** receptor. This suggests that the receptor is not interacting with

phosphate. The water and 10 mM phosphate spectra are almost identical to each other

and do not indicate that there are interactions between the receptor and phosphate. This is

consistent with our results of the single chain guanidinium receptor **S-guan⁺** and the U-

shaped thiourea **U-thio**. The **S-thio** receptor might be forming interactions from

headgroup to headgroup via hydrogen bonding of the closely packed thiourea moieties,

similarly to what was observed for the **S-guan⁺** receptor. It is worth noting that the

neutral thiourea headgroup has demonstrated strong anion recognition capabilities

through the relatively acidic N-H's of the thiourea moiety.[195,237] There are also several

studies of thiourea receptors utilizing metal coordination to the sulfur to help make the N-

Hs a better hydrogen bond donor unit.[238,239] We did not explore these questions further

but could be the source of future research. This is an especially interesting topic as the

changing hydration environment at the air–water interface should have a pronounced

effect on the neutral species.
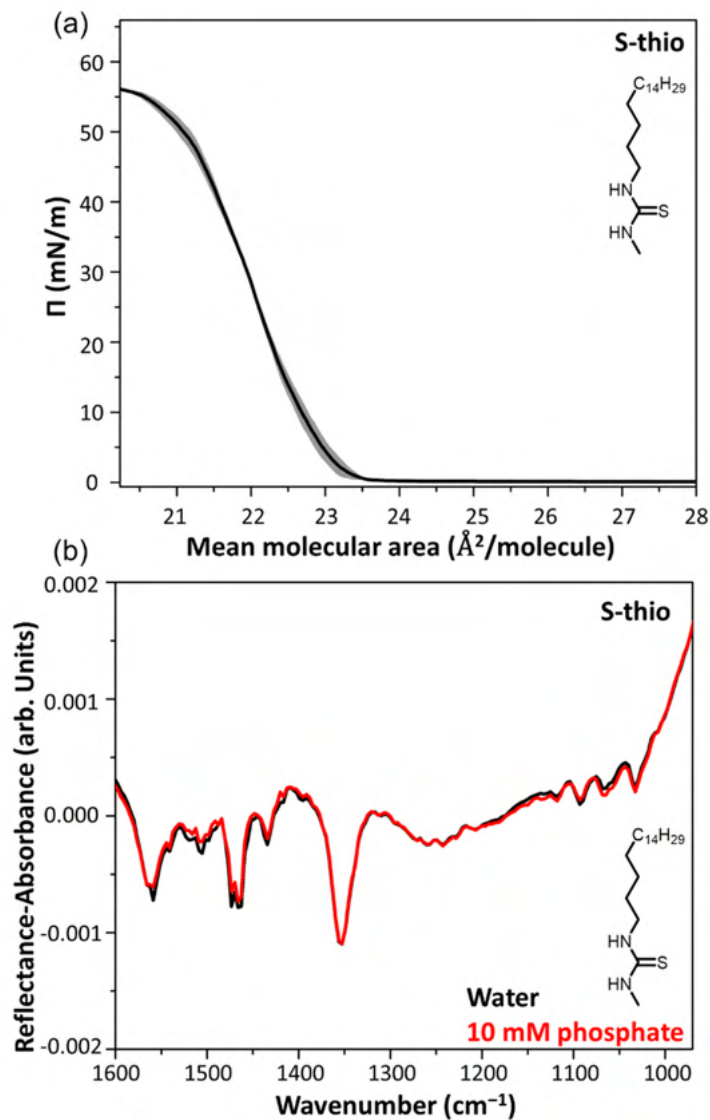
Figure 3.19 Π-A isotherms of (a) **S-thio** on water and (b) IRRAS spectra of **S-thio** on water and 10 mM phosphate at a constant $\Pi = 40$ mN/m.

3.4 Conclusion

We have used a homologous series of amphiphilic receptors to begin to unravel the driving forces for phosphate recognition at the air–water interface. The headgroups and number of alkyl chains were modulated to probe the different chemical and

superstructural features. The guanidinium **U-guan⁺** and thiouronium **U-thiouro⁺** receptors both bound to phosphate through electrostatically assisted hydrogen bonding interactions (chemical). The double alkyl chains of these receptors provided adequate spacing in the confined space of the monolayer surface. The **U-thio** and **S-guan⁺** did not interact with phosphate. The **U-thio** is uncharged and this demonstrates that electrostatically driven binding is an important design feature at the air–water interface. The **S-guan⁺** was the only single chain species tested and the receptor has increased headgroup to headgroup interactions in the condensed region due to the tighter packing of the alkyl chains (superstructural). The **U-thiouro⁺** interestingly underwent a structural change from gauche to trans upon phosphate addition which we attribute to reorganization of the bulky methyl group on the thiouronium headgroup (superstructural). Competition studies between phosphate and chloride revealed that the U-guan+ receptor is selective for phosphate over chloride by a factor of 1000 at low ionic strength conditions. At higher ionic strength ≥10 mM NaCl, there is considerable charge screening of the electrical double layer which weakens interactions (physical). The **U-thiouro⁺** receptor was less selective for phosphate than the **U-guan⁺** receptor (by only a factor of 10). Our results show that the chemical, physical, and supramolecular superstructural driving forces are important for the rational design of surface immobilized receptors. Results from this study advance the field of anion recognition and promote the use of the aqueous interface for its advances over traditional bulk solution studies.

Chapter 4. Specific ion effects for a guanidinium receptor anchored at the air–water interface
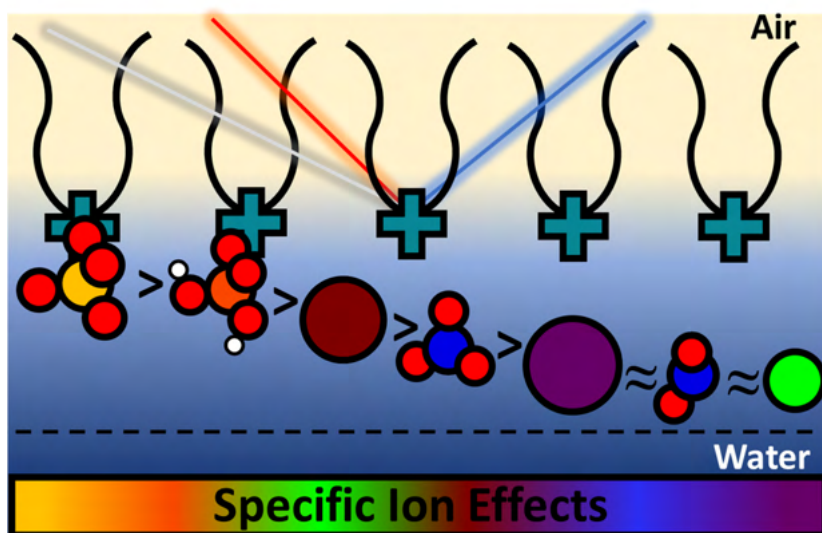
Figure 4.1 Schematic representation of the specific ion effects observed for the **U-guan$^+$** receptor at the air–water interface.

4.1 Introduction

Understanding ion effects at the air–water interface is important to better understand molecular recognition in sensing,[6364] environmental remediation,[5,65,66] and chemical separations[18,34,62] technologies. However, determining anion selectivity at the air–water interface is a non–trivial task that cannot be predicted using conventional bulk techniques.[65,66] Furthermore, predictions using Hofmeister, Collins' rules, or anion/size

dependences have also been found to break convention at the aqueous interface. The Hofmeister series originally provided a relative order of ions for their ability to precipitate egg white proteins but has since then been used to describe the physical phenomena beyond this. Hofmeister order the anion series from $SO_4^{2-} > H_2PO_4^- > Cl^- > Br^- > NO_3^- > I^-$ [230,231] Ions on the left of the series including sulfate have been found to be relatively depleted from the interface[164] whereas ions on the right of the series include iodide are enriched.[240] Molecular dynamics simulations coupled with surface tension and spectroscopic results have ordered anion propensity of the Hofmeister anions to the aqueous interface.[33,164,241] They found that the anions absorb in an inverse Hofmeister series in which iodide> nitrate> sulfate.[33,164]

Furthermore, one study found that combining a weakly and strongly hydrated anion has a nonadditive effect caused by the changing water affinity of the weakly hydrated anion in the mixed solution.[242] With all of this in mind, we seek to explore the interfacial regime of a guanidinium moiety anchored to the air–water interface. We find that this guanidinium receptor has specific ion effects, unrelated to the relative surface propensities of the anions or the dehydration energies.

Studies of bulk guanidinium ions have reported relatively weak hydration[243–246] with an Gibbs free energy of hydration of approximately -318 kJ/mol.[247] Based on surface tension results, the guanidinium ion is relatively excluded from the air–water interface where the single-ion partition coefficient (K_p) of guanidinium is 0.7 (for comparison a $K_p > 1$ indicates surface accumulation).[248,249] Interestingly, the water structure around the guanidinium ion is heterogenous and its structure at the air–water interface is strongly dependent upon orientation.[246,250] Collins' rule or the equal affinities hypothesis states

that species with closely matching hydration energies will bind to each other.[233] Based on this hypothesis and the dehydration energies the guanidinium anion as a representation for the **U-guan⁺** receptor, our receptor should bind to the anions in the order $Cl^- > NO_2^- > Br^- > NO_3^- > I^- > H_2PO_4^- > SO_4^{2-}$. Interestingly, we observe that the **U-guan⁺** receptor interacts with sulfate and phosphate the strongest based on our experimental results which contradicts the prediction using Collins' rule.

A guanidinium receptor has been previously described by Neal *et al.*[65] and was anchored to the air–water interface by two long octadecyl chains. The octadecyl groups act to organize the guanidinium receptor into a U-shaped packing arrangement and thus will be called **U-guan⁺** throughout this work. The **U-guan⁺** receptor is also relevant for the biochemistry community as it can serve as a model system for hindered arginine residue interacting with various anions.
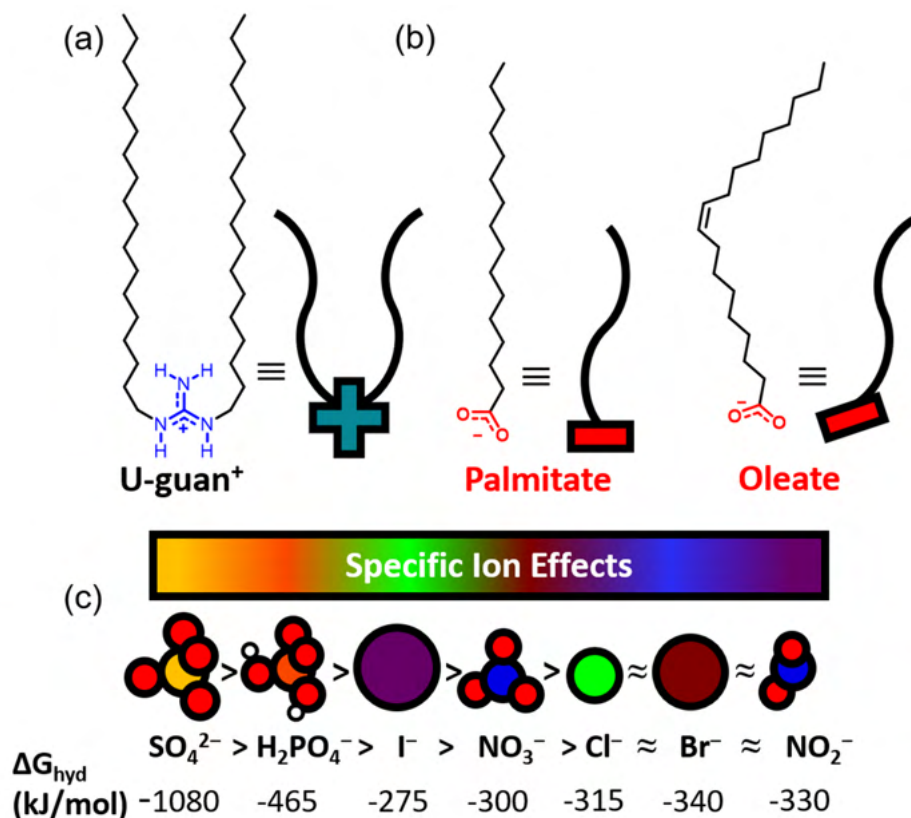
Figure 4.2 (a) Cartoon representation of the **U-guan$^+$** receptor, (b) cartoon representation of palmitate and oleate, (c) the observed ordering of anion selectivity for the **U-guan$^+$** receptor at the air–water interface.

4.2 Materials and Methods

4.2.1 Materials

The aqueous subphases used in this study were made using ultrapure water with a resistivity of 18.2 MΩ·cm (Milli-Q Advantage A10). Sodium phosphate monobasic monohydrate (Sigma, ≥99.5%), sodium nitrite (Fisher, certified ACS), sodium nitrate (Fisher, certified ACS), sodium iodide (Fisher, certified ACS), and sodium bromide (Acros, 99$^+$%, extra pure) were used as received. Sodium sulfate (Fisher, certified ACS) and sodium chloride (Fisher, certified ACS) were baked at 650 °C overnight prior to use.

The procedure to synthesize the **U-guan**[+] receptor has been previously described.[65] The receptor was dissolved in a 9:1 v/v mixture of chloroform (HPLC grade, Fisher) and methanol (HPLC grade, Fisher). Palmitic acid (Sigma, 99%) and oleic acid (Sigma,99%) were used as received and dissolved in chloroform.

4.2.2 Methods

4.2.2.1 Infrared Reflection Absorption Spectroscopy (IRRAS)

Infrared reflection absorption spectroscopy was conducted on a Perkin Elmer Frontier spectrometer with a liquid nitrogen cooled MCT (HgCdTe) detector. The IR spectrometer was modified with a custom–built gold mirror setup (mirror diameter 50.8 mm) to measure reflection off the monolayer surface. The incident angle was set to 48° relative to the surface normal. A Langmuir trough was used for all IRRAS spectra. The background spectrum was taken with the subphase of interest and then the **U-guan**[+] receptor was spread dropwise onto the aqueous surface. A constant surface pressure of 40 mN/m was used for all spectra and controlled using KSV software.

4.2.2.2 Vibrational Sum Frequency Generation Spectroscopy (VSFG)

The broadband sum frequency generation spectrometer used has been previously described.[251] Briefly, the output of a Ti:sapphire amplifier (Spitfire Ace, Spectra-Physics) is split in half and comprises the initial inputs for the visible and tunable IR beams. The IR beam is produced via an optical parametric amplifier (TOPAS-C, Light Conversion) coupled with a noncollinear difference frequency generator (NDFG, Light Conversion). The visible beam goes through an etalon and is overlapped temporally and spatially with the IR beam onto the aqueous sample. The sum frequency beam (SF) is

then directed into the spectrometer (IsoPlane SCT 320, Princeton Instruments) and a liquid nitrogen cooled CCD (PyLon, 1340×400 pixels, Princeton Instruments). The angles of the beam are as follows: SF angle is 52°, visible angle is 50°, and the IR angle is 60°. The spectra shown are the result of background subtraction and averaging two spectra with the standard deviation corresponding to the shaded region on the plots. We normalized our spectra to a reference spectrum of gold which was taken multiple times during the measurement to ensure system stability.

4.3 Results and Discussion
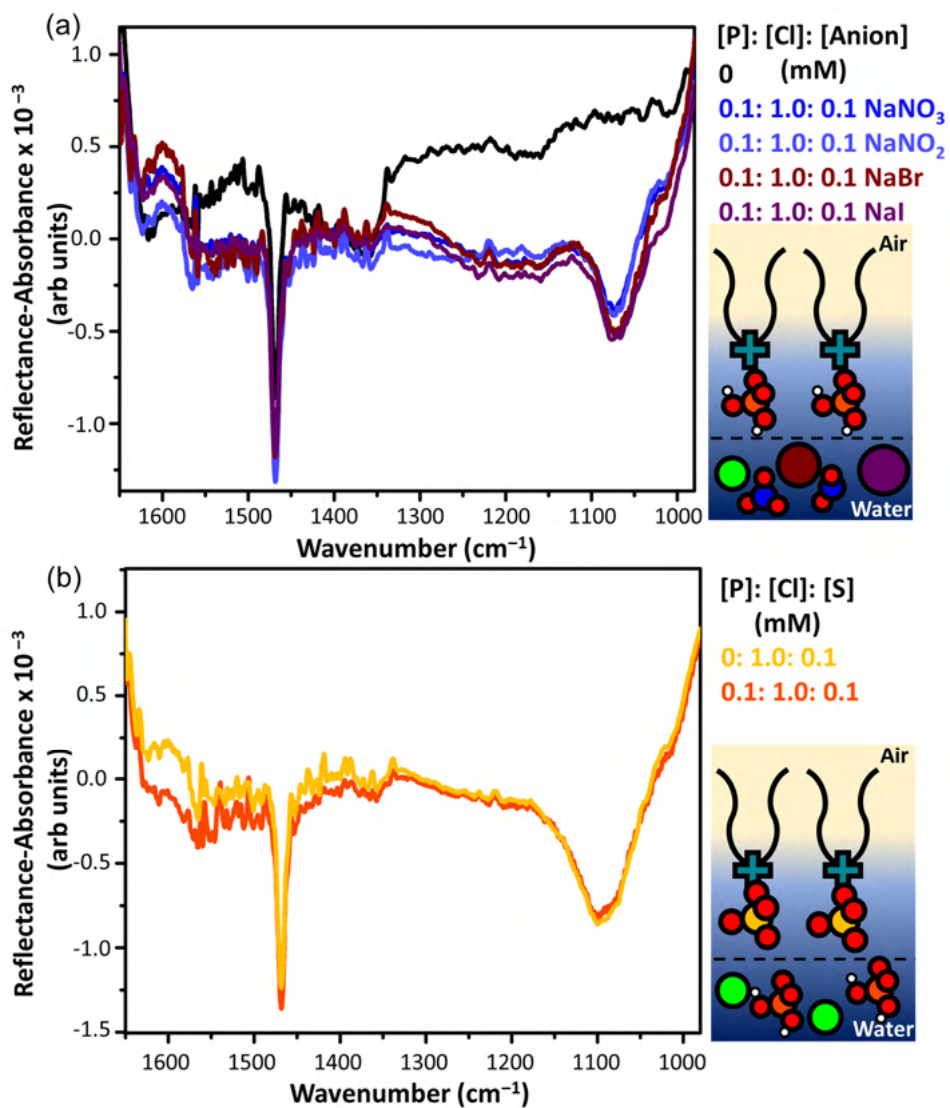
Figure 4.3 IRRAS spectra of the **U-guan**[+] receptor on (a) 1: 0.1: 1 equivalence of aqueous solutions of phosphate, chloride, and either nitrate, nitrite, bromide, or iodide showing the selectivity for the phosphate anion. (b) On solutions of sulfate and phosphate, the receptor is selective for sulfate over phosphate.

We desired to order the relative selectivity of a charged amphiphilic guanidinium receptor, **U-guan**[+] for a series of anions at the air–water interface. To do so, we used a combination of techniques including surface sensitive infrared reflection absorption spectroscopy (IRRAS) and surface specific vibrational sum frequency generation spectroscopy (VSFG) to further support our results.

The IRRAS spectra of the **U-guan**[+] receptor are shown in Figure 4.3. Molar equivalents of phosphate to chloride was maintained at 0.1 to 1 ratio while the anion of interest was also included in this mixture at a 1:1 ratio with phosphate. The spectra for the sodium salts of iodide, bromide, nitrate, and nitrite are shown in Figure 4.3a. We had previously demonstrated that the phosphate modes can be used to track binding interactions between the receptor and aqueous phosphate.[65] The phosphate modes at 1158 and 1074 cm^{-1} are assigned to phosphate's asymmetric (ν_{as} PO$_2$) and symmetric (ν_s PO$_2$) stretches and are indicative of receptor phosphate interactions.[201,202] The IRRAS spectra maintains the spectral features of phosphate with chloride, iodide, nitrate, and nitrite which suggests the receptor is selective towards phosphate over these competing anions (Figure 4.3a).
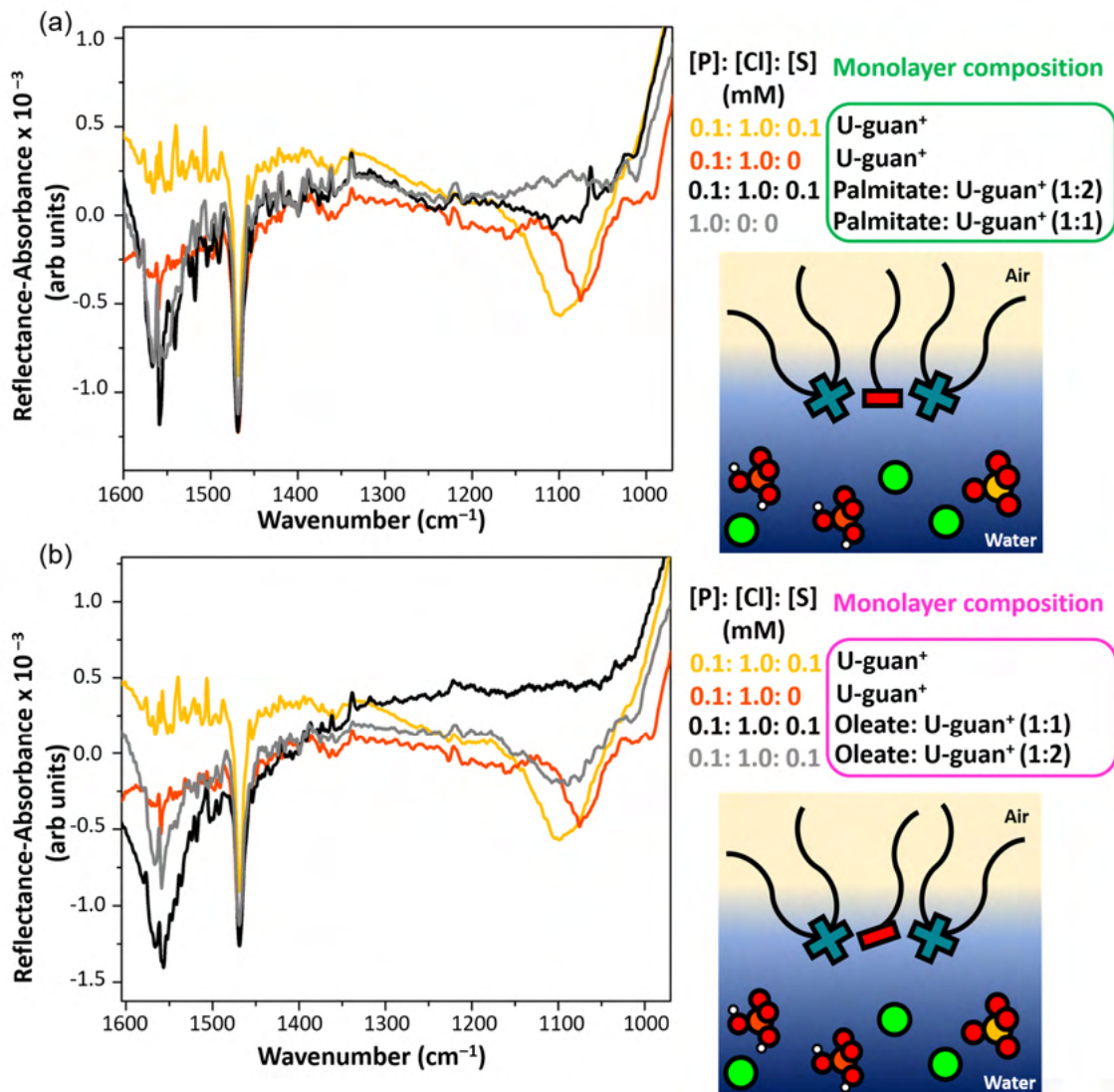
Figure 4.4 (a) Mixed monolayers of the **U-guan⁺** receptor with palmitate on phosphate, sulfate, and chloride and (b) mixed monolayers of the **U-guan⁺** receptor with oleate on phosphate, sulfate and chloride solutions.

However, upon addition of sodium sulfate, the spectra lose the characteristic phosphate modes and a strong peak centered at ~1096 cm^{-1} emerges. This broad peak at ~1096 cm^{-1} is assigned to the ν_{as} SO$_4^{2-}$. [252] At equal equivalence of phosphate and sulfate, the **U-guan⁺** receptor is more selective for sulfate than phosphate (Figure 4.3b). We

verified this by also measuring the spectra of **U-guan**[+] receptor on sulfate without phosphate and the spectra matches the one obtained with phosphate in solution.

Selectivity for phosphate over sulfate is achieved in biology through the phosphate binding protein.[253,254] This selectivity is due to the synergistic effects of phosphate hydrogen bonding with arginine (guanidinium moiety) and a nearby aspartate residue (carboxylate). The carboxylate moiety of aspartate acts as a hydrogen bond acceptor (not donor) and its -1 charge would repel a -2 sulfate anion but phosphate which serves as a hydrogen bond donor and acceptor has also been found to self-associate in its -1 state and is not as affected by this charge repulsion.[255–258] With this in mind, we sought to exploit the intermolecular interactions observed in the phosphate binding protein for our **U-guan**[+] receptor to achieve selectivity for phosphate over sulfate. Mixed monolayers of the **U-guan**[+] receptor with palmitate and oleate would provide an interfacial regime with both the guanidinium and carboxylate moieties necessary to mimic the protein binding pocket. The monolayer spreading solutions were premixed with the **U-guan**[+] receptor and palmitate or oleate at 1:1 or 1:2 equivalences. The oleate molecule was chosen due to its unsaturation and ability to expand the molecular monolayer more than palmitate, with the intent that this would help separate the **U-guan**[+] receptor from the mixed species. Figure 4.4 shows the results from this study on mixed monolayers of the **U-guan**[+] receptor with (a) palmitate and (b) oleate. At a 1:1 equivalence of the receptor with either palmitate or oleate, there is no evidence of interaction with the sulfate or phosphate in the aqueous solution. The phosphate and sulfate modes are not present and there is no other spectral evidence that the receptor or the palmitate and oleate are interacting with phosphate or sulfate. It is however likely that

the positive **U-guan⁺** receptor is aggregating with the negatively charged palmitate and oleate at the surface due to the close proximity of the carboxylate and guanidinium moieties. The peak at ~ 1542 cm^{-1} observed in both the palmitate and oleate spectra is the asymmetric carboxylate stretch (ν_{as} CO$_2^-$). The appearance of this mode and the lack of any phosphate or sulfate modes, suggests that the receptor is not interacting with sulfate or phosphate, but instead forming a hydrogen bonding network with the nearby carboxylate. Furthermore, upon mixing a 2:1 of the **U-guan⁺** receptor (2 equivalence) with one equivalence of either (a) palmitate and (b) oleate, a peak centered at ~1096 cm^{-1} begins to reappear. The reappearance of this peak suggests that the excess **U-guan⁺** receptor is interacting with sulfate. This peak is not as strong as in the spectrum of just the **U-guan⁺** receptor but this is because most of the **U-guan⁺** receptor is interacting with oleate or palmitate and only the excess **U-guan⁺** is interacting with sulfate.   Although we were not able to mimic the active site of the phosphate binding protein in these experiments, these results are still insightful. Based on this, we know that the carboxylate needs to be covalently linked to the guanidinium in order to prevent the aggregation that we observed with the mixed monolayers. Also, these results give further supporting evidence that the phosphate and sulfate modes that appear with the **U-guan⁺** receptor spectra are in fact due to the receptor interacting with these aqueous species. Therefore, these experiment on oleate and palmitate serve as control experiments for the earlier work shown.
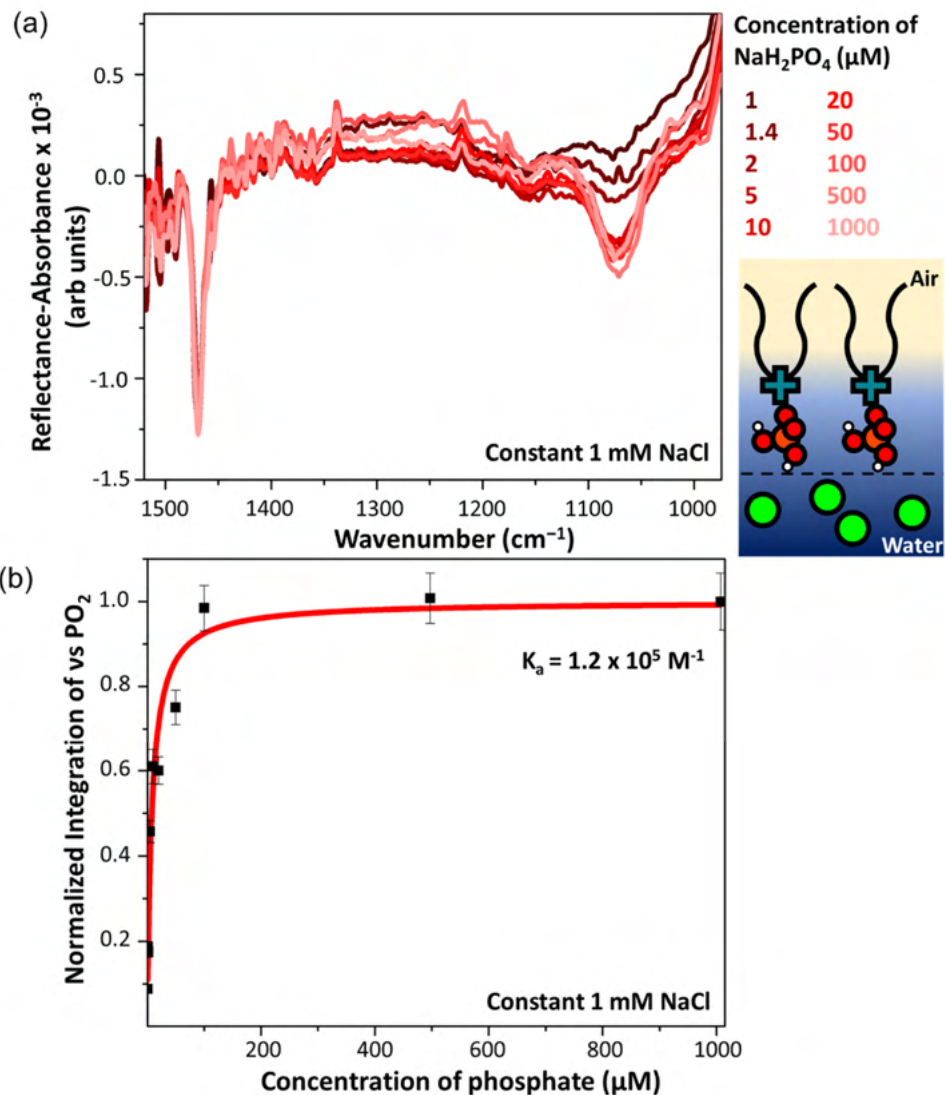
Figure 4.5 (a) IRRAS spectra of the **U-guan**[+] receptor on various concentrations of phosphate with 1 mM constant NaCl background concentration. (b) Langmuir-type fitting using the normalized integration of the $\nu_s PO_2^-$ mode with increasing phosphate. The calculated apparent binding affinity, K_a is 1.2×10^5 M^{-1}.

Although the receptor was shown to be more selective for sulfate over phosphate, we wanted to determine the apparent binding affinity for the **U-guan**[+] receptor towards phosphate because of the relevance of developing phosphate remediation receptors. Figure 4.5 shows the **U-guan**[+] receptor on a background concentration of 1 mM sodium

98

chloride with increasing concentrations of phosphate. The $\nu_s PO_2^-$ mode in particular shows a correlation with increasing phosphate and we used that mode to determine the apparent binding affinity for the receptor. A Langmuir type fitting was used after integrating the $\nu_s PO_2^-$ mode and normalizing it to the highest and lowest concentrations of phosphate tested. The apparent binding affinity for the **U-guan**$^+$ receptor to phosphate was found to be 1.2×10^5 M^{-1}. Previous work of guanidinium amphiphiles binding to adenosine triphosphate (ATP) and adenosine monophosphate (AMP) at the aqueous interface showed similarly high binding affinities of 1.7×10^7 M^{-1} and 3.2×10^6 M^{-1} for ATP and AMP respectively.[43] This was partly enhanced due multifunctional interactions at the binding event.[43,166]
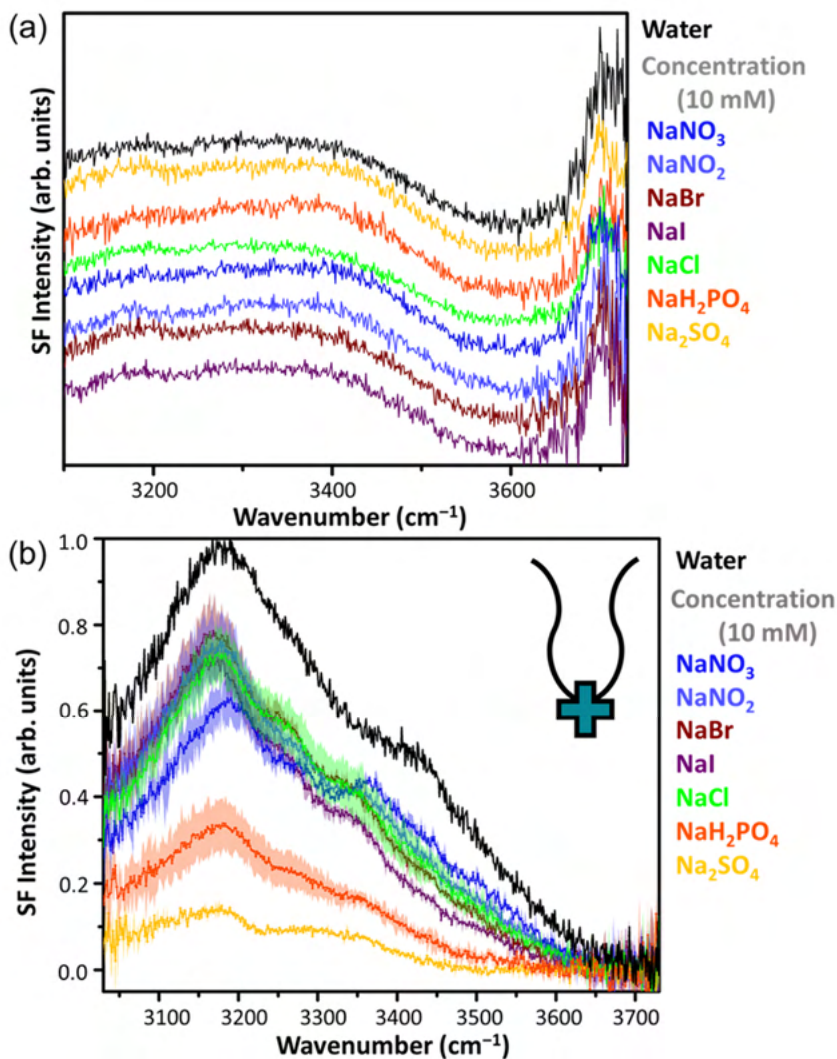
Figure 4.6 VSFG spectra in the *ssp* polarization combination of the (a) the bare aqueous solutions of NaNO₃, NaNO₂, NaBr, NaI, NaCl, NaH₂PO₄, and Na₂SO₄ at 10 mM concentration without the **U-guan⁺** receptor and (b) the **U-guan⁺** receptor at a constant monolayer density of 38 Å²/molecule on top of each aqueous subphase.

The results from the IRRAS showed that the **U-guan⁺** receptor is selective for

sulfate over phosphate, but the receptor is selective for phosphate over chloride, bromide,

nitrate, and nitrite. Our IRRAS results however do not allow us to order the relative

affinities of the anions to the **U-guan⁺** receptor. We know that the **U-guan⁺** receptor is

100

the most selective for sulfate followed by phosphate, but the other anions are group together without knowledge of their selectivity between each other. To order the rest of the anions, we needed to use vibrational sum frequency generation spectroscopy (VSFG). VSFG is a surface specific spectroscopic technique where the aqueous surface is selectively probed due to selection rules that allow only signal from non-centrosymmetric species. At the interface there is an inherent breakdown of centrosymmetry and therefore the interfacial molecules are probed.
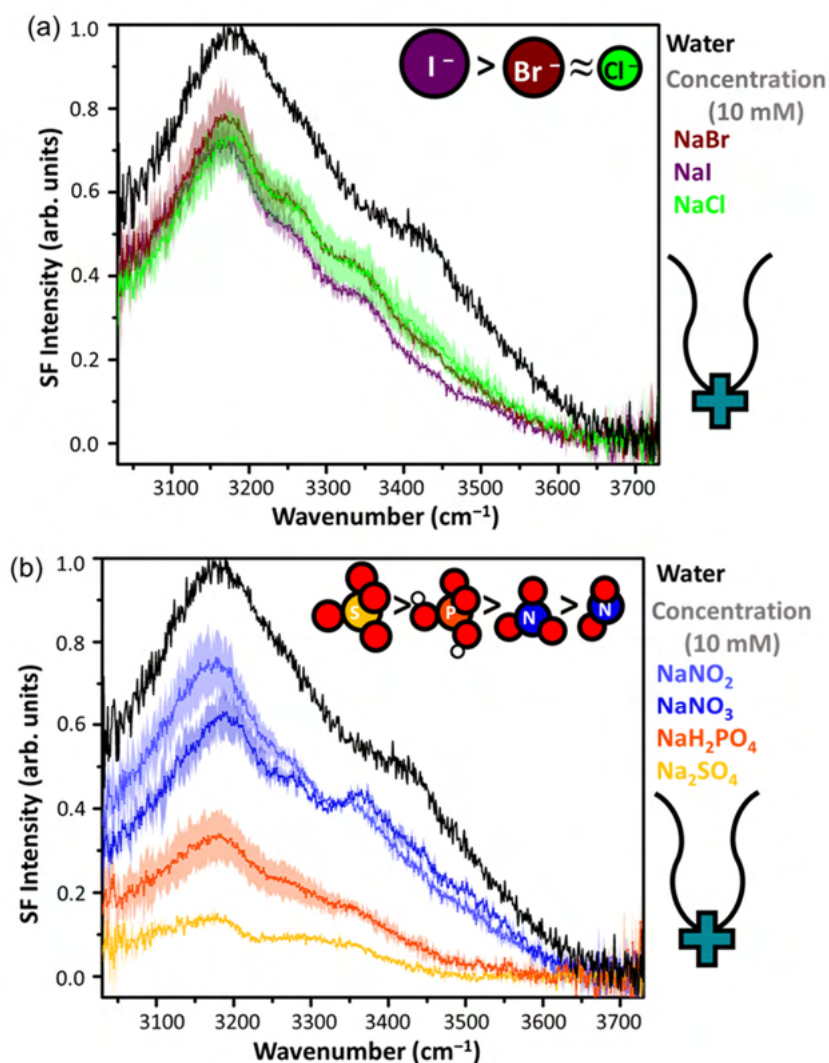
Figure 4.7 VSFG spectra of the **U-guan**$^+$ receptor on the (a) halide series studied bromide, iodide, and chloride, and (b) the sodium salts of the oxoanions nitrite, nitrate, phosphate, and sulfate.

The VSFG spectra were taken in the *ssp* polarization combination (*s*-SGF signal, *s*-visible, *p*-infrared) from ~3800 to 3000 cm^{-1}. The 10 mM aqueous subphases without the **U-guan**$^+$ receptor spectra match closely with the pure water spectrum (Figure 4.6a). We do not observe spectral features that lead to the anions coming up to the surface because the concentration is very low. Figure 4.6b shows the **U-guan**$^+$ receptor at a constant

102

molecular area of 38 Å^2/molecule on pure water and on 10 mM aqueous solutions of sulfate, phosphate, nitrate, nitrite, chloride, bromide, and iodide. Upon adding the **U-guan$^+$** receptor on top of pure water, we observe a significant enhancement in the water region. This increase in SF intensity is attribute to both the positive charge of the guanidinium moiety ordering the interfacial waters and also the vibrational mode of the v N-H on the **U-guan$^+$** receptor headgroup. Of all the anions tested, the positive **U-guan$^+$** receptor shows the strongest interactions with sulfate because we observed the largest changes in this spectrum. The water signal and N-H peaks are significantly diminished upon the **U-guan$^+$** receptor interacting with sulfate. Sulfate has been previously shown to act destructively on the water region with a fatty amine monolayer.[259] Interestingly, SFG spectra and MD stimulations of sodium sulfate and ammonium sulfate at high concentration (1 M) have shown that the sulfate anion is repelled from the aqueous interface, even further than the counter cations sodium or ammonium.[241,260] MD simulations revealed that the sulfate anion is so remarkably excluded from the interfacial region that there is a ~ 7 Å thick anion-free surface layer[241] and SFG spectra show an enhancement in the 3250 cm^{-1} peak corresponding to a thickening of the interfacial regime.[241,260] Based on the large dehydration penalty of sulfate (ΔG= -1080 kJ/mol) and the paucity of sulfate in the interfacial regime, we would predict that the **U-guan$^+$** receptor would interact the least with sulfate. Interestingly, this is not the case. It is clear that the **U-guan$^+$** receptor interacts the strongest with sulfate over phosphate, chloride, nitrate, nitrite, and iodide. However, sulfate was the only dianion tested and its strong interactions with the **U-guan$^+$** receptor can be rationalized by the high charge. The stabilizing intermolecular forces drive the sulfate- **U-guan$^+$** binding interactions due to

the –2 charge on the sulfate and its ability to act as a hydrogen bond acceptor to the positive guanidinium headgroup of the **U-guan$^+$** receptor. It is also reasonable to postulate that the binding stoichiometry of the sulfate to the guanidinium might not follow a 1:1 interaction but instead a 1:2 where two receptors are needed to bind with one sulfate. To better distinguish between the selectivity of the **U-guan$^+$** receptor, we separated the halide series shown in Figure 4.7a from the oxoanions which are shown in Figure 4.7b. The halide series does not alter the ~3192 cm^{-1} peak significantly whereas the phosphate and sulfate of the oxoanions shows a significant diminishing of this peak.

Clearly, the halide series shows much weaker binding affinity to the **U-guan$^+$** receptor than the oxoanion series. This could be attributed to the hydrogen bonding nature of the **U-guan$^+$** receptor which can act as a hydrogen bond donor to the oxygens on the oxoanions. It is however still challenging to break apart the ordering of the anions without further analysis. Figure 4.8 is the integrated region from 3098 to 3650 cm^{-1} showing the trend that we observed more clearly.
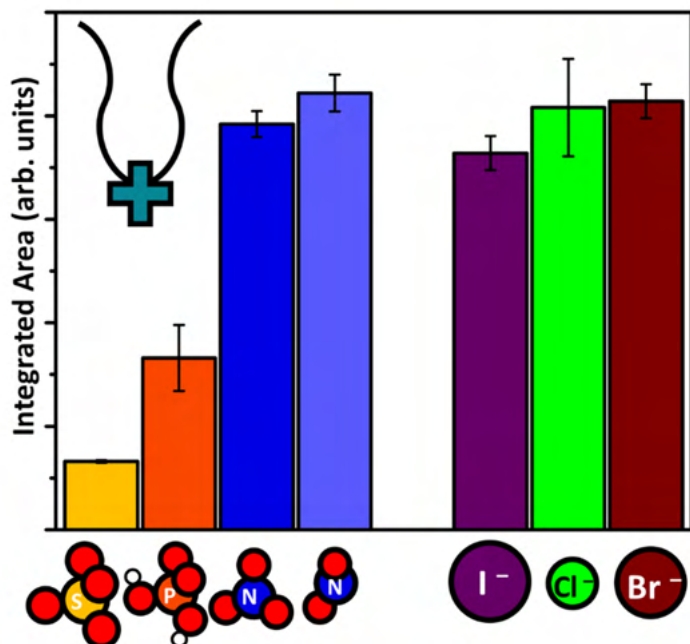
Figure 4.8 The integrated area in the water region for the **U-guan⁺** receptor on aqueous solutions of sulfate, phosphate, nitrate, nitrite, iodide, chloride, and bromide.

4.4 Conclusions

We observe specific ion effects for the **U-guan⁺** receptor binding to a series of anions at the aqueous interface. Using a combination of VSFG and IRRAS, we were able to quantitatively determine the anion selectivity for the **U-guan⁺** receptor. The receptor binds in the order of sulfate> phosphate> iodide> nitrate >chloride~ bromide~ nitrite. In attempts to achieve selectivity for phosphate over sulfate, mixed monolayers of **U-guan⁺** with palmitate or oleate were created. These mixed monolayers formed guanidinium-carboxylate interactions due to the close proximity in the molecular monolayer and therefore, the phosphate selectivity was not achievable. However, the **U-guan⁺** receptor binds extremely well to phosphate with an apparent binding constant of 1.2×10^5 M^{-1}.

(a)
U-guan⁺ receptor orders interfacial water molecules.

(b)
U-guan⁺ receptor is selective for the halides in the order ($I^- > Br^- \approx Cl^-$).

(c)
U-guan⁺ receptor is selective for the oxoanions in the order ($SO_4^{2-} > H_2PO_4^- > NO_3^- > NO_2^-$).
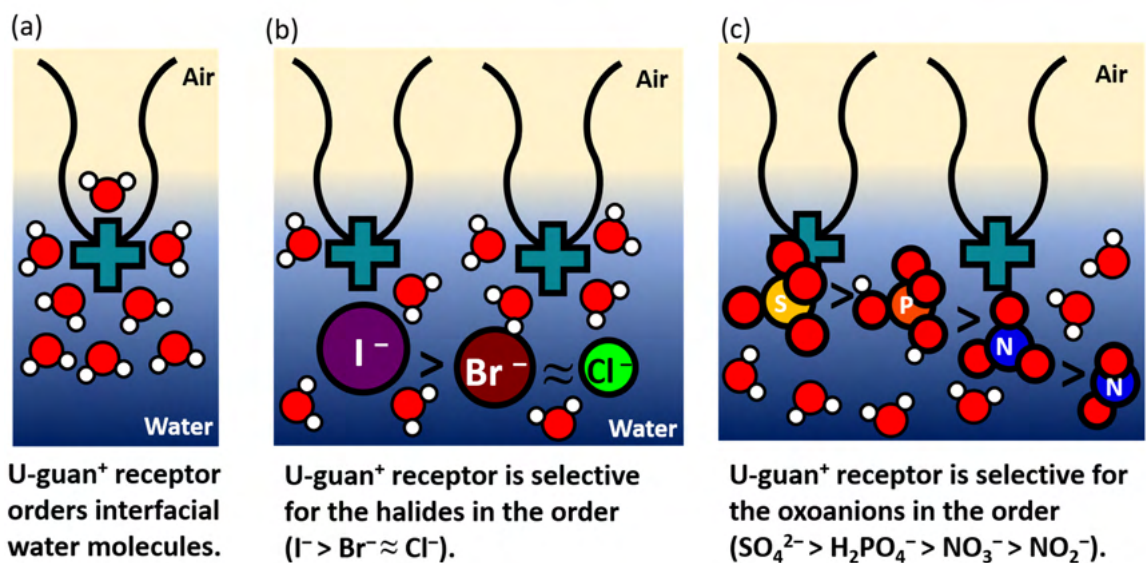
Figure 4.9 Schematic representation of the (a) **U-guan⁺** receptor ordering interfacial water molecules on pure water, (b) the **U-guan⁺** receptor showing selectivity for iodide> bromide ≈ chloride, and (c) the **U-guan⁺** receptor showing selectivity for sulfate > phosphate > nitrate > nitrite at the air–water interface.

Chapter 5. Competitive binding interactions for semi-soluble phosphoric and phosphonic acid species at aqueous interfaces

Abstract

Organic phosphates and phosphonate represent important yet understudied molecules in our chemical understanding of the ocean. We have selected a series of semi-soluble organic phosphonate and phosphate species to better understand the role of pH and sodium binding in surface activity. We chose to conduct this study in an acidic pH range to represent the aging process for sea spray aerosols. We found that increasing acidity and sodium chloride led to increased surface activity for the semi-soluble species. Consistently, the semi-soluble species was less surface active and desorbed into bulk solution with increasing pH without sodium chloride present. The phosphonate species was studied further to decipher the onset of the deprotonated species in a competition study between sodium complexation and acid-base equilibrium. Results reveal a critical sodium chloride concentration ≥ 2 M NaCl at pH 2 necessary to outcompete the acid-base protonation equilibrium. Our results demonstrate that ion pairing at the aqueous interface can shift these competitive processes towards the sodium complexed phosphonate and that this may be more relevant than pH in determining speciation. Our study helps to

better understand the competitive equilibria processes in an aged sea spray aerosol environment and the unique interfacial properties that drive these processes.
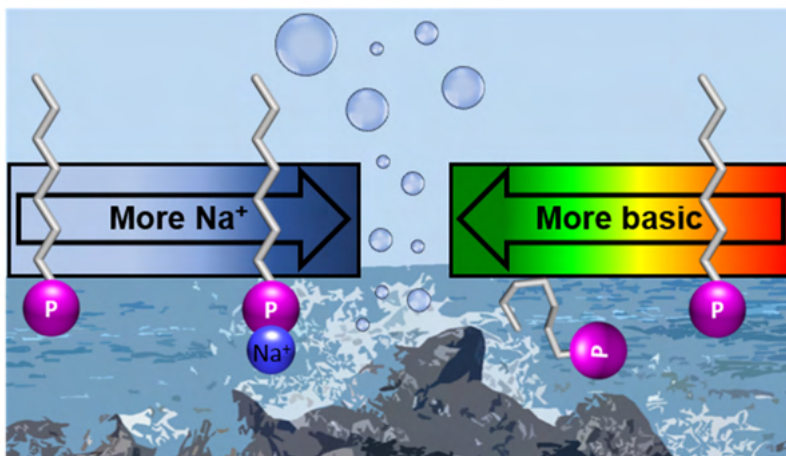
Figure 5.1 Schematic representation of the phosphonic acid and phosphonate equilibria occurring with increasing sodium chloride and pH.

5.1 Introduction

The aqueous interface provides a unique microenvironment that has been previously shown to shift acid-base equilibria,[261,262] alter the hydration state of ions,[16,17,93] and enhance binding affinities[43,65,66,167] relative to the bulk solution equivalent. We chose to study organic phosphoric and phosphonic acids at the aqueous interface in the low pH range (1 to 5.6) with increasing concentrations of sodium chloride. Our acidic model was selected to represent the aging process of sea spray aerosols (SSAs) where the local environment of aged SSAs can transcend a pH of 2.[263] Organic phosphoric and phosphonic acids are important yet understudied species in our molecular understanding ocean chemistry and SSAs, where both play a role in primary production as nutrients.[264,265] Interesting, the phosphonate species were found to have higher

proportions in surface waters than phosphates and this was attributed to the stability of

the C-P bond which is less susceptible to hydrolysis.[266,267]
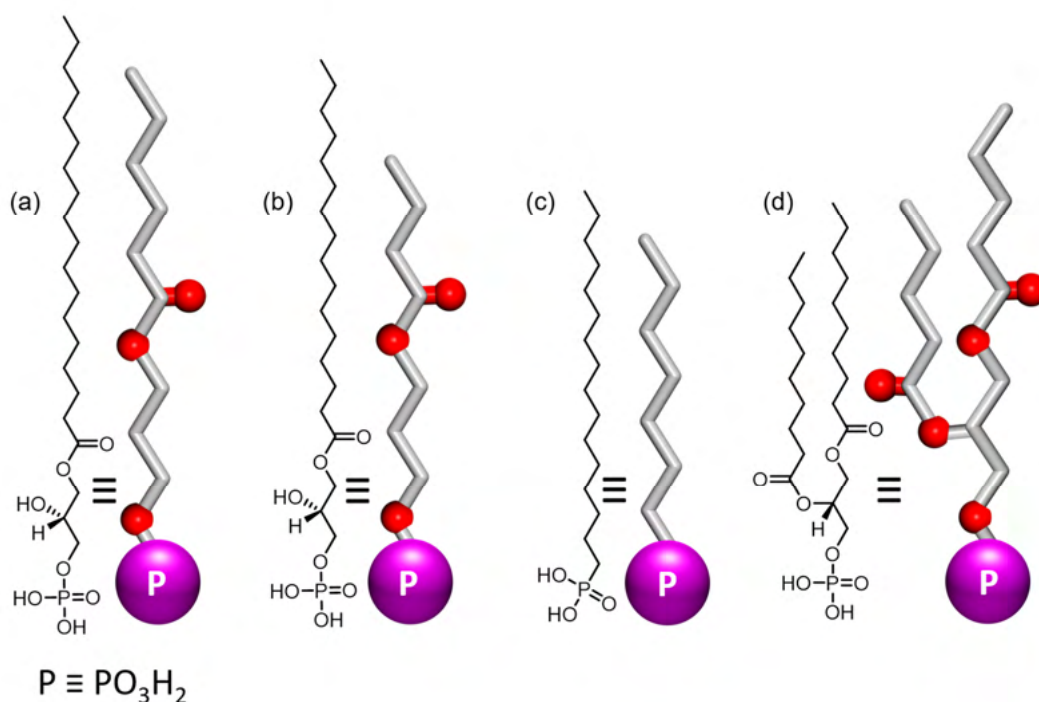
Figure 5.2 The structures of the semi-soluble species used in this study. (a) 1-stearoyl lysophosphatidic acid (C_{18} LPA), (b) 1-palmitoyl lysophosphatidic acid (C_{16} LPA), (c) hexadecylphosphonic acid (C_{16} phosphonic), (d) 1,2-didecanoyl-3-phosphatidic acid (didecanoyl PA). The hydroxyl groups were omitted in the schematic representations of C_{16} and C_{18} LPA for simplicity.

In this study we seek to explore the intermolecular interactions of these organic

phosphoric and phosphonic acids by studying them at the surface of acidic aqueous

solutions with and without the addition of sodium chloride. Figure 5.2 shows the

molecules used in this study in their fully protonated forms. We first determined their

protonation state qualitatively by tracking changes in surface pressure measurements with

varying pH. The surface pressure measurements showed a net desorption process for the deprotonated species which was found to occur in the low pH range studied between 1 and 5.6. Additionally, interfacial acid-base equilibria are still widely debated in the literature.[261,262,268–274] There are still questions over the apparent pKa shifts at the interface as compared to a bulk solution equivalent as well as whether the water interface is acidic, basic, or neutral.[273,275–278] To address these questions, previous studies of organic phosphoric and phosphonic acids at the aqueous interface revealed significant changes in the hydration structure and intermolecular interactions as the bulk pH environment changed.[87,279–281] In this study, we employ surface pressure area isotherms and infrared reflection absorption spectroscopy (IRRAS) to probe the changing speciation of the semi-soluble species as they changed from neutral to singly deprotonated. We demonstrate that changes in speciation has a profound impact in the surface activity of these phosphoric and phosphonic acids. This in turn would greatly affect the surface coatings of SSAs as the partitioning of molecules changes with proton and sodium chloride concentrations.

Besides the acid-base properties, we also seek to explore the concept of competitive equilibria at the air–water interface. The single chain phosphonic acid was used for this additional study but the results could also apply to other acidic semi-soluble species including organic phosphoric acids. Figure 5.3 shows the sodium phosphonate complexation equilibrium and the phosphonate and phosphonic acid equilibrium. Through constant addition of sodium chloride at pH 2, we can determine the concentration of sodium chloride necessary to outcompete the acid-base equilibrium and shift it towards the phosphonate species. We have resolved the concentration of sodium

(>2 M NaCl at pH 2) necessary to outcompete the acid-base protonation equilibrium and shift the phosphonic acid species towards the phosphonate-sodium bound complex. Our results demonstrate that sodium chloride can have a profound effect on the speciation by driving the equilibrium towards the deprotonated species.

This finding shows that the air–water interface has unique properties that should be considered in SSA modeling to accurately predict the surface composition as the pH of these aerosols change. The low dielectric constant at the aqueous interface (~2)[28] combined with the preorganization of a confined surface active species deeply affect the protonation state and sodium binding capabilities of these semi-soluble organic phosphoric and phosphonic acids. The results from this study give further insights into the molecular understanding of the stability, speciation, and sodium binding properties of model SSA interfaces and opens new avenues for research on SSAs and the competition binding equilibria that are present at these interfaces.
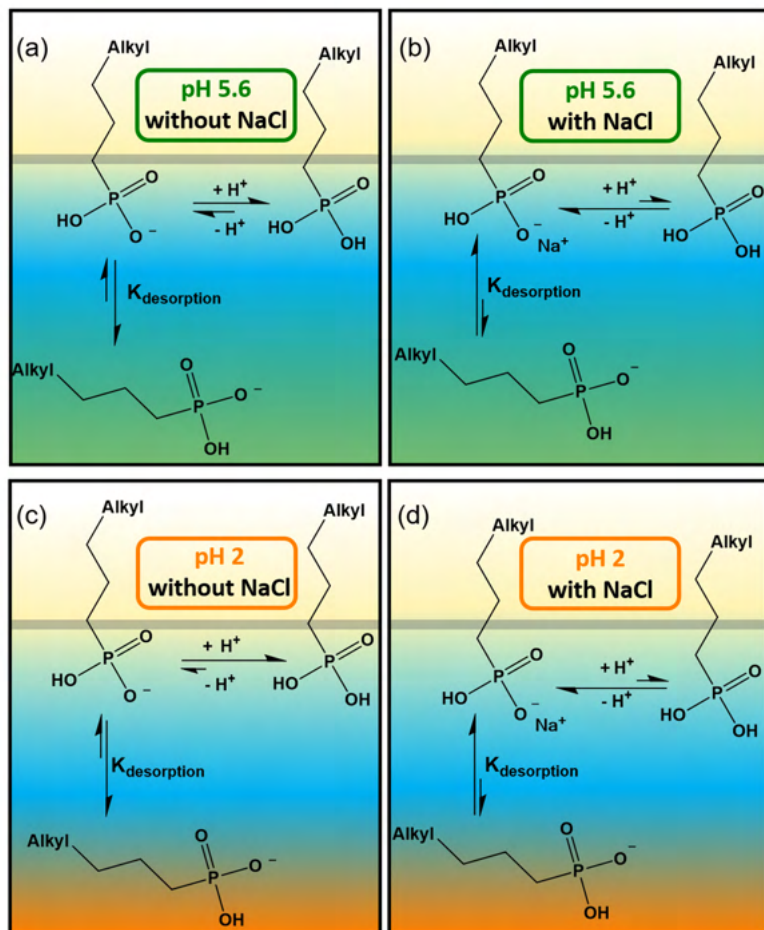
Figure 5.3 The competitive binding equilibria explored in this study. (a) The acid-base equilibrium without sodium chloride showing the phosphonate desorbing into bulk solution at increasing pH. (b) The acid-base equilibrium with sodium chloride showing the surface stability of the phosphonate-sodium complex. (c) The acid-base equilibrium at low pH showing the phosphonic acid species dominating the interfacial region. (d) The acid-base equilibrium at low pH showing the competition between sodium complexation and protonation state.

5.2 Materials and Methods
5.2.1 Materials

All the organic phosphonic and phosphoric acids were purchased in high purity and used without further purification. 1-palmitoyl-2-hydroxy-sn-glycero-3-phosphate sodium salt (>99%, Avanti Polar Lipids), 1,2-didecanoyl-sn-glycero-3-phosphate sodium salt (>99%, Avanti Polar Lipids), 1,2-dioctanoyl-sn-glycero-3-phosphate sodium salt (>99%,

Avanti Polar Lipids), and 1-stearoyl-2-hydroxy-sn-glycero-3-phosphate sodium salt

(>99%, Avanti Polar Lipids) were dissolved in a mixture of chloroform to methanol to

water at 65:35:8 (v/v/v) (HPLC grades, Fisher Scientific). The stock solutions of

hexadecylphosphonic acid (97%, Sigma Aldrich) and octadecylphosphonic acid (97%,

Sigma Aldrich) were dissolved in a mixture of 4:1 chloroform/methanol (v/v) and/or pure

chloroform (HPLC grade, Fisher Scientific). Sodium chloride (ACS certified, Fisher) was

baked at 650 °C for at least 10 hours prior to use to remove organic impurities as outlined

by Hua et al.[282] The pH was adjusted using hydrochloric acid (trace metal grade, Fisher

Scientific) in ultrapure water with a resistivity of 18.2 MΩ·cm (Milli-Q Advantage A10).

The pH of pure water and sodium chloride solutions was 5.6 due to the dissolved

atmospheric CO_2. The bulk pH values are referred to in their nearest integer value which

is within $\pm$ 0.25 pH units. All experiments were performed at ambient conditions (22.3 $\pm$

0.8 °C and a relative humidity of 38% $\pm$ 10%).

5.2.2   Surface pressure-area isotherms

The procedure for surface pressure-area isotherms has been previously described

elsewhere.[66] The semi-soluble species in their respective solvent solutions were spread

dropwise using a Hamilton micro-syringe onto the pH adjusted solutions in a Langmuir

trough (Biolin Scientific USA, Paramus, NJ). Delrin barriers compressed symmetrically

at a rate of 5 mm/min per barrier while the surface pressure was recorded using the

Wilhelmy plate method using pre-cut filter paper plates (Ashless grade, Whatman). All

isotherms were performed in at least triplet and processed with OriginLab software where

the average and standard deviation is shown as the solid line and shaded region,

respectively.

5.2.3   Infrared reflection absorption spectroscopy (IRRAS)

Infrared reflection–absorption spectroscopy (IRRAS) spectra were recorded on an

FTIR spectrometer (Frontier, Perkin Elmer, United States) equipped with a liquid

nitrogen cooled HgCdTe (MCT) detector. Petri dishes were placed inside the

spectrometer and the gold mirrors were optimized to collect the reflectivity at an incident

angle of 48° (relative to the surface normal). The IRRAS spectra are plotted as the

reflectance-absorbance which is the -$log\ (R_m/R_0)$ where R_m is the reflectivity off the

monolayer and R_0 is the reflectivity of the initial aqueous solution where in this case it is

water, pH adjusted water, or sodium chloride solutions.

5.2.4   Brewster angle microscopy (BAM)

The Brewster angle microscopy (BAM) microscope used was custom built. A 543

nm p-polarized laser was reflected off the aqueous surface at the Brewster angle and

images were collected by an Andor CCD camera. The final images were cropped from

their full size (800 μm x 800 μm) to (480 μm x 480 μm) to show the most resolved region

of the image and an artificial blue color scale was used to enhance the image contrast

(gray level range 1-100).

5.3 Results and Discussion
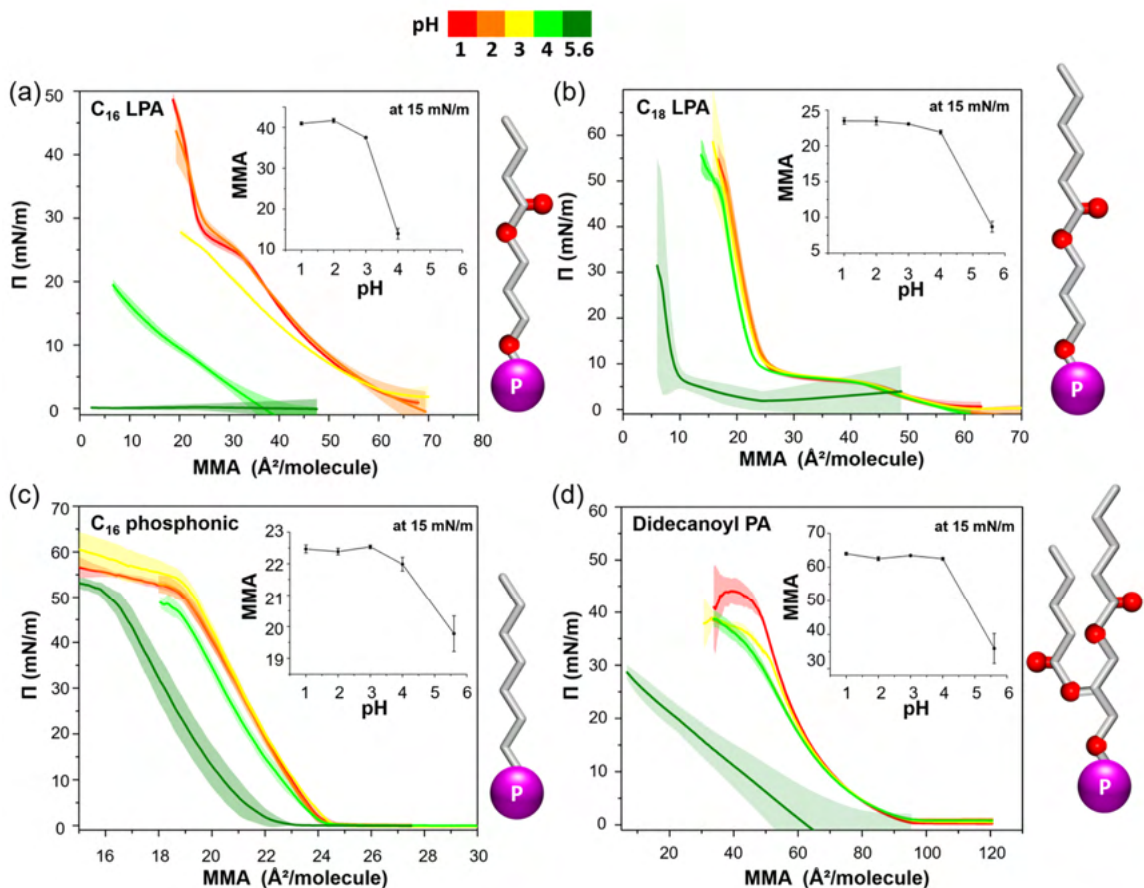
Figure 5.4 Surface pressure- area isotherms for the semi-soluble species at pH 1, 2, 3, 4, and 5.6 (a) C_{16} LPA, (b) C_{18} LPA, (c) C_{16} phosphonic, and (d) didecanoyl PA. The insets are the apparent mean molecular areas taken at a surface pressure of 15 mN/m and show the net loss of the surface molecules at increasing pH.

To access the relative protonation state of the semi-soluble organic phosphoric and phosphonic acid species, we first employed surface pressure-mean molecular area isotherms as a method to track surface activity. Figure 5.4 shows the isotherms at pH 1, 2, 3, 4, and 5.6 in which there is a net loss of the surface-active species at increasing pH. The net loss of the monolayer is observed as a lowering of the apparent mean molecular area. In this case, the apparent mean molecular area describes the lowering of the mean

molecular area as the molecules desorb into the bulk solution. The insets on Figure 5.4 show the apparent mean molecular areas at a surface pressure of 15 mN/m. Clearly, the onset of the deprotonated species is observed in the low pH range studied. The desorption of the C_{16} LPA shows a sharp drop in the apparent MMA between pH 3 and 4 while the C_{18} LPA desorption occurs between pH 4 and 5.6. The combination of the two methylene units rendering the molecule less soluble with the changes in packing structure. As the chain length increases and there is a tighter molecular packing arrangement, the phosphate headgroups are also closer together. It is more difficult to deprotonate a phosphoric headgroup that is arranged in a hydrogen bonding network with neighboring phosphoric acids.[272,283] The C_{18} phosphonic acid and dioctanoyl PA were also tested but these molecules did not result in a semi-soluble species. Figure 5.5 shows the Π-A isotherms for the C_{18} phosphonic on pH 3 and pH 5.6 where an expansion in MMA is observed. This expansion is at first perplexing because the size of the deprotonated, negative phosphonate is larger than the neutral phosphonic acid. However, the C_{18} phosphonate is a better hydrogen bonding acceptor than the neutral C_{18} phosphonic acid species. Therefore, at higher pH (pH 5.6) the molecules are hydrogen bonding to each other, and the area per molecule in the monolayer is condensed due to this. This also indicates that the pKa for the C_{18} phosphonic acid is above 3 and likely close to 5.6. Previous studies of C_{18} phosphoric acid and partially protonated fatty acids also ascribed the monolayer condensing as a result of increasing headgroup-headgroup interactions.[98,279,284]
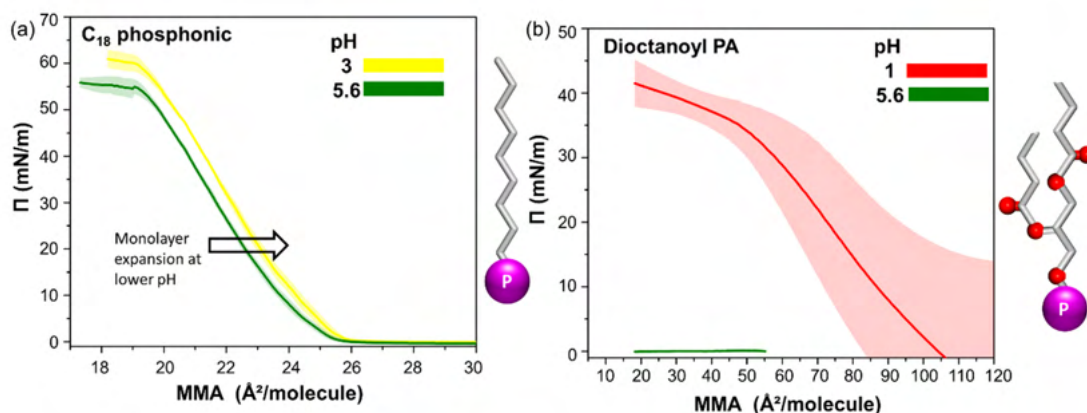
Figure 5.5 Surface pressure-mean molecular area isotherms for (a) C_{18} phosphonic acid at pH 3 and 5.6 and (b) dioctanoyl PA at pH 1 and pH 5.6.

The dioctanoyl PA was far too soluble and did not show a rise in surface pressure at pH 5.6 (Figure 5.5). The dioctanoyl PA showed a variable monolayer and inconsistent liftoff points even at pH 1. It is reasonable to assume that at pH 1 the dioctanoyl PA species should be fully protonated given the pK_{a1} of phosphoric acid in water is ~2.2.[285] Comparing to dioctanoyl PA to the didecanoyl PA, there is a noticeable different in the isotherms by lengthening each alkyl chain by two methylene units. The didecanoyl PA has a much larger liftoff point than what would be reasonably expected for a higher packed molecular monolayer. The liftoff point is approximately 98 $Å^2$/molecule at pH 1 for didecanoyl PA and is greater than 105 $Å^2$/molecule at pH 1 for the dioctanoyl PA species. For reference, the dihexadecanoyl PA (DPPA) has a liftoff point of approximately 47.5 $Å^2$/molecule.[87]
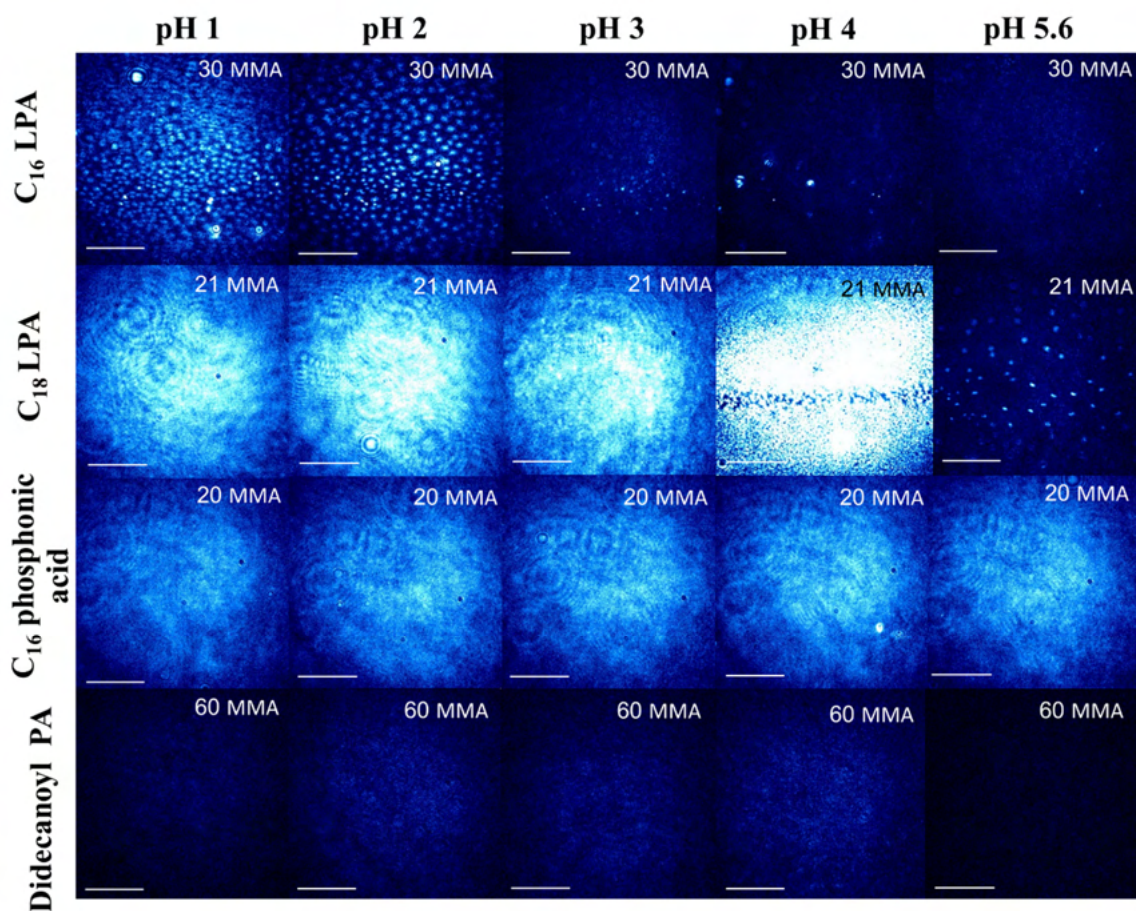
Figure 5.6 Brewster angle microscopy images of (a) C_{16} LPA, (b) C_{18} LPA, (c) C_{16} phosphonic, and (d) didecanoyl PA at pH 1, 2, 3, 4, and 5.6. The scale bar represents 50 μm.

The Brewster angle microscopy (BAM) images of these molecules are shown in Figure 5.6. BAM domain structures are intimately linked with a balance of line tension and long range electrostatic forces.[286–288] The intermolecular interactions between the semi-soluble molecules and the molecules with the aqueous solutions influences the domain structures. The morphologically changes of the monolayer packing is nicely illustrated by observing different packing arrangements using BAM at various pH as the

118

speciation changes. There are changes in the brightness and domain structures upon pH

changes. Interestingly, the BAM images of the C_{16} LPA and C_{18} LPA are very different.

At pH 1, we observe small circular domains for the C_{16} LPA species while the C_{18} LPA is

more of a homogenous sheet. Figures 5.7 and 5.8 show the C_{16} LPA and C_{18} LPA

species at different pH values during multiple MMAs during the isotherm. Clearly there

is a dramatic effect on the packing structures of these species as the speciation (and pH)

change. The alkyl chain dispersion forces must also play an influential role in the

packing as the C_{16} LPA and C_{18} LPA species only differ by two methylene units and the

domain structures are different for these two species.
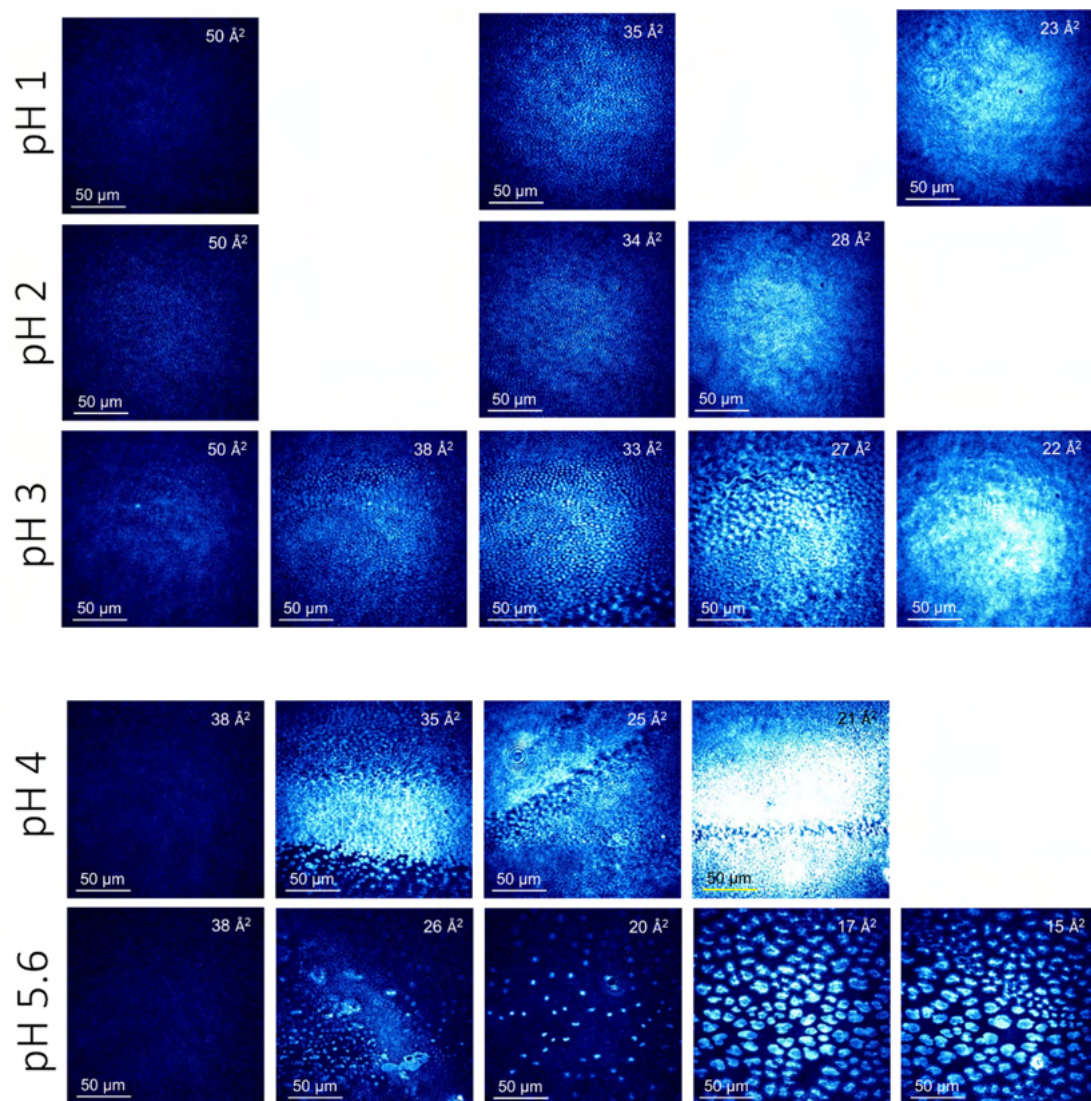
Figure 5.7 BAM images of C_{18} LPA from pH 1 to 5.6 at multiple MMAs through the Π-A isotherm.
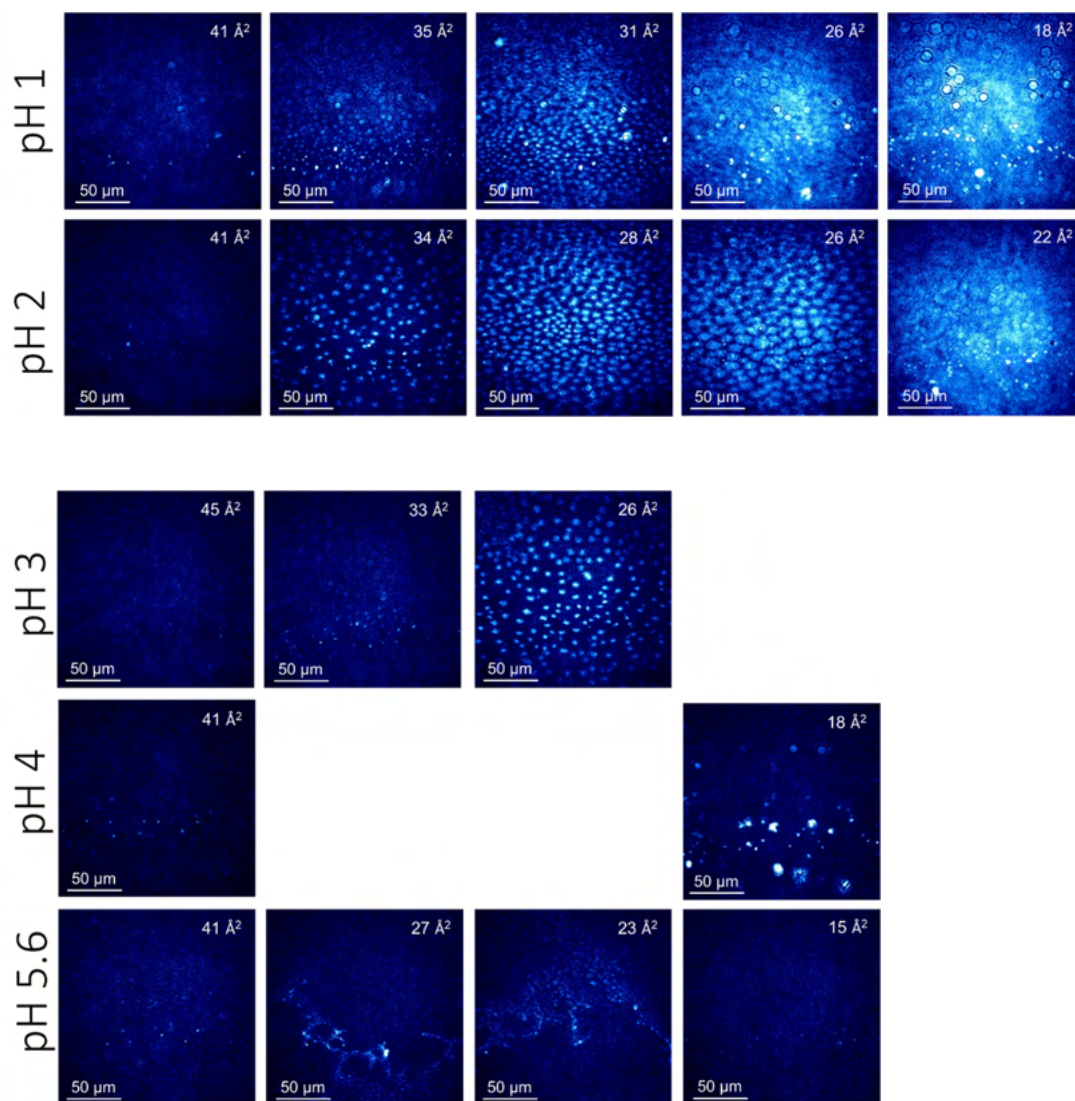
Figure 5.8 BAM images of C_{16} LPA from pH 1 to 5.6 at multiple MMAs through the Π-A isotherm.

Consistent with the earlier result from Π-A isotherms and BAM, the infrared reflection absorption spectra shown in Figure 5.9 show a net loss of the semi-soluble species at pH 5.6. Our results show that the onset of the deprotonation event occurs in the

low pH range studied here. Clearly, the onset of the deprotonated semi-soluble species is
occurring in the pH range chosen for this study.
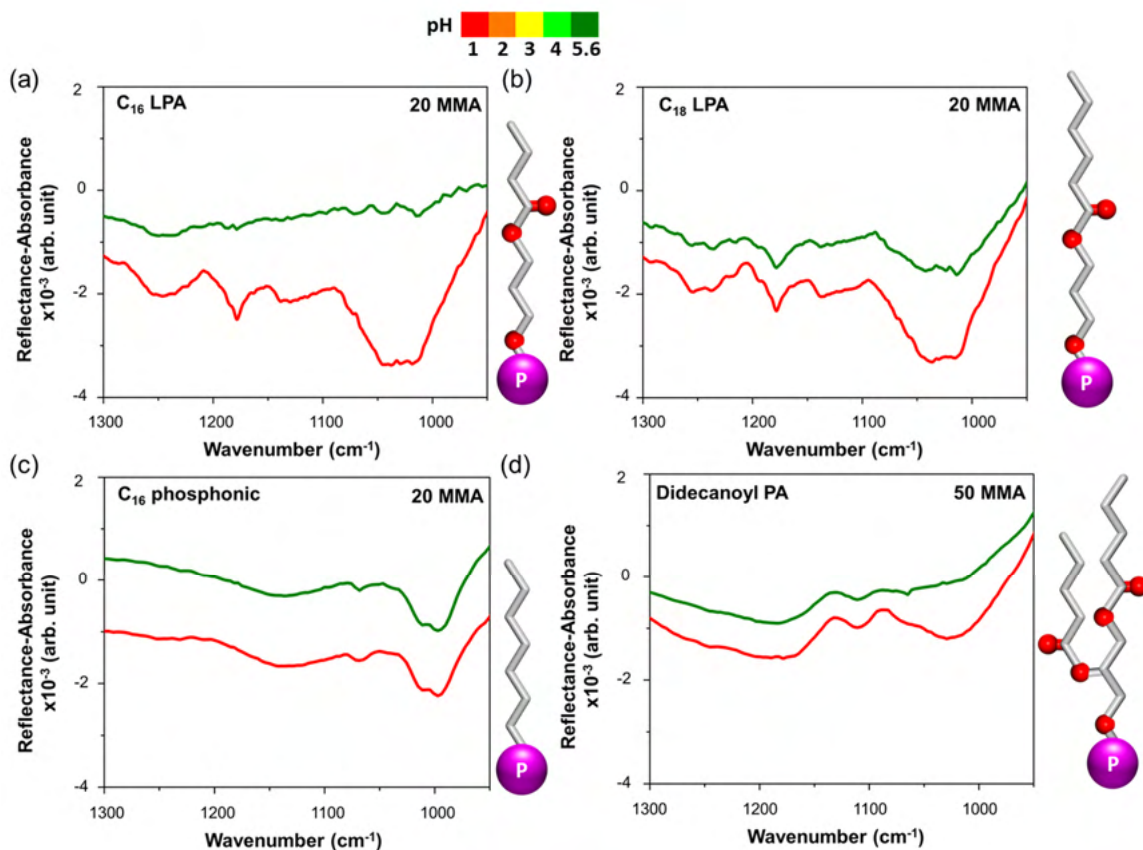
Figure 5.9 IRRAS spectra at pH 1 and pH 5.6 for the (a) C_{16} LPA at 20 MMA, (b) C_{18}
LPA at 20 MMA, (c) C_{16} phosphonic at 20 MMA, and (d) didecanoyl PA at 50 MMA.

We also wanted to determine the role of sodium in driving the semi-soluble
species back to the interface through stabilizing electrostatic binding interactions. Figure
5.10 shows the Π-A isotherms of the semi-soluble species on 0.1 M NaCl at pH 5.6. The
addition of sodium chloride acts to restore the monolayer and there is a drastic difference
between the isotherms with and without salt. Sodium ions bind strongly to the phosphate

and phosphonate species through electrostatic interactions. Previous studies have shown that electrostatic binding interactions are very strong driving forces for noncovalent interactions in the low dielectric constant regime at the aqueous interface.[65,66] The final part of this study was designed to look at the competitive binding equilibria between protonation and sodium complexation.
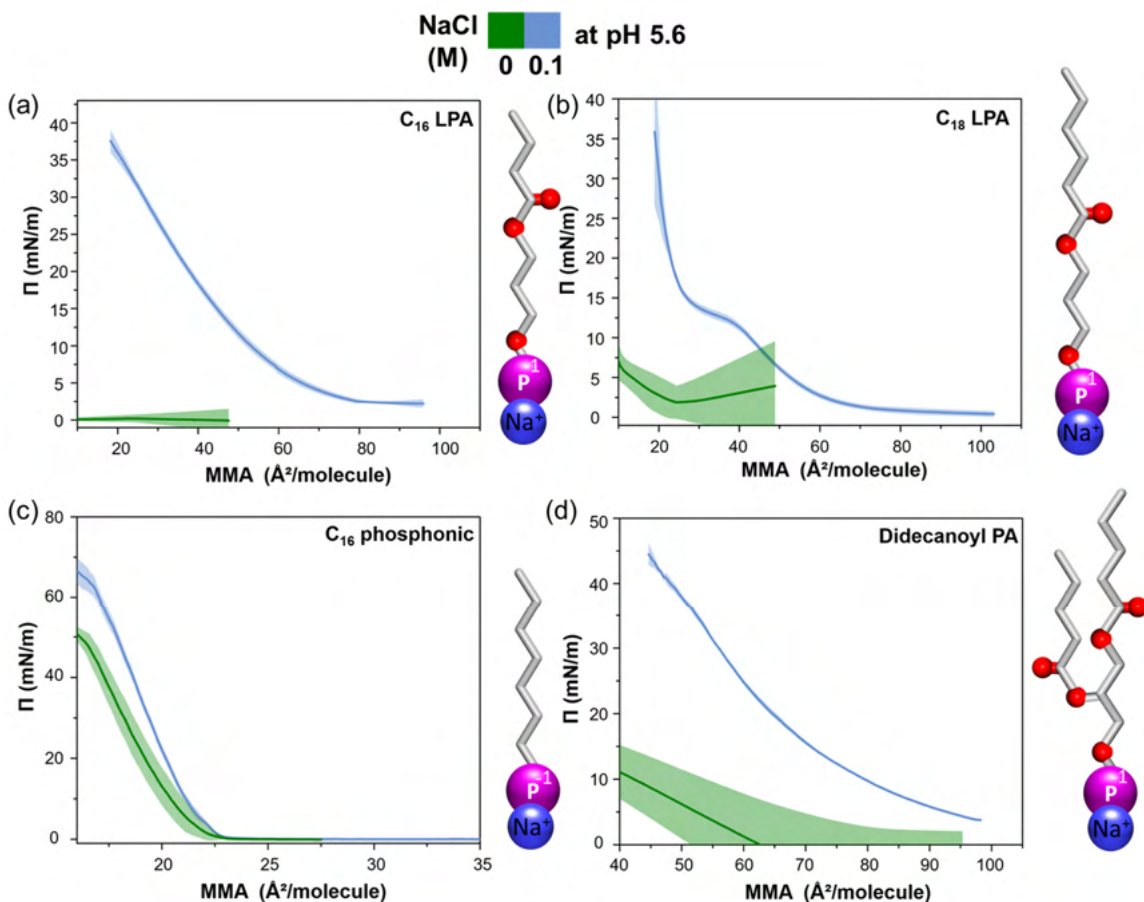
Figure 5.10 Surface pressure-area isotherms at pH 5.6 with no sodium chloride and with 0.1 M sodium chloride for the (a) C_{16} LPA, (b) C_{18} LPA, (c) C_{16} phosphonic, and (d) didecanoyl PA semi-soluble species. The low concentration of sodium chloride acts to restore the surface activity of the semi-soluble species by forming stabilizing electrostatic interactions.

Results from this study show that at low pH where the molecular monolayer is fully protonated, sodium can begin to shift this by influencing the acid-base speciation. This is extremely important in model systems of sea spray aerosols where changes in pKa can affect surface activity predictions. We used the C_{16} phosphonic acid for the model system to interrogate the effect of increasing sodium chloride concentrations on the acid-base equilibrium. Figure 5.11 shows the IRRAS spectra of the C_{16} phosphonic acid at pH 2 and pH 5.6. There are some significant changes observed in these spectra with increasing sodium chloride concentrations. The peak at 942 cm^{-1} is assigned to the symmetric phosphonate stretch, ν_s (O=P-O$^-$) which only begins to appear with increasing sodium concentrations. This mode is especially diagnostic to determine the speciation as it is not present in the spectrum at pH 2. The phosphonate bending mode at 998 cm^{-1} δ(POH) is also diagnostic because it undergoes a red shift upon sodium addition. The phosphonate species forms electrostatically stabilized ion pairing with the negative phosphonate and positive sodium ions. We see this shift even at a pH of 2 in which the sodium is driving the neutral phosphonic acid species towards the phosphonate-sodium complex.
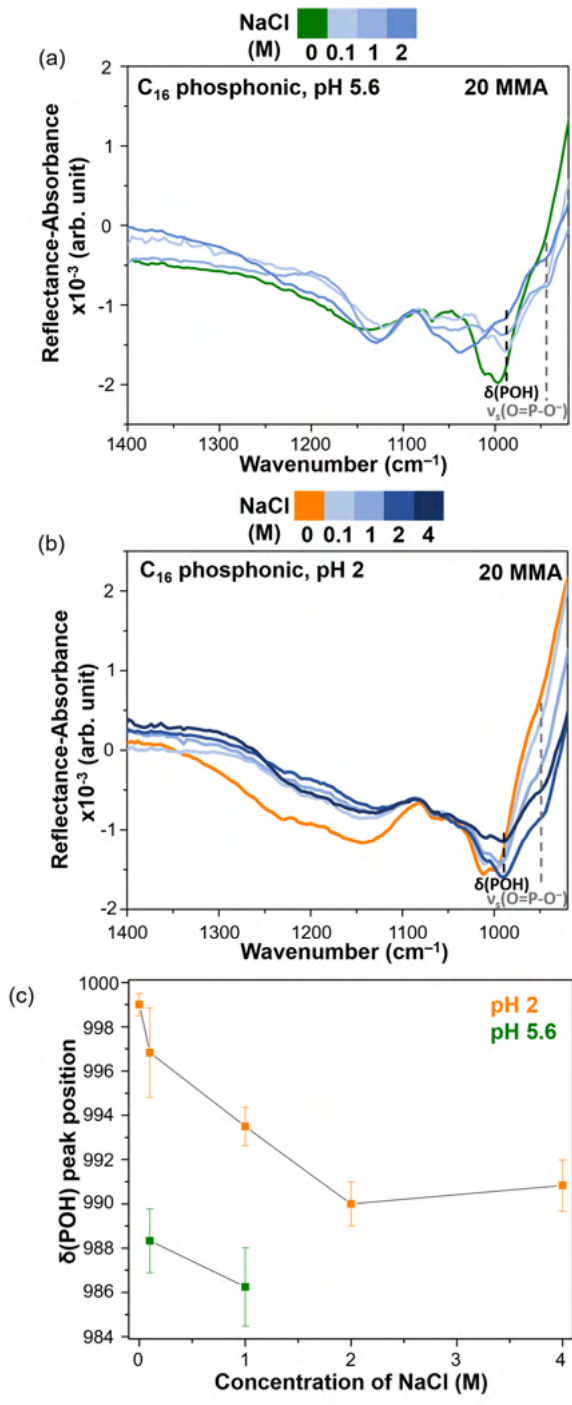
Figure 5.11 (a) The C16 phosphonate species binding to sodium at pH 5.6, (b) at pH of 2, sodium begins to shift the speciation, (c) the normalized peak position of the δ(POH) mode with sodium addition

Upon normalizing the peak position of the phosphonate bending mode δ(POH) to the lowest and highest values ("0" corresponds to the peak position at pH 2 without NaCl and "1" corresponds to the peak position at pH 5.6 with 1 M NaCl). From this normalization, it is more clearly seem that the precipice of the phosphonate-sodium complexation begins at concentrations >0.1 M NaCl and becomes saturated at ≥2 M NaCl at pH 2.
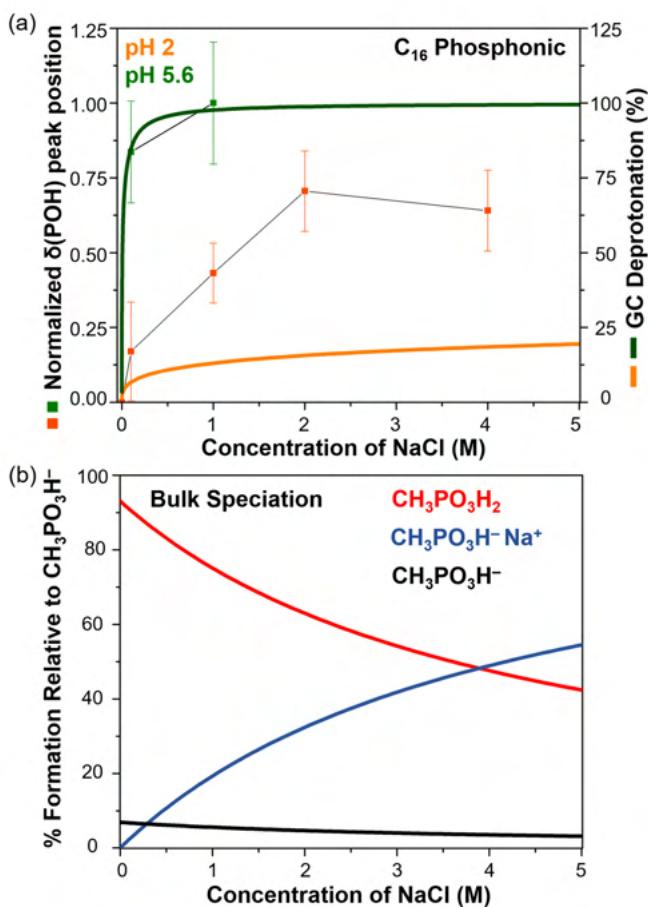
Figure 5.12 (a) The normalized peak position of the δ(POH) mode at pH 2 and pH 5.4 on the left axis and the predicted speciation based on the Gouy Chapman (GC) model (pK_a= 2.13, pH 2 and pH 6) on the right axis. (b) Bulk equilibria of methylphosphonic acid using HySS software.

The presence of sodium chloride is highly influential for the speciation of the C_{16} phosphonic acid species. Figure 5.12 shows the protonation state predictions using Gouy Chapman model modified with the Grahame equation.[289,290] The model can be used to calculate deprotonation (α) with increasing sodium chloride concentrations, $[NaCl]_\infty$.

$$\frac{A_M}{\alpha e} \sinh\left[\frac{1}{2}\left(ln[H^+]_\infty - lnK_a - ln\left(\frac{1-\alpha}{\alpha}\right)\right)\right] = (8\varepsilon\varepsilon_0 kT[NaCl]_\infty)^{-1/2}$$

In this equation, A_M is the mean molecular area (20 Å^2 per phosphonate molecule), e is the elementary charge, K_a is the acid dissociation constant (pK_a= 2.13), ε is the dielectric constant of water, ε_0 is the permittivity of free space, and k is the Boltzmann constant. The results using the theoretical predictions are consistent with our results at pH 5.6. However, the model fails to recognize the importance of high concentrations of sodium chloride at low pH. Therefore, the Gouy Chapman model begins to break down at high concentrations and low pH in an overall high ionic strength environment.

Bulk speciation was predicted using HySS software[291] for the soluble methylphosphonic acid species. These predictions show that it takes concentrations exceeding 4 M sodium chloride to begin to outcompete the acid-base equilibrium at a pH of 1. Clearly, bulk speciation cannot be used to explain the surface relevant results that we observed.
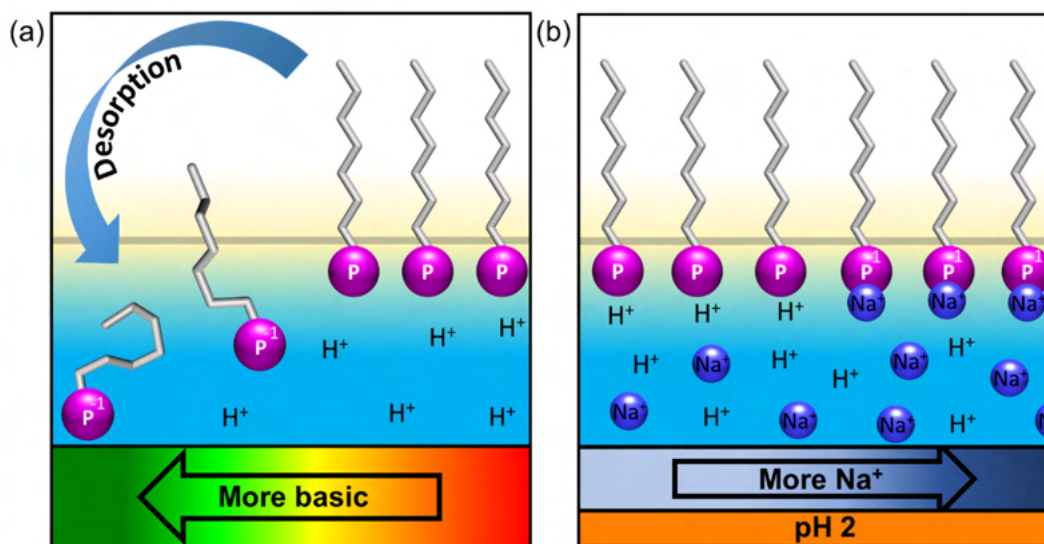
Figure 5.13 Schematic representation of (a) the C_{16} phosphonic desorbing into bulk solution at increasing pH and (b) the competitive equilibria between pH and sodium chloride concentrations at low pH.

5.4 Conclusion

Competitive equilibrium at the aqueous interface is an important concept for sea spray aerosol modeling. Our results reveal that low concentrations of sodium chloride and acidic conditions (pH 1 to 5.6) greatly affect the surface activity for semi-soluble phosphoric and phosphonic acids. This suggests that during an aerosol aging process, more species could partition to the interface and affect the lifetime. The phosphonic acid species was studied further in a competition study between protonation and sodium complexation. We have discovered that there is a critical concentration of sodium chloride (≥ 2 M NaCl at pH 2) necessary to shift the equilibria towards the phosphonate-sodium complex. The concentration of sodium can be more influential than pH to determine the protonation state, contrarily to what might be expected an acidic semi-soluble species.

References

(1)   Kubik, S. Anion Recognition in Water. *Chem. Soc. Rev.* **2010**, *39* (10), 3648–3663.

(2)   Langton, M. J.; Serpell, C. J.; Beer, P. D. Anion Recognition in Water: Recent Advances from a Supramolecular and Macromolecular Perspective. *Angew. Chem. Int. Ed.* **2016**, *55* (6), 1974–1987.

(3)   Pal, S.; Ghosh, T. K.; Ghosh, R.; Mondal, S.; Ghosh, P. Recent Advances in Recognition, Sensing and Extraction of Phosphates: 2015 Onwards. *Coord. Chem. Rev.* **2020**, *405*, 213128.

(4)   Liu, Y.; Sengupta, A.; Raghavachari, K.; Flood, A. H. Anion Binding in Solution: Beyond the Electrostatic Regime. *Chem* **2017**, *3* (3), 411–427.

(5)   Cremer, P. S.; Flood, A. H.; Gibb, B. C.; Mobley, D. L. Collaborative Routes to Clarifying the Murky Waters of Aqueous Supramolecular Chemistry. *Nat. Chem.* **2018**, *10*, 8–16.

(6)   Dragan, A. I.; Read, C. M.; Crane-Robinson, C. Enthalpy–Entropy Compensation: The Role of Solvation. *Eur. Biophys. J.* **2017**, *46* (4), 301–308.

(7)   Schalley, C. A. *Analytical Methods in Supramolecular Chemistry*; Wiley, 2012.

(8)   Shimoyama, D.; Haino, T. Entropy-Driven Cooperativity in the Guest Binding of an Octaphosphonate Bis-Cavitand. *Chem. – A Eur. J.* **2019**, *n/a* (n/a).

(9)   Cram, D. J. The Design of Molecular Hosts, Guests, and Their Complexes (Nobel

Lecture). *Angew. Chem. Int. Ed. Engl.* **1988**, *27* (8), 1009–1020.

(10)   Cram, D. J. Preorganization—From Solvents to Spherands. *Angew. Chem. Int. Ed. Engl.* **1986**, *25* (12), 1039–1057.

(11)   Neal, T. A.; Wang, W.; Zhiquan, L.; Peng, R.; Soni, P.; Xie, H.; Badjić, J. D. A Hexavalent Basket for Bottom-Up Construction of Functional Soft Materials and Polyvalent Drugs through a "Click" Reaction. *Chem. – A Eur. J.* **2019**, *25* (5), 1242–1248.

(12)   Wang, L.; Neal, T.; Chen, S.; Badjić, J. D. Multivalent and Photoresponsive Assembly of Dual-Cavity Baskets in Water. *Chem. – A Eur. J.* **2017**, *23* (37), 8829–8833.

(13)   Liu, Y.; Zhao, W.; Chen, C.-H.; Flood, A. H. Chloride Capture Using a C–H Hydrogen Bonding Cage. *Science* **2019**, eaaw5145.

(14)   Steed, J. W.; Turner, D. R.; Wallace, K. *Core Concepts in Supramolecular Chemistry and Nanochemistry*; Wiley, 2007.

(15)   Mohsen-Nia, M.; Amiri, H.; Jazi, B. Dielectric Constants of Water, Methanol, Ethanol, Butanol and Acetone: Measurement and Computational Study. *J. Solution Chem.* **2010**, *39* (5), 701–708.

(16)   Flores, S. C.; Kherb, J.; Cremer, P. S. Direct and Reverse Hofmeister Effects on Interfacial Water Structure. *J. Phys. Chem. C* **2012**, *116* (27), 14408–14413.

(17)   Allen, H. C.; Casillas-Ituarte, N. N.; Sierra-Hernández, M. R.; Chen, X.; Tang, C. Y. Shedding Light on Water Structure at Air–Aqueous Interfaces: Ions, Lipids, and Hydration. *Phys. Chem. Chem. Phys.* **2009**, *11* (27), 5538–5549.

(18)   Uysal, A.; Rock, W.; Qiao, B.; Bu, W.; Lin, B. Two-Step Adsorption of $PtCl_6^{2-}$

Complexes at a Charged Langmuir Monolayer: Role of Hydration and Ion Correlations. *J. Phys. Chem. C* **2017**, *121* (45), 25377–25383.

(19)   Schwan, H. P.; Takashima, S.; Miyamoto, V. K.; Stoeckenius, W. Electrical Properties of Phospholipid Vesicles. *Biophys. J.* **1970**, *10* (11), 1102–1119.

(20)   Demchak, R. J.; Fort, T. Surface Dipole Moments of Close-Packed Un-Ionized Monolayers at the Air-Water Interface. *J. Colloid Interface Sci.* **1974**, *46* (2), 191–202.

(21)   Sakurai, M.; Tamagawa, H.; Inoue, Y.; Ariga, K.; Kunitake, T. Theoretical Study of Intermolecular Interaction at the Lipid−Water Interface. 1. Quantum Chemical Analysis Using a Reaction Field Theory. *J. Phys. Chem. B* **1997**, *101* (24), 4810–4816.

(22)   Vogel, V.; Möbius, D. Hydrated Polar Groups in Lipid Monolayers: Effective Local Dipole Moments and Dielectric Properties. *Thin Solid Films* **1988**, *159* (1), 73–81.

(23)   Westwell, M. S.; Bardsley, B.; Dancer, R. J.; Try, A. C.; Williams, D. H. Cooperativity in Ligand Binding Expressed at a Model Cell Membrane by the Vancomycin Group Antibiotics. *Chem. Commun.* **1996**, No. 5, 589–590.

(24)   Abed, A. El; Faure, M. C.; Hamdani, M.; Guittard, F.; Billard, J.; Peretti, P. Molecular Orientation in a Semi-Fluorinated Alkane Monolayer Spread at the Air-Water Interface. *Mol. Cryst. Liq. Cryst. Sci. Technol. Sect. A. Mol. Cryst. Liq. Cryst.* **1999**, *329* (1), 283–292.

(25)   Doyle, E. L.; Hunter, C. A.; Phillips, H. C.; Webb, S. J.; Williams, N. H. Cooperative Binding at Lipid Bilayer Membrane Surfaces. *J. Am. Chem. Soc.*

2003, *125* (15), 4593–4599.

(26)   Yang, Z.; He, Y.; Lee, J. H.; Chae, W.-S.; Ren, W. X.; Lee, J. H.; Kang, C.; Kim,
          J. S. A Nile Red/BODIPY-Based Bimodal Probe Sensitive to Changes in the
          Micropolarity and Microviscosity of the Endoplasmic Reticulum. *Chem. Commun.*
          2014, *50* (79), 11672–11675.

(27)   Xiao, H.; Li, P.; Zhang, W.; Tang, B. An Ultrasensitive Near-Infrared Ratiometric
          Fluorescent Probe for Imaging Mitochondrial Polarity in Live Cells and in Vivo.
          Chem. Sci. **2016**, *7* (2), 1588–1593.

(28)   Fumagalli, L.; Esfandiar, A.; Fabregas, R.; Hu, S.; Ares, P.; Janardanan, A.; Yang,
          Q.; Radha, B.; Taniguchi, T.; Watanabe, K.; et al. Anomalously Low Dielectric
          Constant of Confined Water. *Science* **2018**, *360* (6395), 1339–1342.

(29)   Jordan, J. H.; Gibb, C. L. D.; Wishard, A.; Pham, T.; Gibb, B. C. Ion–Hydrocarbon
          and/or Ion–Ion Interactions: Direct and Reverse Hofmeister Effects in a Synthetic
          Host. *J. Am. Chem. Soc.* **2018**, *140* (11), 4092–4099.

(30)   Okur, H. I.; Hladílková, J.; Rembert, K. B.; Cho, Y.; Heyda, J.; Dzubiella, J.;
          Cremer, P. S.; Jungwirth, P. Beyond the Hofmeister Series: Ion-Specific Effects on
          Proteins and Their Biological Functions. *J. Phys. Chem. B* **2017**, *121* (9), 1997–
          2014.

(31)   Jungwirth, P.; Cremer, P. S. Beyond Hofmeister. *Nat. Chem.* **2014**, *6* (4), 261–263.

(32)   DeWalt-Kerian, E. L.; Kim, S.; Azam, M. S.; Zeng, H.; Liu, Q.; Gibbs, J. M. PH-
          Dependent Inversion of Hofmeister Trends in the Water Structure of the Electrical
          Double Layer. *J. Phys. Chem. Lett.* **2017**, *8* (13), 2855–2861.

(33)   Tobias, D. J.; Hemminger, J. C. Getting Specific About Specific Ion Effects.

Science **2008**, *319* (5867), 1197–1198.

(34)   Lovering, K.; Nayak, S.; Bu, W.; Uysal, A. The Role of Specific Ion Effects in Ion Transport: The Case of Nitrate and Thiocyanate. *J. Phys. Chem. C* **2020**, *124* (1), 573–581.

(35)   Sakurai, M.; Tamagawa, H.; Furuki, T.; Inoue, Y.; Ariga, K.; Kunitake, T. A Theoretical Interpretation of Remarkable Enhancement of Intermolecular Binding at the Lipid-Water Interface. *Chem. Lett.* **1995**, *24* (11), 1001–1002.

(36)   Tamagawa, H.; Sakurai, M.; Inoue, Y.; Ariga, K.; Kunitake, T. Theoretical Study of Intermolecular Interaction at the Lipid− Water Interface. 2. Analysis Based on the Poisson− Boltzmann Equation. *J. Phys. Chem. B* **1997**, *101* (24), 4817–4825.

(37)   Ikeura, Y.; Kurihara, K.; Kunitake, T. Molecular Recognition at the Air-Water Interface. Specific Binding of Nitrogen Aromatics and Amino Acids by Monolayers of Long-Chain Derivatives of Kemp's Acid. *J. Am. Chem. Soc.* **1991**, *113* (19), 7342–7350.

(38)   Kawahara, T.; Kurihara, K.; Kunitake, T. Cooperative Binding of Adenine via Complementary Hydrogen Bonding to an Imide Functionalized Monolayer at the Air-Water Interface. *Chem. Lett.* **1992**, *21* (9), 1839–1842.

(39)   Kunitake, T. Molecular Recognition at the Air-Water Interface and Two-Dimensional Molecular Organization —Supermolecules Project in Kurume. *Supramol. Sci.* **1996**, *3* (1), 45–51.

(40)   Taguchi, K.; Ariga, K.; Kunitake, T. Multi-Site Recognition of Flavin Adenine Dinucleotide by Mixed Monolayers on Water. *Chem. Lett.* **1995**, *24* (8), 701–702.

(41)   Oishi, Y.; Torii, Y.; Kuramori, M.; Suehiro, K.; Ariga, K.; Taguchi, K.; Kamino,

A.; Kunitake, T. Two-Dimensional Molecular Patterning through Molecular Recognition. *Chem. Lett.* **1996**, *25* (6), 411–412.

(42) Cha, X.; Ariga, K.; Kunitake, T. Multi-Site Binding of Aqueous Dipeptides by Mixed Monolayers at the Air-Water Interface. *Chem. Lett.* **1996**, *25* (1), 73–74.

(43) Sasaki, D. Y.; Kurihara, K.; Kunitake, T. Specific, Multiple-Point Binding of ATP and AMP to a Guanidinium-Functionalized Monolayer. *J. Am. Chem. Soc.* **1991**, *113* (25), 9685–9686.

(44) Kurihara, K.; Ohto, K.; Tanaka, Y.; Aoyama, Y.; Kunitake, T. Binding of Sugars and Water-Soluble Polymers to a Monolayer of Cyclic Resorcinol Tetramer at the Air-Water Interface. *Thin Solid Films* **1989**, *179* (1), 21–26.

(45) Oishi, Y.; Torii, Y.; Kato, T.; Kuramori, M.; Suehiro, K.; Ariga, K.; Taguchi, K.; Kamino, A.; Koyano, H.; Kunitake, T. Molecular Patterning of a Guanidinium/Orotate Mixed Monolayer through Molecular Recognition with Flavin Adenine Dinucleotide. *Langmuir* **1997**, *13* (3), 519–524.

(46) Cha, X.; Ariga, K.; Kunitake, T. Molecular Recognition of Aqueous Dipeptides at Multiple Hydrogen-Bonding Sites of Mixed Peptide Monolayers. *J. Am. Chem. Soc.* **1996**, *118* (40), 9545–9551.

(47) Degen, P.; Optenhostert, T.; Rehage, H.; Verhaelen, C.; Lange, M.; Polkowska, J.; Klärner, F. G. Langmuir and Langmuir−Blodgett Monolayers of Molecular Tweezers and Clips. *Langmuir* **2007**, *23* (23), 11611–11616.

(48) Degen, P.; Leick, S.; Rehage, H.; Polkowska, J.; Klärner, F. G. Gemini-like Molecular Clips and Tweezers: The Influence of Structure and Guest Binding on Interfacial Tension. *Langmuir* **2009**, *25* (11), 6094–6099.

(49)   Rehage, H.; Achenbach, B.; Klärner, F. G.; Kamieth, M.; Panitzky, J.
        Characterization of Langmuir-Monolayers of Molecular Tweezers and Clips by
        Means of Brewster-Angle-Microscopy. *Tenside Surfactants Deterg.* **2004**, *41* (3),
        121–125.

(50)   Degen, P.; Rehage, H.; Klärner, F. G.; Polkowska, J. Characterization of
        Langmuir-Monolayers of Molecular Clips by Means of Brewster-Angle-
        Microscopy. *Colloid Polym. Sci.* **2005**, *284* (1), 44–50.

(51)   Marchioni, F.; Juris, A.; Lobert, M.; Seelbach, U. P.; Kahlert, B.; Klarner, F.-G.
        Luminescent Host-Guest Complexes Involving Molecular Clips and Tweezers and
        Tetracyanobenzene. *New J. Chem.* **2005**, *29* (6), 780–784.

(52)   Leblanc, R. M. Molecular Recognition at Langmuir Monolayers. *Curr. Opin.*
        Chem. Biol. **2006**, *10* (6), 529–536.

(53)   Rullaud, V.; Moridi, N.; Shahgaldian, P. Sequence-Specific DNA Interactions with
        Calixarene-Based Langmuir Monolayers. *Langmuir* **2014**, *30* (29), 8675–8679.

(54)   Liu, F.; Lu, G.-Y.; He, W.-J.; Liu, M.-H.; Zhu, L.-G.; Wu, H.-M. Molecular
        Recognition of Nucleotides by a Calix[4]Arene Derivative with Two Alkyl
        Guanidinium Groups at the Air–Water Interface. *New J. Chem.* **2002**, *26* (5), 601–
        606.

(55)   Eddaif, L.; Shaban, A.; Telegdi, J. Application of the Langmuir Technique to
        Study the Response of C-Dec-9-En-1-Ylcalix[4]Resorcinarene and C-
        Undecylcalix[4]Resorcinarene Ultra-Thin Films' Interactions with Cd2+, Hg2+,
        Pb2+, and Cu2+ Cations Present in the Subphase. *Water, Air, Soil Pollut.* **2019**,
        230 (12), 279.

(56)   Korchowiec, B.; Trojan, S.; Joly, J.-P.; Korchowiec, J.; Beley, M.; Rogalska, E. The Interaction of an Amphiphile Crown Ether with Divalent Metal Ions. An Electrochemical, Langmuir Film, and Molecular Modeling Study. *Thin Solid Films* **2019**, *683*, 49–56.

(57)   Shahgaldian, P.; Pieles, U.; Hegner, M. Enantioselective Recognition of Phenylalanine by a Chiral Amphiphilic Macrocycle at the Air−Water Interface: A Copper-Mediated Mechanism. *Langmuir* **2005**, *21* (14), 6503–6507.

(58)   Ariga, K.; Nakanishi, T.; Terasaka, Y.; Tsuji, H.; Sakai, D.; Kikuchi, J. Piezoluminescence at the Air−Water Interface through Dynamic Molecular Recognition Driven by Lateral Pressure Application. *Langmuir* **2005**, *21* (3), 976– 981.

(59)   Ariga, K.; Terasaka, Y.; Sakai, D.; Tsuji, H.; Kikuchi, J. Piezoluminescence Based on Molecular Recognition by Dynamic Cavity Array of Steroid Cyclophanes at the Air−Water Interface. *J. Am. Chem. Soc.* **2000**, *122* (32), 7835–7836.

(60)   Ariga, K.; Terasaka, Y.; Tsuji, H.; Sakai, D.; Kikuchi, J. Dynamic Cavity Array of Steroid Cyclophanes at Membrane Surface. In *Proceedings of the International Conference on Colloid and Surface Science*; Iwasawa, Y., Oyama, N., Kunieda, H. B. T.-S. in S. S. and C., Eds.; Elsevier, 2001; Vol. 132, pp 443–446.

(61)   Ariga, K.; Nakanishi, T.; Hill, J. P.; Terasaka, Y.; Sakai, D.; Kikuchi, J. Effect of Guest Capture Modes on Molecular Recognition by a Dynamic Cavity Array at the Air–Water Interface: Soft vs. Tight and Fast vs. Slow. *Soft Matter* **2005**, *1* (2), 132–137.

(62)   Rock, W.; Oruc, M. E.; Ellis, R. J.; Uysal, A. Molecular Scale Description of

Anion Competition on Amine-Functionalized Surfaces. *Langmuir* **2016**, *32* (44), 11532–11539.

(63) Cobben, P. L. H. M.; Egberink, R. J. M.; Bomer, J. G.; Bergveld, P.; Verboom, W.; Reinhoudt, D. N. Transduction of Selective Recognition of Heavy Metal Ions by Chemically Modified Field Effect Transistors (CHEMFETs). *J. Am. Chem. Soc.* **1992**, *114* (26), 10573–10582.

(64) Golub, E.; Pelossof, G.; Freeman, R.; Zhang, H.; Willner, I. Electrochemical, Photoelectrochemical, and Surface Plasmon Resonance Detection of Cocaine Using Supramolecular Aptamer Complexes and Metallic or Semiconductor Nanoparticles. *Anal. Chem.* **2009**, *81* (22), 9291–9298.

(65) Neal, J. F.; Zhao, W.; Grooms, A. J.; Smeltzer, M. A.; Shook, B. M.; Flood, A. H.; Allen, H. C. Interfacial Supramolecular Structures of Amphiphilic Receptors Drive Aqueous Phosphate Recognition. *J. Am. Chem. Soc.* **2019**, *141* (19), 7876–7886.

(66) Neal, J. F.; Zhao, W.; Grooms, A. J.; Flood, A. H.; Allen, H. C. Arginine–Phosphate Recognition Enhanced in Phospholipid Monolayers at Aqueous Interfaces. *J. Phys. Chem. C* **2018**, *122* (46), 26362–26371.

(67) Mori, T.; Okamoto, K.; Endo, H.; Sakakibara, K.; Hill, J. P.; Shinoda, S.; Matsukura, M.; Tsukube, H.; Suzuki, Y.; Kanekiyo, Y.; et al. Mechanical Tuning of Molecular Machines for Nucleotide Recognition at the Air-Water Interface. *Nanoscale Res. Lett.* **2011**, *6* (1), 304.

(68) Sakakibara, K.; Fujisawa, T.; Hill, J. P.; Ariga, K. Conformational Interchange of a Carbohydrate by Mechanical Compression at the Air–Water Interface. *Phys. Chem. Chem. Phys.* **2014**, *16* (22), 10286–10294.

(69) Nørgaard, K.; Laursen, B. W.; Nygaard, S.; Kjaer, K.; Tseng, H.-R.; Flood, A. H.; Stoddart, J. F.; Bjørnholm, T. Structural Evidence of Mechanical Shuttling in Condensed Monolayers of Bistable Rotaxane Molecules. *Angew. Chem. Int. Ed.* **2005**, *44* (43), 7035–7039.

(70) Jang, S. S.; Jang, Y. H.; Kim, Y.-H.; Goddard, W. A.; Choi, J. W.; Heath, J. R.; Laursen, B. W.; Flood, A. H.; Stoddart, J. F.; Nørgaard, K.; et al. Molecular Dynamics Simulation of Amphiphilic Bistable [2]Rotaxane Langmuir Monolayers at the Air/Water Interface. *J. Am. Chem. Soc.* **2005**, *127* (42), 14804–14816.

(71) Quinn, P. K.; Collins, D. B.; Grassian, V. H.; Prather, K. A.; Bates, T. S. Chemistry and Related Properties of Freshly Emitted Sea Spray Aerosol. *Chem. Rev.* **2015**, *115* (10), 4383–4399.

(72) Prather, K. A.; Bertram, T. H.; Grassian, V. H.; Deane, G. B.; Stokes, M. D.; DeMott, P. J.; Aluwihare, L. I.; Palenik, B. P.; Azam, F.; Seinfeld, J. H.; et al. Bringing the Ocean into the Laboratory to Probe the Chemical Complexity of Sea Spray Aerosol. *Proc. Natl. Acad. Sci. U. S. A.* **2013**, *110* (19), 7550.

(73) Ault, A. P.; Moffet, R. C.; Baltrusaitis, J.; Collins, D. B.; Ruppel, M. J.; Cuadra-Rodriguez, L. A.; Zhao, D. F.; Guasco, T. L.; Ebben, C. J.; Geiger, F. M.; et al. Size-Dependent Changes in Sea Spray Aerosol Composition and Properties with Different Seawater Conditions. *Environ. Sci. Technol.* **2013**, *47* (11), 5603.

(74) Engel, A.; Bange, H. W.; Cunliffe, M.; Burrows, S. M.; Friedrichs, G.; Galgani, L.; Herrmann, H.; Hertkorn, N.; Johnson, M.; Liss, P. S.; et al. The Ocean's Vital Skin: Toward an Integrated Understanding of the Sea Surface Microlayer . *Frontiers in Marine Science* . 2017, p 165.

(75)   Cochran, R. E.; Laskina, O.; Trueblood, J. V; Estillore, A. D.; Morris, H. S.; Jayarathne, T.; Sultana, C. M.; Lee, C.; Lin, P.; Laskin, J.; et al. Molecular Diversity of Sea Spray Aerosol Particles: Impact of Ocean Biology on Particle Composition and Hygroscopicity. *Chem* **2017**, *2* (5), 655–667.

(76)   Hawkins, L. N.; Russell, L. M. Polysaccharides, Proteins, and Phytoplankton Fragments: Four Chemically Distinct Types of Marine Primary Organic Aerosol Classified by Single Particle Spectromicroscopy. *Adv. Meteorol.* **2010**, Article ID 612132.

(77)   Laß, K.; Friedrichs, G. Revealing Structural Properties of the Marine Nanolayer from Vibrational Sum Frequency Generation Spectra. *J. Geophys. Res. Ocean.* **2011**, *116* (C8).

(78)   Russell, L. M.; Hawkins, L. N.; Frossard, A. A.; Quinn, P. K.; Bates, T. S. Carbohydrate-like Composition of Submicron Atmospheric Particles and Their Production from Ocean Bubble Bursting. *Proc. Natl. Acad. Sci.* **2010**, *107* (15), 6652–6657.

(79)   Jayarathne, T.; Sultana, C. M.; Lee, C.; Malfatti, F.; Cox, J. L.; Pendergraft, M. A.; Moore, K. A.; Azam, F.; Tivanski, A. V; Cappa, C. D.; et al. Enrichment of Saccharides and Divalent Cations in Sea Spray Aerosol during Two Phytoplankton Blooms. *Environ. Sci. Technol.* **2016**, *50* (21), 11511.

(80)   Link, K. A.; Spurzem, G. N.; Tuladhar, A.; Chase, Z.; Wang, Z.; Wang, H.; Walker, R. A. Cooperative Adsorption of Trehalose to DPPC Monolayers at the Water–Air Interface Studied with Vibrational Sum Frequency Generation. *J. Phys. Chem. B* **2019**, *123* (42), 8931–8938.

(81)   Hasenecz, E. S.; Kaluarachchi, C. P.; Lee, H. D.; Tivanski, A. V; Stone, E. A. Saccharide Transfer to Sea Spray Aerosol Enhanced by Surface Activity, Calcium, and Protein Interactions. *ACS Earth Sp. Chem.* **2019**, *3* (11), 2539–2548.

(82)   Link, K. A.; Hsieh, C.-Y.; Tuladhar, A.; Chase, Z.; Wang, Z.; Wang, H.; Walker, R. A. Vibrational Studies of Saccharide-Induced Lipid Film Reorganization at Aqueous/Air Interfaces. *Chem. Phys.* **2018**.

(83)   Burrows, S. M.; Gobrogge, E.; Fu, L.; Link, K.; Elliott, S. M.; Wang, H.; Walker, R. OCEANFILMS-2: Representing Coadsorption of Saccharides in Marine Films and Potential Impacts on Modeled Marine Aerosol Chemistry. *Geophys. Res. Lett.* **2016**, *43* (15), 8306–8313.

(84)   Schill, S.R.; Burrows, S.M.; Hasenecz, E.S.; Stone, E.A.; Bertram, T. H. The Impact of Divalent Cations on the Enrichment of Soluble Saccharides in Primary Sea Spray Aerosol. *Atmosphere* **2018**, *9* (12), 476.

(85)   Adams, E. M.; Allen, H. C. Palmitic Acid on Salt Subphases and in Mixed Monolayers of Cerebrosides: Application to Atmospheric Aerosol Chemistry. *Atmosphere* **2013**, *4* (4), 315–336.

(86)   Casillas-Ituarte, N. N.; Chen, X.; Castada, H.; Allen, H. C. Na^+ and Ca^{2+} Effect on the Hydration and Orientation of the Phosphate Group of DPPC at Air−Water and Air−Hydrated Silica Interfaces. *J. Phys. Chem. B* **2010**, *114* (29), 9485–9495.

(87)   Zhang, T.; Cathcart, M. G.; Vidalis, A. S.; Allen, H. C. Cation Effects on Phosphatidic Acid Monolayers at Various PH Conditions. *Chem. Phys. Lipids* **2016**, *200*, 24–31.

(88)   Casper, C. B.; Verreault, D.; Adams, E. M.; Hua, W.; Allen, H. C. Surface

Potential of DPPC Monolayers on Concentrated Aqueous Salt Solutions. *J. Phys. Chem. B* **2016**, *120* (8), 2043–2052.

(89) Adams, E. M.; Verreault, D.; Jayarathne, T.; Cochran, R. E.; Stone, E. A.; Allen, H. C. Surface Organization of a DPPC Monolayer on Concentrated SrCl2 and ZnCl2 Solutions. *Phys. Chem. Chem. Phys.* **2016**, *18* (47), 32345–32357.

(90) Adams, E. M.; Casper, C. B.; Allen, H. C. Effect of Cation Enrichment on Dipalmitoylphosphatidylcholine (DPPC) Monolayers at the Air-Water Interface. *J. Colloid Interface Sci.* **2016**, *478*, 353–364.

(91) Zhang, T.; Fiamingo, M.; Allen, H. C. Trace Metal Enrichment Driven by Phosphate Functional Group Binding Selectivity. *J. Geophys. Res. Ocean.* **2018**, *123* (8), 5286–5297.

(92) Cochran, R. E.; Laskina, O.; Jayarathne, T.; Laskin, A.; Laskin, J.; Lin, P.; Sultana, C.; Lee, C.; Moore, K. A.; Cappa, C. D.; et al. Analysis of Organic Anionic Surfactants in Fine and Coarse Fractions of Freshly Emitted Sea Spray Aerosol. *Environ. Sci. Technol.* **2016**, *50* (5), 2477–2486.

(93) Tang, C. Y.; Allen, H. C. Ionic Binding of Na+ versus K+ to the Carboxylic Acid Headgroup of Palmitic Acid Monolayers Studied by Vibrational Sum Frequency Generation Spectroscopy. *J. Phys. Chem. A* **2009**, *113* (26), 7383–7393.

(94) Tang, C. Y.; Huang, Z.; Allen, H. C. Interfacial Water Structure and Effects of Mg2+ and Ca2+ Binding to the COOH Headgroup of a Palmitic Acid Monolayer Studied by Sum Frequency Spectroscopy. *J. Phys. Chem. B* **2011**, *115* (1), 34–40.

(95) Tang, C. Y.; Huang, Z. S. A.; Allen, H. C. Binding of Mg2+ and Ca2+ to Palmitic Acid and Deprotonation of the COOH Headgroup Studied by Vibrational Sum

Frequency Generation Spectroscopy. *J. Phys. Chem. B* **2010**, *114* (51), 17068.

(96)   Gericke, A.; Hühnerfuss, H. The Effect of Cations on the Order of Saturated Fatty
       Acid Monolayers at the Air-Water Interface as Determined by Infrared Reflection-
       Absorption Spectrometry. *Thin Solid Films* **1994**, *245* (1), 74–82.

(97)   Adams, E. M.; Wellen, B. A.; Thiraux, R.; Reddy, S. K.; Vidalis, A. S.; Paesani,
       F.; Allen, H. C. Sodium-Carboxylate Contact Ion Pair Formation Induces
       Stabilization of Palmitic Acid Monolayers at High PH. *Phys. Chem. Chem. Phys.*
       2017, *19* (16), 10481–10490.

(98)   Gaines, G. L. *Insoluble Monolayers at Liquid-Gas Interfaces*; Interscience
       Publishers: New York, 1966.

(99)   Jalal, I. M.; Zografi, G.; Rakshit, A. K.; Gunstone, F. D. Monolayer Properties of
       Fatty Acids. I. Thermodynamics of Spreading. *J. Colloid Interface Sci.* **1980**, *76*
       (1), 146–156.

(100) Wellen Rudd, B. A.; Vidalis, A. S.; Allen, H. C. Thermodynamic versus Non-
       Equilibrium Stability of Palmitic Acid Monolayers in Calcium-Enriched Sea Spray
       Aerosol Proxy Systems. *Phys. Chem. Chem. Phys.* **2018**, *20* (24), 16320–16332.

(101) May, N. W.; Olson, N. E.; Panas, M.; Axson, J. L.; Tirella, P. S.; Kirpes, R. M.;
       Craig, R. L.; Gunsch, M. J.; China, S.; Laskin, A.; et al. Aerosol Emissions from
       Great Lakes Harmful Algal Blooms. *Environ. Sci. Technol.* **2018**, *52* (2), 397–405.

(102) Olson, N. E.; May, N. W.; Kirpes, R. M.; Watson, A. E.; Hajny, K. D.; Slade, J.
       H.; Shepson, P. B.; Stirm, B. H.; Pratt, K. A.; Ault, A. P. Lake Spray Aerosol
       Incorporated into Great Lakes Clouds. *ACS Earth Sp. Chem.* **2019**, *3* (12), 2765–
       2774.

(103) May, N. W.; Gunsch, M. J.; Olson, N. E.; Bondy, A. L.; Kirpes, R. M.; Bertman, S. B.; China, S.; Laskin, A.; Hopke, P. K.; Ault, A. P.; et al. Unexpected Contributions of Sea Spray and Lake Spray Aerosol to Inland Particulate Matter. *Environ. Sci. Technol. Lett.* **2018**, *5* (7), 405–412.

(104) Axson, J. L.; May, N. W.; Colón-Bernal, I. D.; Pratt, K. A.; Ault, A. P. Lake Spray Aerosol: A Chemical Signature from Individual Ambient Particles. *Environ. Sci. Technol.* **2016**, *50* (18), 9835–9845.

(105) Stefaniu, C.; Brezesinski, G.; Möhwald, H. Langmuir Monolayers as Models to Study Processes at Membrane Surfaces. *Adv. Colloid Interface Sci.* **2014**, *208*, 197–213.

(106) Maget-Dana, R. The Monolayer Technique: A Potent Tool for Studying the Interfacial Properties of Antimicrobial and Membrane-Lytic Peptides and Their Interactions with Lipid Membranes. *Biochim. Biophys. Acta, Biomembr.* **1999**, *1462* (1), 109–140.

(107) Brezesinski, G.; Möhwald, H. Langmuir Monolayers to Study Interactions at Model Membrane Surfaces. *Adv. Colloid Interface Sci.* **2003**, *100–102*, 563–584.

(108) Dynarowicz-Łątka, P.; Dhanabalan, A.; Oliveira, O. N. Modern Physicochemical Research on Langmuir Monolayers. *Adv. Colloid Interface Sci.* **2001**, *91* (2), 221–293.

(109) Flach, C. R.; Prendergast, F. G.; Mendelsohn, R. Infrared Reflection-Absorption of Melittin Interaction with Phospholipid Monolayers at the Air/Water Interface. *Biophys. J.* **1996**, *70* (1), 539–546.

(110) Bartkowiak, A.; Rojewska, M.; Prochaska, K. Study of Mucin Interaction with

Model Phospholipid Membrane at the Air–Water Interface. *Colloids Surfaces A Physicochem. Eng. Asp.* **2019**, *578*, 123587.

(111) Boisselier, É.; Demers, É.; Cantin, L.; Salesse, C. How to Gather Useful and Valuable Information from Protein Binding Measurements Using Langmuir Lipid Monolayers. *Adv. Colloid Interface Sci.* **2017**, *243*, 60–76.

(112) Vollhardt, D.; Fainerman, V. B. Penetration of Dissolved Amphiphiles into Two-Dimensional Aggregating Lipid Monolayers. *Adv. Colloid Interface Sci.* **2000**, *86* (1), 103–151.

(113) Crawford, N. F.; Leblanc, R. M. Serum Albumin in 2D: A Langmuir Monolayer Approach. *Adv. Colloid Interface Sci.* **2014**, *207*, 131–138.

(114) Demers, E.; Boisselier, E.; Horchani, H.; Blaudez, D.; Calvez, P.; Cantin, L.; Belley, N.; Champagne, S.; Desbat, B.; Salesse, C. Lipid Selectivity, Orientation, and Extent of Membrane Binding of Nonacylated RP2. *Biochemistry* **2015**, *54* (16), 2560–2570.

(115) Boisselier, É.; Calvez, P.; Demers, É.; Cantin, L.; Salesse, C. Influence of the Physical State of Phospholipid Monolayers on Protein Binding. *Langmuir* **2012**, *28* (25), 9680–9688.

(116) Dalchand, N.; Cui, Q.; Geiger, F. M. Electrostatics, Hydrogen Bonding, and Molecular Structure at Polycation and Peptide:Lipid Membrane Interfaces. *ACS Appl. Mater. Interfaces* **2019**.

(117) McGeachy, A. C.; Dalchand, N.; Caudill, E. R.; Li, T.; Doğangün, M.; Olenick, L. L.; Chang, H.; Pedersen, J. A.; Geiger, F. M. Interfacial Electrostatics of Poly(Vinylamine Hydrochloride), Poly(Diallyldimethylammonium Chloride),

Poly-l-Lysine, and Poly-l-Arginine Interacting with Lipid Bilayers. *Phys. Chem. Chem. Phys.* **2018**, *20* (16), 10846–10856.

(118) Hädicke, A.; Blume, A. Binding of the Cationic Peptide (KL)4K to Lipid Monolayers at the Air–Water Interface: Effect of Lipid Headgroup Charge, Acyl Chain Length, and Acyl Chain Saturation. *J. Phys. Chem. B* **2016**, *120* (16), 3880–3887.

(119) Hädicke, A.; Schwieger, C.; Blume, A. Cospreading of Anionic Phospholipids with Peptides of the Structure (KX)4K at the Air–Water Interface: Influence of Lipid Headgroup Structure and Hydrophobicity of the Peptide on Monolayer Behavior. *Langmuir* **2017**, *33* (43), 12204–12217.

(120) Petelska, A. D.; Naumowicz, M.; Figaszewski, Z. A. The Equilibrium of Phosphatidylcholine–Amino Acid System in Monolayer at the Air/Water Interface. *Cell Biochem. Biophys.* **2011**, *60* (3), 155–160.

(121) Zhang, J.; Yang, W.; Tan, J.; Ye, S. In Situ Examination of a Charged Amino Acid-Induced Structural Change in Lipid Bilayers by Sum Frequency Generation Vibrational Spectroscopy. *Phys. Chem. Chem. Phys.* **2018**, *20* (8), 5657–5665.

(122) Schmidt, T. F.; Caseli, L.; Oliveira, O. N.; Itri, R. Binding of Methylene Blue onto Langmuir Monolayers Representing Cell Membranes May Explain Its Efficiency as Photosensitizer in Photodynamic Therapy. *Langmuir* **2015**, *31* (14), 4205–4212.

(123) Thorpe, W. P.; Toner, M.; Ezzell, R. M.; Tompkins, R. G.; Yarmush, M. L. Dynamics of Photoinduced Cell Plasma Membrane Injury. *Biophys. J.* **1995**, *68* (5), 2198–2206.

(124) Itri, R.; Junqueira, H. C.; Mertins, O.; Baptista, M. S. Membrane Changes under

Oxidative Stress: The Impact of Oxidized Lipids. *Biophys. Rev.* **2014**, *6* (1), 47–61.

(125) Aoki, P. H. B.; Morato, L. F. C.; Pavinatto, F. J.; Nobre, T. M.; Constantino, C. J. L.; Oliveira, O. N. Molecular-Level Modifications Induced by Photo-Oxidation of Lipid Monolayers Interacting with Erythrosin. *Langmuir* **2016**, *32* (15), 3766–3773.

(126) Maximino, M. D.; Constantino, C. J. L.; Oliveira, O. N.; Alessio, P. Synergy in the Interaction of Amoxicillin and Methylene Blue with Dipalmitoyl Phosphatidyl Choline (DPPC) Monolayers. *Appl. Surf. Sci.* **2019**, *476*, 493–500.

(127) de Souza, R. M.; Siani, P.; Schmidt, T. F.; Itri, R.; Dias, L. G. Methylene Blue Location in (Hydroperoxized) Cardiolipin Monolayer: Implication in Membrane Photodegradation. *J. Phys. Chem. B* **2017**, *121* (36), 8512–8522.

(128) Fernández-Botello, A.; Comelles, F.; Alsina, M. A.; Cea, P.; Reig, F. A Monolayer Study on Interactions of Docetaxel with Model Lipid Membranes. *J. Phys. Chem. B* **2008**, *112* (44), 13834–13841.

(129) Chou, T.-H.; Chu, I.-M.; Chang, C.-H. Interaction of Paclitaxel with DSPC in Monolayers at the Air/Water Interface at Different Temperatures. *Colloids Surf., B* **2002**, *25* (2), 147–155.

(130) Zhao, L.; Feng, S.-S. Effects of Cholesterol Component on Molecular Interactions between Paclitaxel and Phospholipid within the Lipid Monolayer at the Air–Water Interface. *J. Colloid Interface Sci.* **2006**, *300* (1), 314–326.

(131) Feng, S.-S.; Gong, K.; Chew, J. Molecular Interactions between a Lipid and an Antineoplastic Drug Paclitaxel (Taxol) within the Lipid Monolayer at the

Air/Water Interface. *Langmuir* **2002**, *18* (10), 4061–4070.

(132) Heredia, V.; Maggio, B.; Beltramo, D. M.; Dupuy, F. G. Interfacial Stabilization of the Antitumoral Drug Paclitaxel in Monolayers of GM1 and GD1a Gangliosides. *Biochim. Biophys. Acta, Biomembr.* **2015**, *1848* (10, Part A), 2163–2171.

(133) Zhao, L.; Feng, S.-S. Effects of Lipid Chain Unsaturation and Headgroup Type on Molecular Interactions between Paclitaxel and Phospholipid within Model Biomembrane. *J. Colloid Interface Sci.* **2005**, *285* (1), 326–335.

(134) Romão, R. I. S.; Maçôas, E.; Martinho, J. M. G.; Gonçalves da Silva, A. M. P. S. Interaction of Toremifene with Dipalmitoyl-Phosphatidyl-Glycerol in Monolayers at the Air–Water Interface Followed by Fluorescence Microscopy in Langmuir–Blodgett Films. *Thin Solid Films* **2013**, *534*, 584–590.

(135) Sreekanth, V.; Bajaj, A. Fluorescence (Fluidity/Hydration) and Calorimetric Studies of Interactions of Bile Acid–Drug Conjugates with Model Membranes. *J. Phys. Chem. B* **2013**, *117* (7), 2123–2133.

(136) Rodrigues, J. C.; Caseli, L. Incorporation of Bacitracin in Langmuir Films of Phospholipids at the Air-Water Interface. *Thin Solid Films* **2017**, *622*, 95–103.

(137) Rodrigues, J. C.; Caseli, L. Lipids Mediating the Interaction of Metronidazole with Cell Membrane Models at the Air-Water Interface. *Colloids Surf., B* **2018**, *171*, 377–382.

(138) Yin, T.; Cao, X.; Liu, X.; Wang, J.; Shi, C.; Su, J.; Zhang, Y.; Gou, J.; He, H.; Guo, H.; et al. Interfacial Molecular Interactions Based on the Conformation Recognition between the Insoluble Antitumor Drug AD-1 and DSPC. *Colloids Surf., B* **2016**, *146*, 902–909.

(139) de Souza, K. D.; Perez, K. R.; Durán, N.; Justo, G. Z.; Caseli, L. Interaction of Violacein in Models for Cellular Membranes: Regulation of the Interaction by the Lipid Composition at the Air-Water Interface. *Colloids Surf., B* **2017**, *160*, 247– 253.

(140) Bilkova, E.; Pleskot, R.; Rissanen, S.; Sun, S.; Czogalla, A.; Cwiklik, L.; Róg, T.; Vattulainen, I.; Cremer, P. S.; Jungwirth, P.; et al. Calcium Directly Regulates Phosphatidylinositol 4,5-Bisphosphate Headgroup Conformation and Recognition. *J. Am. Chem. Soc.* **2017**, *139* (11), 4019–4024.

(141) Shi, J.; Yang, T.; Kataoka, S.; Zhang, Y.; Diaz, A. J.; Cremer, P. S. GM1 Clustering Inhibits Cholera Toxin Binding in Supported Phospholipid Membranes. *J. Am. Chem. Soc.* **2007**, *129* (18), 5954–5961.

(142) Monson, C. F.; Cong, X.; Robison, A. D.; Pace, H. P.; Liu, C.; Poyton, M. F.; Cremer, P. S. Phosphatidylserine Reversibly Binds Cu2+ with Extremely High Affinity. *J. Am. Chem. Soc.* **2012**, *134* (18), 7773–7779.

(143) Sun, S.; Sendecki, A. M.; Pullanchery, S.; Huang, D.; Yang, T.; Cremer, P. S. Multistep Interactions between Ibuprofen and Lipid Membranes. *Langmuir* **2018**, *34* (36), 10782–10792.

(144) Melcrová, A.; Pokorna, S.; Pullanchery, S.; Kohagen, M.; Jurkiewicz, P.; Hof, M.; Jungwirth, P.; Cremer, P. S.; Cwiklik, L. The Complex Nature of Calcium Cation Interactions with Phospholipid Bilayers. *Sci. Rep.* **2016**, *6* (1), 38035.

(145) Pullanchery, S.; Yang, T.; Cremer, P. S. Introduction of Positive Charges into Zwitterionic Phospholipid Monolayers Disrupts Water Structure Whereas Negative Charges Enhances It. *J. Phys. Chem. B* **2018**, *122* (51), 12260–12270.

(146) Sutton M.A.; Bleeker A.; Bekunda M.; Grizzetti B.; de Vries W.; van Grinsven H.J.M.; Abrol Y.P.; Adhya T.K.; Billen G.; Davidson E.A.; et al. *Our Nutrient World: The Challenge to Produce More Food and Energy with Less Pollution*; Centre for Ecology and Hydrology (CEH): Edinburgh, U.K., 2013.

(147) Cordell, D.; Drangert, J.-O.; White, S. The Story of Phosphorus: Global Food Security and Food for Thought. *Glob. Environ. Chang.* **2009**, *19* (2), 292–305.

(148) Elrashidi, M. A.; Mays, M. D.; Harder, J.; Schroeder, D.; Brakhage, P.; Peaslee, S.; Seybold, C.; Schaecher, C. Loss of Phosphorus by Runoff for Agricultural Watersheds. *Soil Sci.* **2005**, *170* (7), 543–558.

(149) Correll, D. L. The Role of Phosphorus in the Eutrophication of Receiving Waters: A Review. *J. Environ. Qual.* **1998**, *27*, 261–266.

(150) Hargrove, A. E.; Nieto, S.; Zhang, T.; Sessler, J. L.; Anslyn, E. V. Artificial Receptors for the Recognition of Phosphorylated Molecules. *Chem. Rev.* **2011**, *111* (11), 6603–6782.

(151) Gavette, J. V; Mills, N. S.; Zakharov, L. N.; Johnson, C. A.; Johnson, D. W.; Haley, M. M. An Anion-Modulated Three-Way Supramolecular Switch That Selectively Binds Dihydrogen Phosphate, $H_2PO_4{}^-$. *Angew. Chem. Int. Ed.* **2013**, *52* (39), 10270–10274.

(152) Harris, S. M.; Nguyen, J. T.; Pailloux, S. L.; Mansergh, J. P.; Dresel, M. J.; Swanholm, T. B.; Gao, T.; Pierre, V. C. Gadolinium Complex for the Catch and Release of Phosphate from Water. *Environ. Sci. Technol.* **2017**, *51* (8), 4549–4558.

(153) Mungalpara, D.; Valkonen, A.; Rissanen, K.; Kubik, S. Efficient Stabilisation of a Dihydrogenphosphate Tetramer and a Dihydrogenpyrophosphate Dimer by a

Cyclic Pseudopeptide Containing 1,4-Disubstituted 1,2,3-Triazole Moieties. *Chem. Sci.* **2017**, *8* (9), 6005–6013.

(154) Hristova, K.; Wimley, W. C. A Look at Arginine in Membranes. *J. Membr. Biol.* **2011**, *239* (1), 49–56.

(155) Schow, E. V; Freites, J. A.; Cheng, P.; Bernsel, A.; von Heijne, G.; White, S. H.; Tobias, D. J. Arginine in Membranes: The Connection Between Molecular Dynamics Simulations and Translocon-Mediated Insertion Experiments. *J. Membr. Biol.* **2011**, *239* (1), 35–48.

(156) Pantos, A.; Tsogas, I.; Paleos, C. M. Guanidinium Group: A Versatile Moiety Inducing Transport and Multicompartmentalization in Complementary Membranes. *Biochim. Biophys. Acta, Biomembr.* **2008**, *1778* (4), 811–823.

(157) Kuznetsova, M.; Lee, C.; Aller, J. Characterization of the Proteinaceous Matter in Marine Aerosols. *Mar. Chem.* **2005**, *96* (3), 359–377.

(158) Bertram, T. H.; Cochran, R. E.; Grassian, V. H.; Stone, E. A. Sea Spray Aerosol Chemical Composition: Elemental and Molecular Mimics for Laboratory Studies of Heterogeneous and Multiphase Reactions. *Chem. Soc. Rev.* **2018**, *47*, 2374–2400.

(159) Angyal, S. J.; Warburton, W. K. 549. The Basic Strengths of Methylated Guanidines. *J. Chem. Soc.* **1951**, 2492–2494.

(160) Chen, X.; Hua, W.; Huang, Z.; Allen, H. C. Interfacial Water Structure Associated with Phospholipid Membranes Studied by Phase-Sensitive Vibrational Sum Frequency Generation Spectroscopy. *J. Am. Chem. Soc.* **2010**, *132* (32), 11336–11342.

(161) Kim, J.; Kim, G.; Cremer, P. S. Investigations of Water Structure at the Solid/Liquid Interface in the Presence of Supported Lipid Bilayers by Vibrational Sum Frequency Spectroscopy. *Langmuir* **2001**, *17* (23), 7255–7260.

(162) Covert, P. A.; Jena, K. C.; Hore, D. K. Throwing Salt into the Mix: Altering Interfacial Water Structure by Electrolyte Addition. *J. Phys. Chem. Lett.* **2014**, *5* (1), 143–148.

(163) Tyrode, E.; Liljeblad, J. F. D. Water Structure Next to Ordered and Disordered Hydrophobic Silane Monolayers: A Vibrational Sum Frequency Spectroscopy Study. *J. Phys. Chem. C* **2013**, *117* (4), 1780–1790.

(164) Jungwirth, P.; Tobias, D. J. Specific Ion Effects at the Air/Water Interface. *Chem. Rev.* **2006**, *106* (4), 1259–1281.

(165) Wu, Y.; Vendome, J.; Shapiro, L.; Ben-Shaul, A.; Honig, B. Transforming Binding Affinities from Three Dimensions to Two with Application to Cadherin Clustering. *Nature* **2011**, *475* (7357), 510–513.

(166) Sasaki, D. Y.; Kurihara, K.; Kunitake, T. Self-Assembled Multifunctional Receptors for Nucleotides at the Air-Water Interface. *J. Am. Chem. Soc.* **1992**, *114* (27), 10994–10995.

(167) Onda, M.; Yoshihara, K.; Koyano, H.; Ariga, K.; Kunitake, T. Molecular Recognition of Nucleotides by the Guanidinium Unit at the Surface of Aqueous Micelles and Bilayers. A Comparison of Microscopic and Macroscopic Interfaces. *J. Am. Chem. Soc.* **1996**, *118* (36), 8524–8530.

(168) Masayuki, D. Y.; Yanagi, M.; Kurihara, K.; Kunitake, T. The Interaction of a Guanidinium Monolayer with ATP and AMP, as Revealed by Surface Potential

and UV Absorption Measurements. *Thin Solid Films* **1992**, *210–211*, 776–779.

(169) Ariga, K.; Kamino, A.; Koyano, H.; Kunitake, T. Recognition of Aqueous Flavin

Mononucleotide on the Surface of Binary Monolayers of Guanidinium and

Melamine Amphiphiles. *J. Mater. Chem.* **1997**, *7* (7), 1155–1161.

(170) Hoenig, D.; Moebius, D. Direct Visualization of Monolayers at the Air-Water

Interface by Brewster Angle Microscopy. *J. Phys. Chem.* **1991**, *95* (12), 4590–

4592.

(171) Vollhardt, D. Morphology and Phase Behavior of Monolayers. *Adv. Colloid*

Interface Sci. **1996**, *64*, 143–171.

(172) Wong, P. T. T.; Mantsch, H. H. High-Pressure Infrared Spectroscopic Evidence of

Water Binding Sites in 1,2-Diacyl Phospholipids. *Chem. Phys. Lipids* **1988**, *46* (3),

213–224.

(173) Mendelsohn, R.; Mao, G.; Flach, C. R. Infrared Reflection-Absorption

Spectroscopy: Principles and Applications to Lipid-Protein Interaction in

Langmuir Films. *Biochim. Biophys. Acta* **2010**, *1798* (4), 788–800.

(174) Ibarguen, C.; Manrique-Moreno, M.; Hadad, C. Z.; David, J.; Restrepo, A.

Microsolvation of Dimethylphosphate: A Molecular Model for the Interaction of

Cell Membranes with Water. *Phys. Chem. Chem. Phys.* **2013**, *15* (9), 3203–3211.

(175) Blume, A.; Hubner, W.; Messner, G. Fourier Transform Infrared Spectroscopy of

^{13}C = O-Labeled Phospholipids Hydrogen Bonding to Carbonyl Groups.

Biochemistry **1988**, *27* (21), 8239–8249.

(176) Lewis, R. N.; McElhaney, R. N.; Pohle, W.; Mantsch, H. H. Components of the

Carbonyl Stretching Band in the Infrared Spectra of Hydrated 1,2-

Diacylglycerolipid Bilayers: A Reevaluation. *Biophys. J.* **1994**, *67* (6), 2367–2375.

(177) Venyaminov, S. Y.; Kalnin, N. N. Quantitative IR Spectrophotometry of Peptide Compounds in Water (H$_2$O) Solutions. I. Spectral Parameters of Amino Acid Residue Absorption Bands. *Biopolymers* **1990**, *30* (13–14), 1243–1257.

(178) Braiman, M. S.; Briercheck, D. M.; Kriger, K. M. Modeling Vibrational Spectra of Amino Acid Side Chains in Proteins: Effects of Protonation State, Counterion, and Solvent on Arginine C−N Stretch Frequencies. *J. Phys. Chem. B* **1999**, *103* (22), 4744–4750.

(179) Chirgadze, Y. N.; Fedorov, O. V.; Trushina, N. P. Estimation of Amino Acid Residue Side-chain Absorption in the Infrared Spectra of Protein Solutions in Heavy Water. *Biopolymers* **1975**, *14*, 679–694.

(180) Schmidtchen, F. P.; Berger, M. Artificial Organic Host Molecules for Anions. *Chem. Rev.* **1997**, *97* (5), 1609–1646.

(181) Tamaru, S.; Hamachi, I. Recent Progress of Phosphate Derivatives Recognition Utilizing Artificial Small Molecular Receptors in Aqueous Media. In *Recognition of Anions. Structure and Bonding*; Vilar, R., Ed.; Springer: Berlin, 2008; pp 95–125.

(182) Jarvie, H. P.; Sharpley, A. N.; Flaten, D.; Kleinman, P. J. A.; Jenkins, A.; Simmons, T. The Pivotal Role of Phosphorus in a Resilient Water–Energy–Food Security Nexus. *J. Environ. Qual.* **2015**, *44* (4), 1049–1062.

(183) Springmann, M.; Clark, M.; Mason-D'Croz, D.; Wiebe, K.; Bodirsky, B. L.; Lassaletta, L.; de Vries, W.; Vermeulen, S. J.; Herrero, M.; Carlson, K. M.; et al. Options for Keeping the Food System within Environmental Limits. *Nature* **2018**,

562 (7728), 519–525.

(184)   Ryther, J. H.; Dunstan, W. M. Nitrogen, Phosphorus, and Eutrophication in the Coastal Marine Environment. *Science* **1971**, *171* (3975), 1008–1013.

(185)   Sharpley, A. N.; Chapra, S. C.; Wedepohl, R.; Sims, J. T.; Daniel, T. C.; Reddy, K. R. Managing Agricultural Phosphorus for Protection of Surface Waters: Issues and Options. *J. Environ. Qual.* **1994**, *23* (3), 437–451.

(186)   Sims, J. T.; Simard, R. R.; Joern, B. C. Phosphorus Loss in Agricultural Drainage: Historical Perspective and Current Research. *J. Environ. Qual.* **1998**, *27*, 277–293.

(187)   Marcus, Y. Thermodynamics of Solvation of Ions. Part 5.-Gibbs Free Energy of Hydration at 298.15 K. *J. Chem. Soc. Faraday Trans.* **1991**, *87* (18), 2995–2999.

(188)   Xiao, K. P.; Bühlmann, P.; Umezawa, Y. Ion-Channel-Mimetic Sensing of Hydrophilic Anions Based on Monolayers of a Hydrogen Bond-Forming Receptor. *Anal. Chem.* **1999**, *71* (6), 1183–1187.

(189)   Kato, R.; Cui, Y.-Y.; Nishizawa, S.; Yokobori, T.; Teramae, N. Thiourea–Isothiouronium Conjugate for Strong and Selective Binding of Very Hydrophilic H2PO4− Anion at the 1,2-Dichloroethane–Water Interface. *Tetrahedron Lett.* **2004**, *45* (22), 4273–4276.

(190)   Bühlmann, P.; Nishizawa, S.; Xiao, K. P.; Umezawa, Y. Strong Hydrogen Bond-Mediated Complexation of H2PO4− by Neutral Bis-Thiourea Hosts. *Tetrahedron* **1997**, *53* (5), 1647–1654.

(191)   Nguyen, Q. P. B.; Kim, J.-N.; Kim, T.-H. Investigation of Isomerism in Anthracene-Isothiouronium Salts and Application of These Salts for Anion Sensing. *Bull. Korean Chem. Soc.* **2009**, *30*, 2093–2097.

(192) Blondeau, P.; Segura, M.; Pérez-Fernández, R.; de Mendoza, J. Molecular Recognition of Oxoanions Based on Guanidinium Receptors. *Chem. Soc. Rev.* **2007**, *36* (2), 198–210.

(193) Schug, K. A.; Lindner, W. Noncovalent Binding between Guanidinium and Anionic Groups: Focus on Biological- and Synthetic-Based Arginine/Guanidinium Interactions with Phosph[on]Ate and Sulf[on]Ate Residues. *Chem. Rev.* **2005**, *105* (1), 67–114.

(194) Dixon, R. P.; Geib, S. J.; Hamilton, A. D. Molecular Recognition: Bis-Acylguanidiniums Provide a Simple Family of Receptors for Phosphodiesters. *J. Am. Chem. Soc.* **1992**, *114* (1), 365–366.

(195) Li, A.-F.; Wang, J.-H.; Wang, F.; Jiang, Y.-B. Anion Complexation and Sensing Using Modified Urea and Thiourea-Based Receptors. *Chem. Soc. Rev.* **2010**, *39* (10), 3729–3745.

(196) Kubo, Y.; Ishihara, S.; Tsukahara, M.; Tokita, S. Isothiouronium-Derived Simple Fluorescent Chemosensors of Anions. *J. Chem. Soc. Perkin Trans. 2* **2002**, No. 8, 1455–1460.

(197) Kubo, Y.; Tsukahara, M.; Ishihara, S.; Tokita, S. A Simple Anion Chemosensor Based on a Naphthalene–Thiouronium Dyad. *Chem. Commun.* **2000**, No. 8, 653–654.

(198) Yeo, W.-S.; Hong, J.-I. Oxoanion Recognition by a Thiouronium Receptor. *Tetrahedron Lett.* **1998**, *39* (44), 8137–8140.

(199) Yeo, W.-S.; Hong, J.-I. Thiouronium-Thymine Conjugate as a New Carrier for Selective Transport of 5′-AMP. *Tetrahedron Lett.* **1998**, *39* (22), 3769–3772.

(200) Misawa, Y.; Kubo, Y.; Tokita, S.; Ohkuma, H.; Nakahara, H. An Isothiouronium-Derived Organized Monolayer at the Air–Water Interface: Design of Film-Based Anion Sensor Systems for H2PO4−. *Chem. Lett.* **2004**, *33*, 1118–1119.

(201) Chapman, A. C.; Thirlwell, L. E. Spectra of Phosphorus Compounds—I the Infra-Red Spectra of Orthophosphates. *Spectrochim. Acta* **1964**, *20* (6), 937–947.

(202) Klähn, M.; Mathias, G.; Kötting, C.; Nonella, M.; Schlitter, J.; Gerwert, K.; Tavan, P. IR Spectra of Phosphate Ions in Aqueous Solution: Predictions of a DFT/MM Approach Compared with Observations. *J. Phys. Chem. A* **2004**, *108* (29), 6186–6194.

(203) Rudolph, W. W. Raman- and Infrared-Spectroscopic Investigations of Dilute Aqueous Phosphoric Acid Solutions. *Dalt. Trans.* **2010**, *39* (40), 9642–9653.

(204) Ma, G.; Allen, H. C. DPPC Langmuir Monolayer at the Air−Water Interface: Probing the Tail and Head Groups by Vibrational Sum Frequency Generation Spectroscopy. *Langmuir* **2006**, *22* (12), 5341–5349.

(205) Jubb, A. M.; Allen, H. C. Bisulfate Dehydration at Air/Solution Interfaces Probed by Vibrational Sum Frequency Generation Spectroscopy. *J. Phys. Chem. C* **2012**, *116* (24), 13161–13168.

(206) Carboxamides, Ureas, Thioureas, Imidazolidinones, Caffeine, Isocaffeine, Uracils, Imides, Hydantoins, and s-Triazine(1H, 3H, 5H)-Triones. In *Interpreting Infrared, Raman, and Nuclear Magnetic Resonance Spectra*; Nyquist, R. A., Ed.; Academic Press: San Diego, CA, 2001; pp 213–266.

(207) Mido, Y.; Kitagawa, I.; Hashimoto, M.; Matsuura, H. Vibrational Spectra and Normal Coordinate Analysis of N-Methylthiourea and Three Deuterated

Analogues. *Spectrochim. Acta Part A Mol. Biomol. Spectrosc.* **1999**, *55* (13), 2623–2633.

(208) Jensen, K. A.; Nielsen, P. H. Infrared Spectra of Thioamides and Selenoamides. *Acta Chem. Scand.* **1966**, *20* (3), 597–629.

(209) Sovago, M.; Wurpel, G. W. H.; Smits, M.; Müller, M.; Bonn, M. Calcium-Induced Phospholipid Ordering Depends on Surface Pressure. *J. Am. Chem. Soc.* **2007**, *129* (36), 11079–11084.

(210) Badis, M.; Tomaszkiewicz, I.; Joly, J.-P.; Rogalska, E. Enantiomeric Recognition of Amino Acids by Amphiphilic Crown Ethers in Langmuir Monolayers. *Langmuir* **2004**, *20* (15), 6259–6267.

(211) Blankenburg, R.; Meller, P.; Ringsdorf, H.; Salesse, C. Interaction between Biotin Lipids and Streptavidin in Monolayers: Formation of Oriented Two-Dimensional Protein Domains Induced by Surface Recognition. *Biochemistry* **1989**, *28* (20), 8214–8221.

(212) Vazdar, M.; Heyda, J.; Mason, P. E.; Tesei, G.; Allolio, C.; Lund, M.; Jungwirth, P. Arginine "Magic": Guanidinium Like-Charge Ion Pairing from Aqueous Salts to Cell Penetrating Peptides. *Acc. Chem. Res.* **2018**, *51* (6), 1455–1464.

(213) Vondrášek, J.; Mason, P. E.; Heyda, J.; Collins, K. D.; Jungwirth, P. The Molecular Origin of Like-Charge Arginine−Arginine Pairing in Water. *J. Phys. Chem. B* **2009**, *113* (27), 9041–9045.

(214) Soetens, J.-C.; Millot, C.; Chipot, C.; Jansen, G.; Ángyán, J. G.; Maigret, B. Effect of Polarizability on the Potential of Mean Force of Two Cations. The Guanidinium−Guanidinium Ion Pair in Water. *J. Phys. Chem. B* **1997**, *101* (50),

10910–10917.

(215) No, K. T.; Nam, K.-Y.; Scheraga, H. A. Stability of Like and Oppositely Charged Organic Ion Pairs in Aqueous Solution. *J. Am. Chem. Soc.* **1997**, *119* (52), 12917–12922.

(216) Masunov, A.; Lazaridis, T. Potentials of Mean Force between Ionizable Amino Acid Side Chains in Water. *J. Am. Chem. Soc.* **2003**, *125* (7), 1722–1730.

(217) Shih, O.; England, A. H.; Dallinger, G. C.; Smith, J. W.; Duffey, K. C.; Cohen, R. C.; Prendergast, D.; Saykally, R. J. Cation-Cation Contact Pairing in Water: Guanidinium. *J. Chem. Phys.* **2013**, *139* (3), 35104.

(218) Mendelsohn, R.; Brauner, J. W.; Gericke, A. External Infrared Reflection Absorption Spectrometry of Monolayer Films at the Air-Water Interface. *Annu. Rev. Phys. Chem.* **1995**, *46* (1), 305–334.

(219) Papahadjopoulos, D.; Vail, W. J.; Newton, C.; Nir, S.; Jacobson, K.; Poste, G.; Lazo, R. Studies on Membrane Fusion. III. The Role of Calcium-Induced Phase Changes. *Biochim. Biophys. Acta, Biomembr.* **1977**, *465* (3), 579–598.

(220) Cotmore, J. M.; Nichols, G.; Wuthier, R. E. Phospholipid—Calcium Phosphate Complex: Enhanced Calcium Migration in the Presence of Phosphate. *Science* **1971**, *172* (3990), 1339–1341.

(221) Kimelberg, H. K.; Papahadjopoulos, D. Phospholipid-Protein Interactions: Membrane Permeability Correlated with Monolayer "Penetration." *Biochim. Biophys. Acta, Biomembr.* **1971**, *223* (3), 805–809.

(222) Papahadjopoulos, D.; Moscarello, M.; Eylar, E. H.; Isac, T. Effects of Proteins on the Thermotropic Phase Transitions of Phospholipid Membranes. *Biochim.*

Biophys. Acta, Biomembr. **1975**, *401* (3), 317–335.

(223) de Meyer, F.; Smit, B. Effect of Cholesterol on the Structure of a Phospholipid Bilayer. *Proc. Natl. Acad. Sci.* **2009**, *106* (10), 3654–3658.

(224) Magarkar, A.; Dhawan, V.; Kallinteri, P.; Viitala, T.; Elmowafy, M.; Róg, T.; Bunker, A. Cholesterol Level Affects Surface Charge of Lipid Membranes in Saline Solution. *Sci. Rep.* **2014**, *4*, 5005.

(225) McMullen, T. P. W.; Lewis, R. N. A. H.; McElhaney, R. N. Cholesterol–Phospholipid Interactions, the Liquid-Ordered Phase and Lipid Rafts in Model and Biological Membranes. *Curr. Opin. Colloid Interface Sci.* **2004**, *8* (6), 459–468.

(226) Gardner, K. M.; Royer, T. V. Effect of Road Salt Application on Seasonal Chloride Concentrations and Toxicity in South-Central Indiana Streams. *J. Environ. Qual.* **2010**, *39*, 1036–1042.

(227) Zhou, H.-X. Disparate Ionic-Strength Dependencies of on and off Rates in Protein–Protein Association. *Biopolymers* **2001**, *59* (6), 427–433.

(228) Schreiber, G.; Haran, G.; Zhou, H.-X. Fundamental Aspects of Protein−Protein Association Kinetics. *Chem. Rev.* **2009**, *109* (3), 839–860.

(229) Wang, Q.; Liang, K.-C.; Czader, A.; Waxham, M. N.; Cheung, M. S. The Effect of Macromolecular Crowding, Ionic Strength and Calcium Binding on Calmodulin Dynamics. *PLoS Comput. Biol.* **2011**, *7* (7), e1002114.

(230) Hofmeister, F. Zur Lehre von Der Wirkung Der Salze. *Arch. für Exp. Pathol. und Pharmakologie* **1888**, *24* (4), 247–260.

(231) Kunz, W.; Henle, J.; Ninham, B. W. 'Zur Lehre von Der Wirkung Der Salze' (about the Science of the Effect of Salts): Franz Hofmeister's Historical Papers.

Curr. Opin. Colloid Interface Sci. **2004**, *9* (1), 19–37.

(232) Zhang, Y.; Cremer, P. S. The Inverse and Direct Hofmeister Series for Lysozyme. *Proc. Natl. Acad. Sci.* **2009**, *106* (36), 15249–15253.

(233) Collins, K. D. Charge Density-Dependent Strength of Hydration and Biological Structure. *Biophys. J.* **1997**, *72* (1), 65–76.

(234) Salis, A.; Ninham, B. W. Models and Mechanisms of Hofmeister Effects in Electrolyte Solutions, and Colloid and Protein Systems Revisited. *Chem. Soc. Rev.* **2014**, *43* (21), 7358–7377.

(235) Smith, H. A.; Fuzek, J. F. The Adsorption of Fatty Acids on Nickel and Platinum Catalysts. *J. Am. Chem. Soc.* **1946**, *68* (2), 229–231.

(236) Adam, N. K. *The Physics and Chemistry of Surfaces.*; Dover Publications: New York, 1968.

(237) Blažek Bregović, V.; Basarić, N.; Mlinarić-Majerski, K. Anion Binding with Urea and Thiourea Derivatives. *Coord. Chem. Rev.* **2015**, *295*, 80–124.

(238) Amendola, V.; Boiocchi, M.; Fabbrizzi, L.; Mosca, L. Metal-Controlled Anion-Binding Tendencies of the Thiourea Unit of Thiosemicarbazones. *Chem. – A Eur. J.* **2008**, *14* (31), 9683–9696.

(239) Soriano, M. L.; Lenthall, J. T.; Anderson, K. M.; Smith, S. J.; Steed, J. W. Enhanced Anion Binding from Unusual Coordination Modes of Bis(Thiourea) Ligands in Platinum Group Metal Complexes. *Chem. – A Eur. J.* **2010**, *16* (35), 10818–10831.

(240) Jungwirth, P.; Tobias, D. J. Molecular Structure of Salt Solutions: A New View of the Interface with Implications for Heterogeneous Atmospheric Chemistry. *J.*

Phys. Chem. B **2001**, *105* (43), 10468–10472.

(241) Gopalakrishnan, S.; Jungwirth, P.; Tobias, D. J.; Allen, H. C. Air−Liquid

Interfaces of Aqueous Solutions Containing Ammonium and Sulfate:

Spectroscopic and Molecular Dynamics Studies. *J. Phys. Chem. B* **2005**, *109* (18),

8861–8872.

(242) Bruce, E. E.; Bui, P. T.; Rogers, B. A.; Cremer, P. S.; van der Vegt, N. F. A.

Nonadditive Ion Effects Drive Both Collapse and Swelling of Thermoresponsive

Polymers in Water. *J. Am. Chem. Soc.* **2019**, *141* (16), 6609–6616.

(243) Mason, P. E.; Neilson, G. W.; Dempsey, C. E.; Barnes, A. C.; Cruickshank, J. M.

The Hydration Structure of Guanidinium and Thiocyanate Ions: Implications for

Protein Stability in Aqueous Solution. *Proc. Natl. Acad. Sci.* **2003**, *100* (8), 4557

LP – 4561.

(244) Marcus, Y. The Guanidinium Ion. *J. Chem. Thermodyn.* **2012**, *48*, 70–74.

(245) Rosseinsky, D. R. Electrode Potentials and Hydration Energies. Theories and

Correlations. *Chem. Rev.* **1965**, *65* (4), 467–490.

(246) Werner, J.; Wernersson, E.; Ekholm, V.; Ottosson, N.; Öhrwall, G.; Heyda, J.;

Persson, I.; Söderström, J.; Jungwirth, P.; Björneholm, O. Surface Behavior of

Hydrated Guanidinium and Ammonium Ions: A Comparative Study by

Photoelectron Spectroscopy and Molecular Dynamics. *J. Phys. Chem. B* **2014**, *118*

(25), 7119–7127.

(247) Houriez, C.; Meot-Ner (Mautner), M.; Masella, M. Solvation of the Guanidinium

Ion in Pure Aqueous Environments: A Theoretical Study from an "Ab Initio"-

Based Polarizable Force Field. *J. Phys. Chem. B* **2017**, *121* (50), 11219–11228.

(248) Pegram, L. M.; Record, M. T. Hofmeister Salt Effects on Surface Tension Arise from Partitioning of Anions and Cations between Bulk Water and the Air−Water Interface. *J. Phys. Chem. B* **2007**, *111* (19), 5411–5417.

(249) Breslow, R.; Guo, T. Surface Tension Measurements Show That Chaotropic Salting-in Denaturants Are Not Just Water-Structure Breakers. *Proc. Natl. Acad. Sci. U. S. A.* **1990**, *87* (1), 167–169.

(250) Wernersson, E.; Heyda, J.; Vazdar, M.; Lund, M.; Mason, P. E.; Jungwirth, P. Orientational Dependence of the Affinity of Guanidinium Ions to the Water Surface. *J. Phys. Chem. B* **2011**, *115* (43), 12521–12526.

(251) Lin, L.; Husek, J.; Biswas, S.; Baumler, S. M.; Adel, T.; Ng, K. C.; Baker, L. R.; Allen, H. C. Iron(III) Speciation Observed at Aqueous and Glycerol Surfaces: Vibrational Sum Frequency and X-Ray. *J. Am. Chem. Soc.* **2019**, *141* (34), 13525–13535.

(252) Hug, S. J. In SituFourier Transform Infrared Measurements of Sulfate Adsorption on Hematite in Aqueous Solutions. *J. Colloid Interface Sci.* **1997**, *188* (2), 415–422.

(253) Luecke, H.; Quiocho, F. High Specificity of a Phosphate Transport Protein Determined by Hydrogen Bonds. *Nature* **1990**, *347*, 402–406.

(254) Wang, Z.; Luecke, H.; Yao, N.; Quiocho, F. A. A Low Energy Short Hydrogen Bond in Very High Resolution Structures of Protein Receptor-Phosphate Complexes. *Nat. Struct. Mol. Biol.* **1997**, *4* (7), 519–522.

(255) Zhao, W.; Qiao, B.; Chen, C.-H.; Flood, A. H. High-Fidelity Multistate Switching with Anion–Anion and Acid–Anion Dimers of Organophosphates in Cyanostar

Complexes. *Angew. Chem. Int. Ed.* **2017**, *56* (42), 13083–13087.

(256) Fatila, E. M.; Pink, M.; Twum, E. B.; Karty, J. A.; Flood, A. H. Phosphate-
Phosphate Oligomerization Drives Higher Order Co-Assemblies with Stacks of
Cyanostar Macrocycles. *Chem. Sci.* **2018**, *9* (11), 2863–2872.

(257) Syed, K. A.; Pang, S.-F.; Zhang, Y.; Zeng, G.; Zhang, Y.-H. Micro-Raman
Observation on the HPO42– Association Structures in an Individual Dipotassium
Hydrogen Phosphate (K2HPO4) Droplet. *J. Phys. Chem. A* **2012**, *116* (6), 1558–
1564.

(258) Cerreta, M. K.; Berglund, K. A. The Structure of Aqueous Solutions of Some
Dihydrogen Orthophosphates by Laser Raman Spectroscopy. *J. Cryst. Growth*
1987, *84* (4), 577–588.

(259) Gurau, M. C.; Lim, S.-M.; Castellana, E. T.; Albertorio, F.; Kataoka, S.; Cremer,
P. S. On the Mechanism of the Hofmeister Effect. *J. Am. Chem. Soc.* **2004**, *126*
(34), 10522–10523.

(260) Tian, C.; Byrnes, S. J.; Han, H.-L.; Shen, Y. R. Surface Propensities of
Atmospherically Relevant Ions in Salt Solutions Revealed by Phase-Sensitive Sum
Frequency Vibrational Spectroscopy. *J. Phys. Chem. Lett.* **2011**, *2* (15), 1946–
1949.

(261) Griffith, E. C.; Vaida, V. Ionization State of L-Phenylalanine at the Air–Water
Interface. *J. Am. Chem. Soc.* **2013**, *135* (2), 710–716.

(262) Wellen, B. A.; Lach, E. A.; Allen, H. C. Surface PKa of Octanoic, Nonanoic, and
Decanoic Fatty Acids at the Air-Water Interface: Applications to Atmospheric
Aerosol Chemistry. *Phys. Chem. Chem. Phys.* **2017**, *19* (39), 26551–26558.

(263)   Fridlind, A. M.; Jacobson, M. Z. A Study of Gas-Aerosol Equilibrium and Aerosol

PH in the Remote Marine Boundary Layer during the First Aerosol

Characterization Experiment (ACE 1). *J. Geophys. Res-Atmos.* **2000**, *105* (D13),

17325–17340.

(264)   Dyhrman, S. T.; Benitez-Nelson, C. R.; Orchard, E. D.; Haley, S. T.; Pellechia, P.

J. A Microbial Source of Phosphonates in Oligotrophic Marine Systems. *Nat.

Geosci.* **2009**, *2* (10), 696–699.

(265)   Karl, D. M. Microbially Mediated Transformations of Phosphorus in the Sea: New

Views of an Old Cycle. *Ann. Rev. Mar. Sci.* **2014**, *6* (1), 279–337.

(266)   Clark, L. L.; Ingall, E. D.; Benner, R. Marine Phosphorus Is Selectively

Remineralized. *Nature* **1998**, *393*, 426.

(267)   Clark, K. L.; Ingall, E. D.; Ronald, B. Composition and Cycling of Marine Organic

Phosphorus. *Limnol. Oceanogr.* **2001**, *46* (2), 309–320.

(268)   Ariga, K.; Lee, M. V; Labuta, J.; Okamoto, K.; Hill, J. P. Studies on Langmuir

Monolayers of Polyprenyl Phosphates towards a Possible Scenario for Origin of

Life. *Colloids Surf., B* **2009**, *74* (2), 426–435.

(269)   Cheng, J.; Psillakis, E.; Hoffmann, M. R.; Colussi, A. J. Acid Dissociation versus

Molecular Association of Perfluoroalkyl Oxoacids: Environmental Implications. *J.

Phys. Chem. A* **2009**, *113* (29), 8152–8156.

(270)   Eugene, A. J.; Pillar, E. A.; Colussi, A. J.; Guzman, M. I. Enhanced Acidity of

Acetic and Pyruvic Acids on the Surface of Water. *Langmuir* **2018**, *34* (31), 9307–

9313.

(271)   Kanicky, J. R.; Shah, D. O. Effect of Degree, Type, and Position of Unsaturation

on the PKa of Long-Chain Fatty Acids. *J. Colloid Interface Sci.* **2002**, *256* (1), 201–207.

(272) Kanicky, J. R.; Poniatowski, A. F.; Mehta, N. R.; Shah, D. O. Cooperativity among Molecules at Interfaces in Relation to Various Technological Processes: Effect of Chain Length on the PKa of Fatty Acid Salt Solutions. *Langmuir* **2000**, *16* (1), 172–177.

(273) Mishra, H.; Enami, S.; Nielsen, R. J.; Stewart, L. A.; Hoffmann, M. R.; Goddard, W. A.; Colussi, A. J. Brønsted Basicity of the Air–Water Interface. *Proc. Natl. Acad. Sci.* **2012**, *109* (46), 18679 LP – 18683.

(274) Zhang, T.; Brantley, S. L.; Verreault, D.; Dhankani, R.; Corcelli, S. A.; Allen, H. C. Effect of PH and Salt on Surface-PKa of Phosphatidic Acid Monolayers. *Langmuir* **2018**, *34* (1), 530–539.

(275) Saykally, R. J. Two Sides of the Acid–Base Story. *Nat. Chem.* **2013**, *5* (2), 82–84.

(276) Cecchi, T. Chromatography and the Hotly Debated Enigma of Aqueous Surface's Acid–Base Character. *J. Phys. Chem. C* **2013**, *117* (48), 25579–25585.

(277) Manciu, M.; Ruckenstein, E. Ions near the Air/Water Interface. II: Is the Water/Air Interface Acidic or Basic? Predictions of a Simple Model. *Colloids Surfaces A Physicochem. Eng. Asp.* **2012**, *404*, 93–100.

(278) Mucha, M.; Frigato, T.; Levering, L. M.; Allen, H. C.; Tobias, D. J.; Dang, L. X.; Jungwirth, P. Unified Molecular Picture of the Surfaces of Aqueous Acid, Base, and Salt Solutions. *J. Phys. Chem. B* **2005**, *109* (16), 7617–7623.

(279) Gershfeld, N. L.; Pak, C. Y. O. The Surface Chemistry of Monooctadecyl Phosphate at the Air/Water Interface. A Study of Molecular Aggregation in

Monolayers. *J. Colloid Interface Sci.* **1967**, *23* (2), 215–220.

(280)   Parreira, H. C. The Surface Chemistry of Alkyl Phosphoric Acids. *J. Colloid Sci.* **1965**, *20* (7), 742–754.

(281)   Schulz, E. P.; Piñeiro, Á.; Miñones, J.; Miñones Trillo, J.; Frechero, M. A.; Pieroni, O.; Schulz, P. C. Effect of Ionization on the Behavior of N-Eicosanephosphonic Acid Monolayers at the Air/Water Interface. Experimental Determinations and Molecular Dynamics Simulations. *Langmuir* **2015**, *31* (8), 2269–2280.

(282)   Hua, W.; Verreault, D.; Adams, E. M.; Huang, Z.; Allen, H. C. Impact of Salt Purity on Interfacial Water Organization Revealed by Conventional and Heterodyne-Detected Vibrational Sum Frequency Generation Spectroscopy. *J. Phys. Chem. C* **2013**, *117* (38), 19577–19585.

(283)   McLean, D. S.; Vercoe, D.; Stack, K. R.; Richardson, D. The Colloidal PKa, of Lipophilic Extractives Commonly Found in Pinus Radiata. *Appita J.* **2005**, *58*, 362–366.

(284)   Spink, J. A. Ionization of Monolayers of Fatty Acids from C14 to C18. *J. Colloid Sci.* **1963**, *18* (6), 512–525.

(285)   Perrin, D. D. *Ionisation Constants of Inorganic Acids and Bases in Aqueous Solution*; Pergamon Press: New York, 1982.

(286)   Lipp, M. M.; Lee, K. Y.; Waring, A.; Zasadzinski, J. A. Fluorescence, Polarized Fluorescence, and Brewster Angle Microscopy of Palmitic Acid and Lung Surfactant Protein B Monolayers. *Biophys. J.* **1997**, *72* (6), 2783–2804.

(287)   Thirumoorthy, K.; Nandi, N.; Vollhardt, D. Role of Electrostatic Interactions for

the Domain Shapes of Langmuir Monolayers of Monoglycerol Amphiphiles. *J. Phys. Chem. B* **2005**, *109* (21), 10820–10829.

(288) Rivière, S.; Hénon, S.; Meunier, J.; Albrecht, G.; Boissonnade, M. M.; Baszkin, A. Electrostatic Pressure and Line Tension in a Langmuir Monolayer. *Phys. Rev. Lett.* **1995**, *75* (13), 2506–2509.

(289) Tyrode, E.; Corkery, R. Charging of Carboxylic Acid Monolayers with Monovalent Ions at Low Ionic Strengths: Molecular Insight Revealed by Vibrational Sum Frequency Spectroscopy. *J. Phys. Chem. C* **2018**, *122* (50), 28775–28786.

(290) Sthoer, A.; Hladílková, J.; Lund, M.; Tyrode, E. Molecular Insight into Carboxylic Acid–Alkali Metal Cations Interactions: Reversed Affinities and Ion-Pair Formation Revealed by Non-Linear Optics and Simulations. *Phys. Chem. Chem. Phys.* **2019**, *21* (21), 11329–11344.

(291) Alderighi, L.; Gans, P.; Ienco, A.; Peters, D.; Sabatini, A.; Vacca, A. Hyperquad Simulation and Speciation (HySS): A Utility Program for the Investigation of Equilibria Involving Soluble and Partially Soluble Species. *Coord. Chem. Rev.* **1999**, *184* (1), 311–318.

(292) Baumler, S. M.; Hartt V., W. H.; Allen, H. C. Hydration of Ferric Chloride and Nitrate in Aqueous Solutions: Water-Mediated Ion Pairing Revealed by Raman Spectroscopy. *Phys. Chem. Chem. Phys.* **2019**, *21* (35), 19172–19180.

Appendix A. Polarized infrared reflection absorption spectroscopy

A ZnSe Holographic wire grid polarizer (Thorlabs, Inc) was used to obtained polarized

infrared reflection absorption spectroscopy spectra. The polarizer was mounted in a

rotation stage where "0" and "180" degrees corresponds to the *p*-polarization and "90" or

"270" corresponds to the *s*-polarization. Stearic acid and dipalmitoylphosphatidylcholine

were both dissolved in chloroform solutions and spread via the Hamilton syringe method

onto a water surface. The stearic acid surface pressure was maintained at 10 mN/m and

the dipalmitoylphosphatidylcholine surface pressure was maintained at 40 mN/m during

the experiment. The incidence angle of the infrared source was controlled and set to

angles of 48° and 50° relative to the surface normal. The results shown are the result of

averaging three independently collected spectra. The y-axis was offset in each spectrum

for clarity. Figure A.1 shows an example of the *p*-polarized and *s*-polarized spectra for

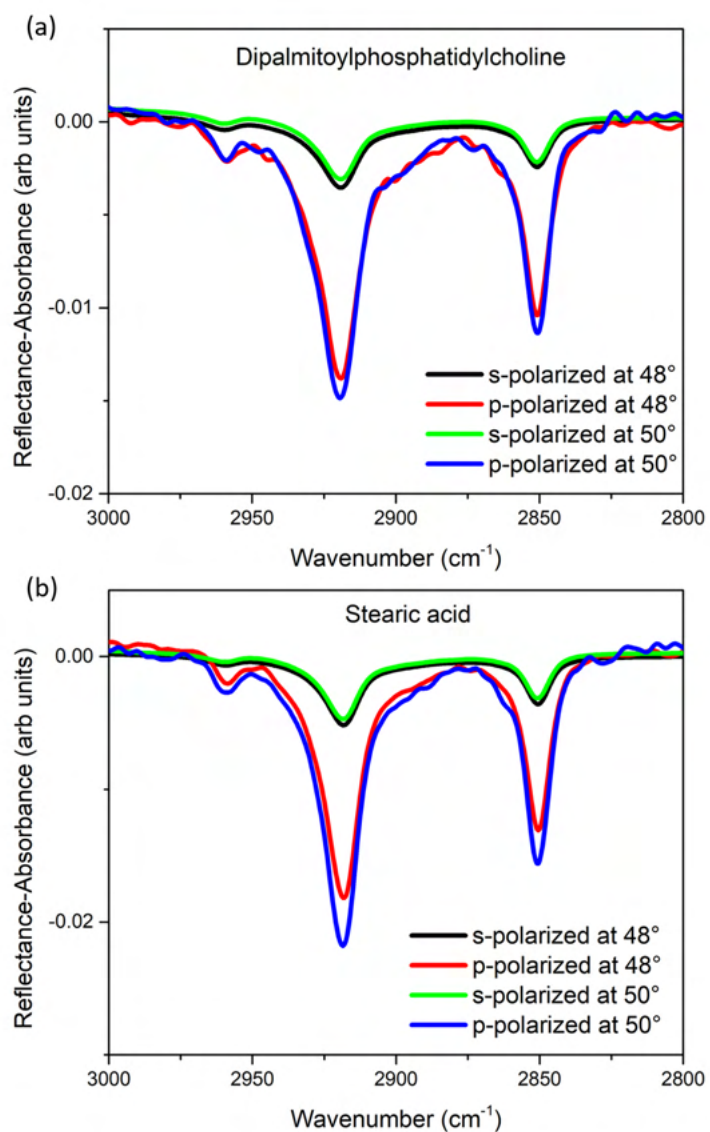these monolayers in the alkyl chain region (from ~3000 to 2800 cm^{-1}).

Figure A.1 IRRAS spectra of (a) dipalmitoylphosphatidylcholine and (b) stearic acid in the alkyl region.

The *s*-polarization spectra are lower in intensity than the *p*-polarization spectra for both the stearic acid and dipalmitoylphosphatidylcholine. By collecting data over a range of

incidence angles the tilt angle of the alkyl chains can be solved for. It is therefore useful

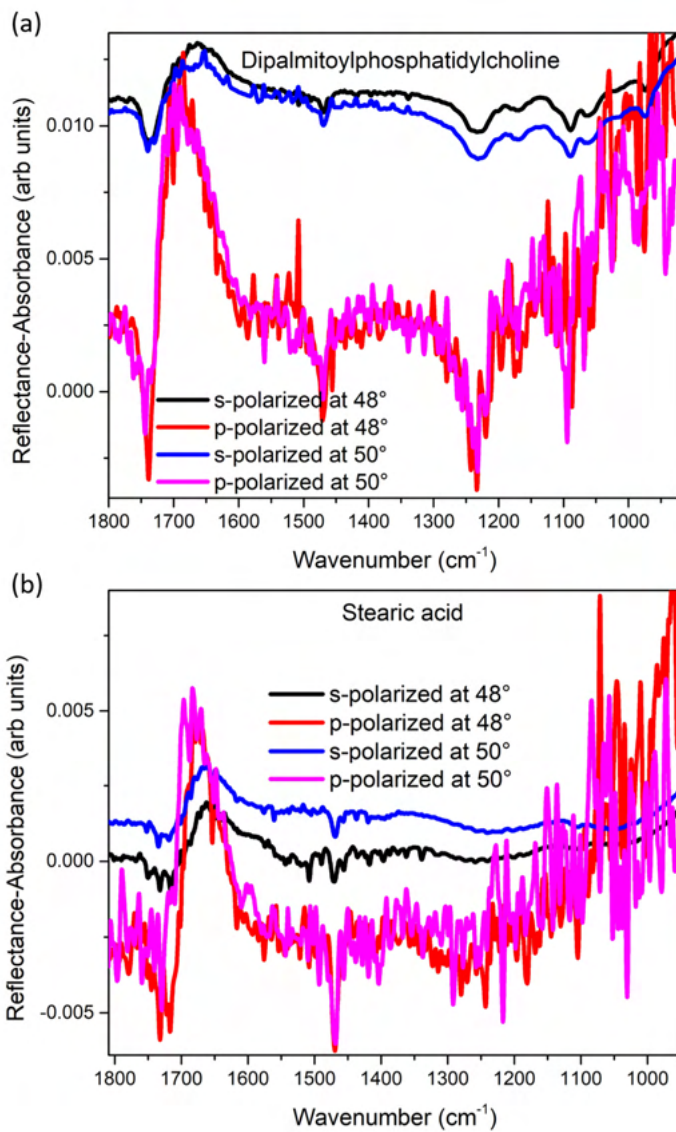to be able to collect polarized IRRAS data.

Figure A.2 IRRAS spectra of (a) dipalmitoylphosphatidylcholine and (b) stearic acid in the low frequency region.

Appendix B. Raman Spectroscopy

Polarized Raman spectroscopy was performed on a custom-built Raman spectrometer described in more detail elsewhere.[292] Briefly, a 532 nm CW laser with CrystaLaser polarization filters (>100:1) was used. The fiber optic polarized probe from InPhotonics scattered light into two fiber optic ports one for the output parallel polarization and the other for the output perpendicular polarization. The two polarization were directed into a Princeton Instruments (IsoPlane 320) spectrometer and liquid nitrogen cooled CCD detector (Pylon, Princeton Instruments). Spectra were taken at different temperatures using a Peltier-driven temperature-controlled cuvette holder (Quantum Northwest). The cuvettes used were Starna Cells Inc UV Quartz windows useable range 170 to 2700 nm with a sealing cap (# 1-Q-10-GL-14-C).

To acquire temperature-controlled spectra, first the temperature probe was calibrated using the setpoints on the temperature controller and a thermocouple. The setpoints are slightly different than the actual temperature readings so it is important to first calibrate this in order to know the real temperature readings. Next, a spectrum of the vial was taken before each run for the day. The vial spectrum is important because it serves as a background subtraction to get rid of artifacts present. When acquiring

171

temperature Raman spectra, it is also important to ensure there is no evaporation from the Raman vial at higher temperatures. Multiple room temperature (at 20 °C) spectra were taken to ensure there were no issues with evaporation. For example, once the 80 °C spectrum was taken, the setpoint would be returned to 20 °C to make sure it matched. Then, the setpoint would be adjusted to 100 °C and this spectrum would be acquired and the setpoint again would be returned to 20 °C to ensure there were no issues with evaporation. Each Raman acquisition was repeated in at least triplet in order to confirm reproducibility.
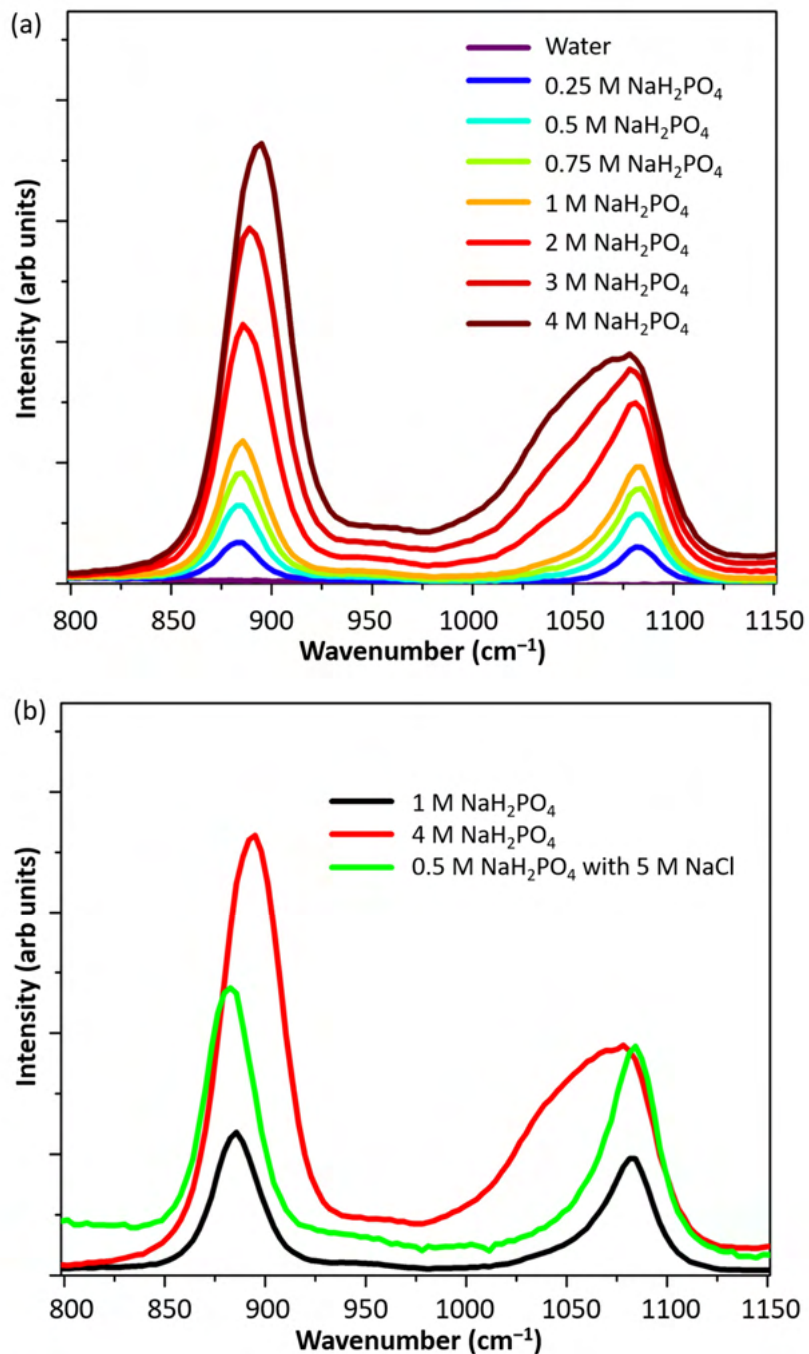
Figure B.1 (a) Raman spectra of sodium phosphate showing the increase in phosphate-phosphate interactions at increasing concentrations and (b) 0.5 M phosphate with sodium chloride (green) multiplied by four to compare with the intensity of the 4 M phosphate spectrum (red).
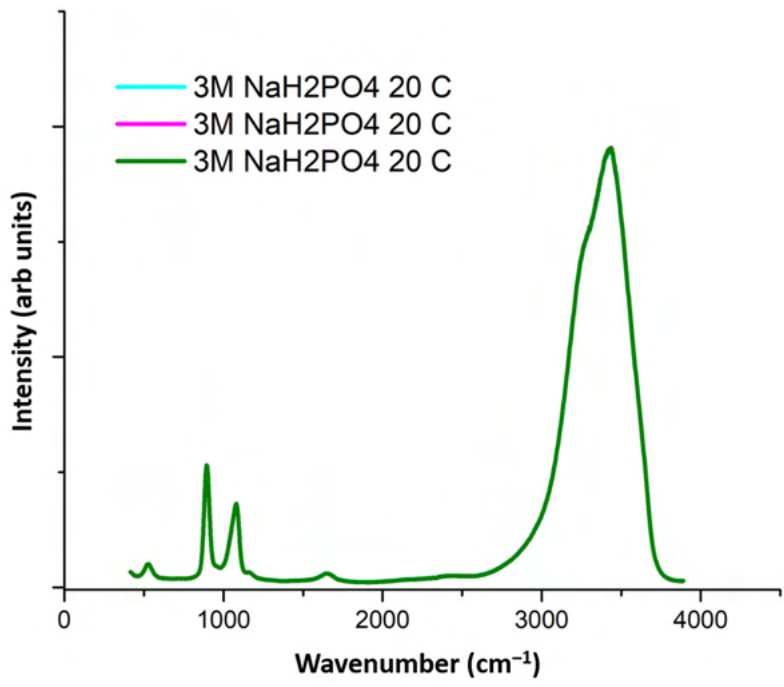
Figure B.2 Raman spectra of sodium phosphate at 20°C showing the reproducibility of the spectra.
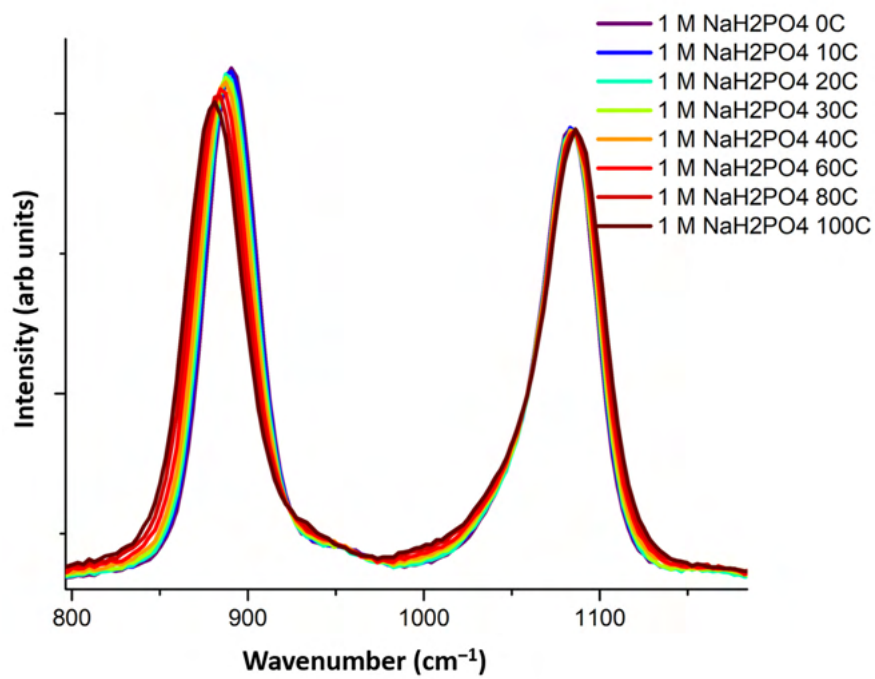
Figure B.3 Raman spectra of 1 M sodium phosphate from 0 °C to 100 °C.
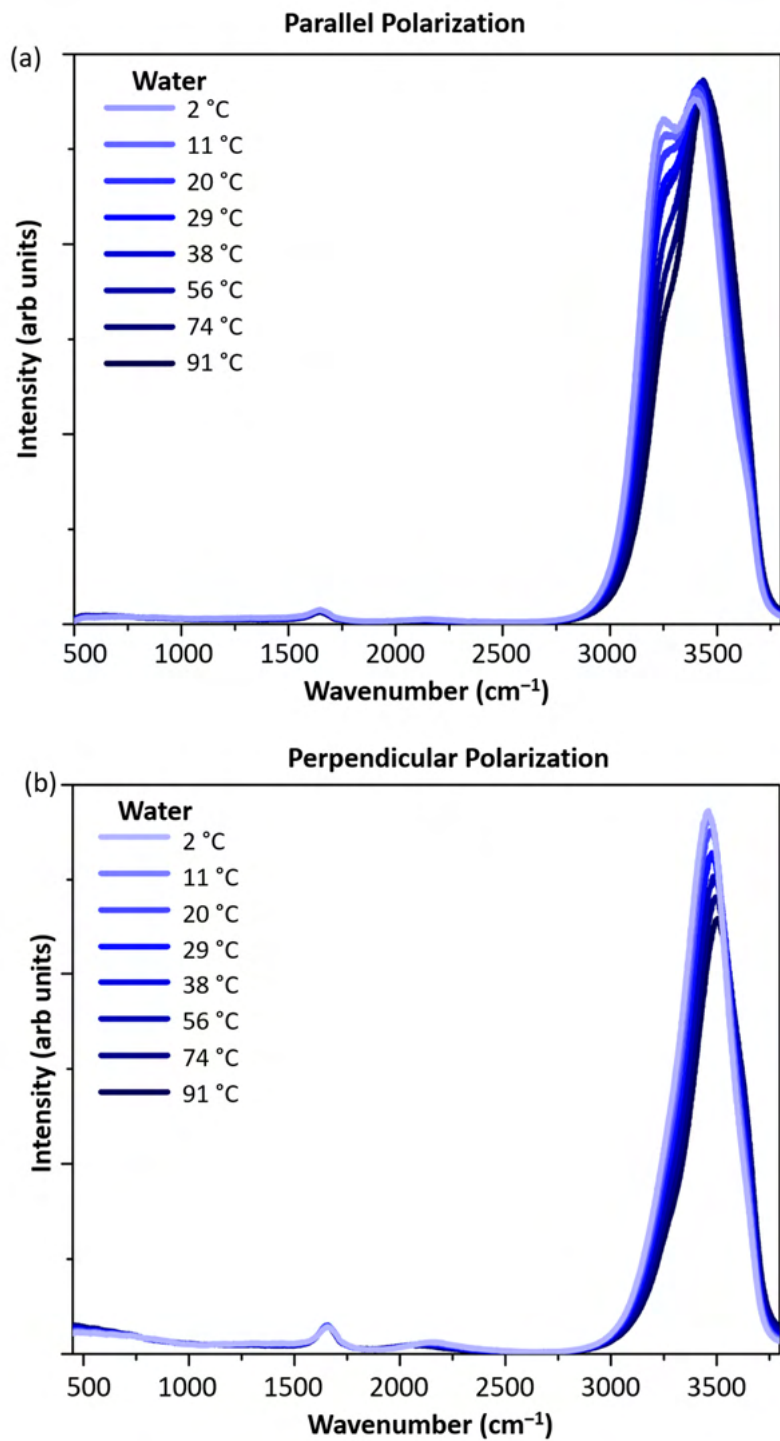
Figure B.4 (a) Parallel polarized Raman spectra of water (b) perpendicular polarized Raman spectra of water.
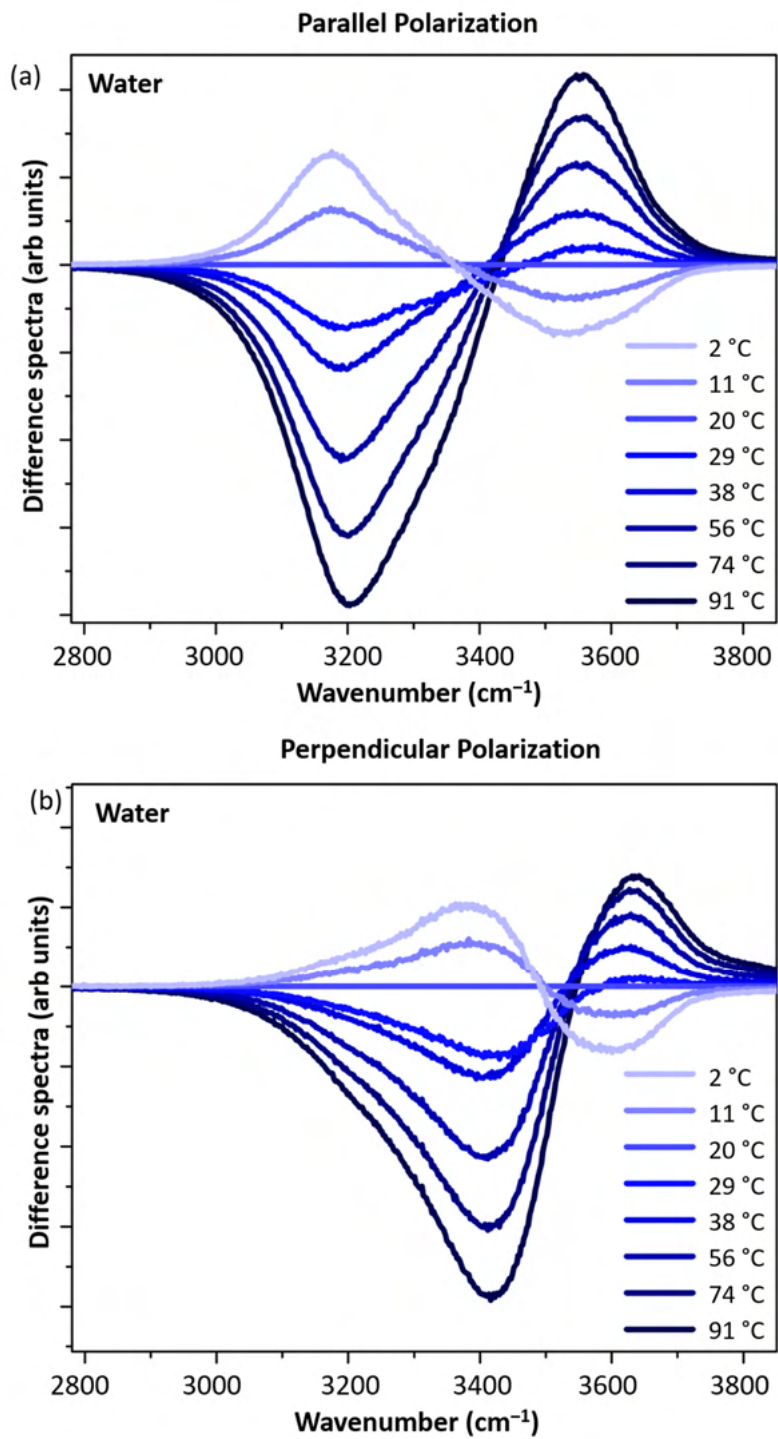
Figure B.5 (a) Difference spectra of the parallel polarized Raman spectra and (b) difference spectra of the perpendicular polarized Raman spectra.